INVESTIGATING BIOLOGICAL ROOT CAUSES OF HYDRAULIC PERFORMANCE CHALLENGES IN DRINKING WATER BIOFILTERS

By

Leili Abkar

Submitted in partial fulfilment of the requirements
for the degree of Doctor of Philosophy

at

Dalhousie University
Halifax, Nova Scotia
Oct 2020

TABLE OF CONTENTS

LIST OF TABLES

LIST OF FIGURES

ABSTRACT

United Nations SDG6 defines that providing safe drinking water to all (goal 6) and SDG12 mandates employing sustainable approaches for all. Utilizing indigenous microbial communities (IMC) to remove water contaminants provides a promising pathway to provide safe and affordable drinking water sustainably. Although drinking water biofiltration already achieves high productivity rates, researchers are pursuing further optimizing the system to improve the overall performance and lower maintenance. Intentional operation of biofilter mandates understanding the microbiome, which provides the foundation for developing educated monitoring, prediction, and optimization strategies. In this study, microbiome analysis was used to monitor the biofilter microbial community in regular and challenging filter events. Challenging filter events refer to events with lower hydraulic performance. In two years, regular operations and events such as diatom algae bloom and a media replacement were investigated. The diatom bloom event, representative of intense source water quality changes, resulted in a significantly lower filter runtime (24.9 h) than the average of 70 h. Beta diversity analysis showed a distinct difference between the fresh media and all other media. Besides to understanding the microbiome changes, the use of a clarification step to improve hydraulic performance was studied. It is known that a clarification step reduces the floc carryovers, however the impact of a clarification step prior to a biofilter has not been studied. Therefore, this study was designed and conducted on a pilot scale to investigate the impact of a sedimentation process prior to a biofilter. Results showed that sedimentation improved FRT up to 30% and reduced head-loss, and head-loss accumulation rate up to 29% and 35%, respectively. The NOM removal in effluent water did not change while the turbidity decreased significantly. Biological activity changed measured as EPS (reduced by 36%). The results of this study triggered the investigation of the biological root causes of the different EPS level observed. Thus, the two most biofilm-producing bacteria were isolated from full-scale biofilters. The isolated bacteria were then identified as *Bacillus mycoides and Paenibacillus tundrae*. The characterization step led to developing a reliable and high-throughput protocol for measuring bacterial growth curves and maximum growth rate. The protocol was developed addressing accuracy and repeatability issues, including (i) lid condensation, (ii) pathlength correction, (iii) inoculation method, and (iv) sampling time interval were investigated. The maximum growth rates were determined for *Bacillus mycoides* (0.99 ± 0.03 h^{-1}) and *Paenibacillus tundrae* (0.85 ± 0.025 h^{-1}). It was hypothesized that the flocs buildup inhibits the nutrient diffusion to the bacteria. Subsequently, the impact of nutrient limitation, specifically P as an essential macronutrient, was studied under different P limited conditions for isolated bacteria. Carbohydrate and protein-EPS were increased when decreasing the available P in the medium while the ATP level decreased and reached a plateau. The results of this study showed that inhibiting nutrient diffusion due to the floc buildup could cause higher EPS production in the biofilter without a clarification step. In conclusion, this study provides a novel insight by combining detailed information about the IMC, traditional filter performance, and biological activity indicators allowing for a deeper understanding of the biological root causes of reduced hydraulic biofilter performance. A fundamental toolkit to predict and subsequently avoid challenging events, leading to a more sustainable and affordable drinking water biofiltration in large and small facilities was presented. The toolkit was examined in a full-scale water treatment facility providing the applicability aspect. Sedimentation as a clarification step was implemented for the first time and proved to be a successful optimization strategy improving water quality and hydraulic performances of the biofilters.

LIST OF ABBREVIATIONS

DBP	Disinfection-by-product
ATP	Adenosine Triphosphate
ASVs	Amplicon Sequence Variants
NMF	Non-Negative Matrix Factorization
DADA	Divisive Amplicon Denoising Algorithm
EBCT	Empty Bed Contact Time
FRT	Filter Runtime
LPS	Lipopolysaccharide
EPS	Extracellular Polymeric Substances
PCR	Polymerase Chain Reaction
NOM	Natural Organic Matter
DOC	Dissolved Organic Matter
PeCOD	Photoelectrochemical Oxygen Demand
UV_{254}	UV absorbance measurements at 254 nm
TOC	Total Organic Carbon
THMs	Trihalomethanes
HAAs	Haloacetic acids
C-F	Coagulation-Flocculation
C-F-S	Coagulation-Flocculation-Sedimentation

OD	Optical Density
TSA	Tryptic Soy Agar
TSB	Tryptic Soy Broth
PBS	Phosphate-buffered Saline
CV	Crystal Violet
RDP	Ribosomal Database Project
NCBI	National Center for Biotechnology Information
MEGA	Molecular Evolutionary Genetics Analysis
CDP	Critical Drying Point
e-DNA	Extracellular DNA
MAFFT	Multiple Alignment Using Fast Fourier Transform

ACKNOWLEDGEMENTS

Chapter I   INTRODUCTION

C.I - 1   INTRODUCTION

The United Nation's 17 interconnected, sustainable development goals (SDGs) include the availability of safe and affordable drinking water (SDG 6), sustainable consumption, and production of natural resources (SDG 12)[1].

Drinking water quality has a considerable impact on human health, given the regular and large volume consumption and, therefore, accessible, clean, and safe drinking water that does not impair human health when consumed long term is of utmost importance [2]. Drinking water is either locally sourced and processed or remotely bottled and shipped. If tap water quality is not satisfactory, it disproportionally affects people in different social sector based on their income level. While high-income populations would use household water treatment technologies or bottled water alternatives[3], low income has to use unsafe tap water. It is noteworthy that bottled water often comes from exploited parts of the world[3] and a considerable environmental footprint for transport, storage and waste management. All of these signify the importance of providing safe and affordable tap water through sustainable water treatment approaches.

Water treatment technologies, such as thermal and membrane desalination, are deemed to be very energy-intensive with low productivity rates, making them not very sustainable options for providing drinking water. While chemical disinfection processes are common, the side-effect of carcinogenic by-products is a significant health concern. Disinfectant by-products result from the reactions between the disinfectant and natural organic matter in the water. Therefore, utilizing naturally occurring microbial communities to consume NOMs and provide clean and safe drinking water is a sustainable approach. Biofiltration is a robust process that is cost and energy-efficient, resulting in lower final water production costs than

other water treatment technologies. Biofiltration can be used over a wide range of operating conditions and removes a vast spectrum of contaminants. Microorganisms remove the contaminants through mineralization and biodegradation rather than transferring them to a waste stream, creating a concentrated stream that requires a series of waste disposal processes. It also reduces the disinfectant requirements for the distribution system by removing the organic contaminant in the water.

This study focuses on drinking water biofiltration as a sustainable water treatment approach. Historically this process was designed and operated based on the regular filtration criteria. It is evident that to run biofiltration optimally; the biological activity must be understood and monitored.

One focus of this thesis is the biological monitoring strategies, such as microbiome structure analysis, applied to provide more insight.

Another focus is the effect of a clarification step, an easy retrofit to existing water facilities, in an attempt to optimize the biofiltration performance. The clarification step reduces the floc carryovers to the biofilter. To understand the floc and bacteria interaction, two species were isolated and characterized from a full-scale biofilter. It is hypothesized that the flocs accumulation inhibits nutrient diffusion to bacteria; thus, more extracellular polymeric substances are produced. Alum carried over to biofilter with flocs may trigger the EPS production pathway in bacteria. These hypotheses were studied in lab experiments and through a literature search.

C.1 - 2 BACKGROUND

Safe drinking water has played an essential role in human civilization since the very beginnings. It has defined broadly where nomads would rest and where settlements were

established. Directing water over long distances (i.e. aqueducts by the Romans) for the first-time allowed settlements to grow into significantly large cities independent of local water sources [4]. Over 4000 years of water treatment documentation showed that water filtration beyond simple straining or boiling as practiced by the Greeks and Egyptians did not develop much further until the microscope's invention enabled new insight into the countless microorganisms present in the water in the 18th Century [5]. This led to using charcoal, sponge, and wool filters to eliminate unwanted organisms and particles by many nations [5]. It is this practice that accidentally introduced biologically active filters into practice.

Biological filtration (biofiltration) in slow-sand filtration operation mode (0.02 to 0.08 gpm/ft^2 or 0.03-0.05 L/m^2/s) started since 1800s providing drinking water. The first commercial biological slow-sand filter built by John Gibb used for water treatment operated in Scotland [6]. The biological activity in slow-sand filtration happened unintentionally. Rapid-sand filtration (2 to 10 gpm/ft^2 or 1.4 to 6.8 L/m^2/s) started in the USA early 1900s after the success of preventing water-borne disease using filtration in Europe[7]. Rapid rate biofilters gained more popularity due to the lower footprint requirement and accommodating water with higher turbidity >10 NTU [8].

In the mid 19th Century, cholera transmission through water and the ability to inactivate it using chlorine resulted in chlorination as a popular form of water purification [9]. Chlorine incorporated with the operation of rapid-rate filters limited the biological activity in the filters [10]. Disinfectant by-product forms as a result of chlorine reaction with organic matter in the water. The identification of carcinogenic properties of DBPs shifted the focus toward eliminating the chlorine addition in the drinking water system. This allowed for microorganism growth on the filter media again and thus the passive operation of biofilters. Biofiltration is a sustainable approach to degrade the contaminants in the water using the microbial community.

Reducing the organics by biofilter decreases the potential of DBPs formation and amounts of organics inflowing to the distribution system. Lower organic levels in the distribution system reduce bacterial regrowth, thus enhancing water's biological stability in the distribution systems[11].

The recognition of biological instability in the drinking water distribution system (DWDS) and the reduction of DBP precursors directed the passive operation of biofiltration toward a more purposeful process. Thus, the biological filtration has been defined recently as the activity of managing, maintaining, and enhancing the biological activity on the filter media so the organic (i.e., DPB precursor) and inorganic contaminant (Mn, Fe, Nitrate, ..) transformation are optimized [12].

Conventional drinking water treatment system includes primary chemical addition (depending on the source water quality varies), coagulation (coagulant type varies based on the source water quality and targeted objectives), flocculation, sedimentation (optional) followed by an array of filters. Direct biofiltration does not include a clarification step.

In the attempt to increase the biofilter productivity and minimize the head-loss accumulation rate, optimizing the operational and design factors such as empty bed contact time (EBCT), the hydraulic loading rate, different backwash strategies and type of media were considered and investigated [13]. The foremost attention of promoting the biological activities focused on the increasing biodegradability of the Natural Organic Matter (NOM) using upstream oxidation (ozone, $UV-H_2O_2$, and UV-Ozone)[14–16] and nutrient supplementation (Phosphate and Nitrogen addition) which promoted the contaminant transformation through microorganism metabolism[17].

C.I - 2.1   Microbiological Community in an Intentional Biofilter

Microorganisms move through the source water to the biofilter media and proliferate. The source water and type of water treatment system applied prior to the biofilter (e.g. type of coagulant, and chemicals addition) determine the microbial community structure in the biofilter media. Not all the microorganisms will stick to the filter media, conditions such as low nutrient level, oxidant addition and backwashing strategy select the microorganisms. Some bacteria slough off, and the rest are categorized as strict (not slough off frequently), and leaky colonizers (leak through the filter media to the effluent water)[18]. Strict colonizers are likely the most biofilm producing bacteria on the media. Apprehending the biofilm characteristics is of utmost significance to understand biofilter performance and productivity. Biofilm formation is the transition of a single-cell to a multicellular lifestyle and from planktonic to a sessile state[19]. Biofilm formation happens in response to the environmental changes. This transition involves changes in cells' metabolic pathways and gene expression, and consequently, the alteration in the cell wall, nutrient consumption and virulence changes helping the cells to survive in undesirable situations. Bacteria (10%) in the biofilm are enveloped with extracellular polymeric substances (EPS), contributing to 90% of the total biofilm biomass[20,21]. EPS mainly compose of proteins, carbohydrates and extracellular deoxyribonucleic acid (e-DNA)[20–24]. The robust structure of biofilms is provided by the nutrient gradient maintenance and regulation utilizing enzyme secretion by bacteria and retaining the adequate water through the H-bond with hydrophilic exopolysaccharides[20]. The robust structure of biofilm keeps the enclosed bacteria sheltered from the harsh and stressful conditions such as desiccation, predation, oxidizing agent, radiation, and other damaging chemicals[20,25–27].

C.I - 2.2   Monitoring Performance and Function of Intentional Biofiltration

To assess biofilter performance and productivity, applying the appropriate monitoring tools and strategies is vital. Biofilter monitoring, in general, includes media inspection, hydraulic, water quality and biological monitoring[28].

The recent move toward a more focused biofilter operation to reach specific goals requires furthering the knowledge about the microbial community structure and function on a deeper level[13]. Shifting from incidental to the intentional operation of biological filtration necessitates state-of-the-art biological monitoring technologies. Now, we have the advanced and cost-effective technologies to analyze and understand the biological activity, and microbial community structure and function. Microbial community characterization advances our knowledge to optimize biofiltration performance more systematically[29].

C.I - 3 THESIS APPROACH

To optimize the biofilter performance understanding the microbial community structure is of utmost importance. This thesis aims to consolidate the state-of-the-art tools for monitoring the dynamics and performance of intentional biofiltration. It further focuses on comprehending the root causes of adverse biofilter performance which requires relating performance monitoring data to the biofilter's biological activity and characterization.

Analyzing and characterizing the bacterial community using 16S rRNA gene analysis provides insights into community structures, and diversity analysis depicts the differences between the microbial communities. Pairing the 16S rRNA sequences with hydraulic performance parameters and biological activity indicators such as ATP measurements helps understand the role of microbial community structures regarding challenging filter events, such as algae bloom and media replacement.

A clarification step (sedimentation tank) before the biofilters was incorporated and investigated to optimize the hydraulic performance of biofilters. The results of this study will establish hypotheses (see C.I-5) further exploring biological approaches for optimizing hydraulic performance in drinking water biofilters. Understanding the flocs and bacteria microorganism.

C.I - 4 RESEARCH QUESTIONS

The research questions addressed in this thesis are:

1) How does the microbial community in a biological filter respond to variation in water quality and challenging filter events?

2) Can the hydraulic performance challenges be explained using biological approaches?

C.I - 5 RESEARCH HYPOTHESES AND OBJECTIVES

The main goal of this research is to understand the biological root causes of challenging filter events. The hypotheses and objectives are defined as follows:

C.I - 5.1 Hypothesis 1

Microbiome analysis is a sensitive monitoring strategy with capabilities to show distinct differences between the regular operation and challenging events.

The following objective and sub-objectives are addressed by hypothesis 1:

Characterize the microbial community structure of a biofilter for two years to identify biomarkers correlating with challenging filter events.

- Understand the microbiome of biofilter under regular operation.
- Understand the impact of filter media replacements as a challenging filter event on the microbial community structure and hydraulic performance.
- Understand the impact of diatom algae bloom as a challenging filter event on the microbiome and hydraulic performance.

C.I - 5.2 Hypothesis 2

Applying a sedimentation tank improves the hydraulic performance of a drinking water biofilter

The following objective and sub-objectives were defined to address the hypothesis 2:

Identify the impact of a sedimentation tank on the hydraulic performance of biofilters.

- Determining the impact of applying a sedimentation tank on biological activity.
- Investigate the impact of a sedimentation tank on hydraulic performance.
- Evaluate the water quality changes when applying the sedimentation process.

After addressing the above-mentioned objectives in pilot-scale biofilters, hypotheses 3 and 4 were formed to understand the root causes of the observations.

C.I - 5.3   Hypothesis 3

The toxicity of alum, carried over in flocs, triggers the EPS pathway in bacteria

The following objective was defined to address the hypothesis 3:

Study the impact of alum toxicity on the EPS production of bacteria.

C.I - 5.4   Hypothesis 4

Floc carryover reduces the diffusion of nutrients to bacteria. Low nutrient conditions cause stress leading to an increased formation of EPS.

The following objective and sub-objectives were defined to explore hypothesis 4:

Isolate biofilm-producing bacteria from a full-scale biofilter and investigate their behavior under nutrient-limited conditions:

- Isolate the two most biofilm-producing bacteria from a full-scale drinking water biofilter.
- Identify and characterize the isolated bacteria.
- Develop a reliable and accurate high-throughput method to measure the maximum growth rate of the isolated biofilm-producing bacteria.
- Investigate the biofilm architecture using SEM imaging.
- Determine the influence of P-limitation on biofilm production.

C.1 - 6   **THESIS OVERVIEW**

This thesis has been written as a publication based cumulative thesis. Therefore, each chapter is intended to stand on its own as a publication with its own introduction, methods, results and discussion and this may lead to redundancies with the literature review.

Chapter I: Introduction

This chapter provides a general introduction and outline for the thesis, including the background and objectives necessary to understand the significance of this work.

Chapter II: Biofilter Monitoring Strategies

This chapter addresses Hypothesis 1, evaluating a monitoring gap for drinking water biofilters. Considering biological activity as the primary driver for biofilter performance, and using tools, such as ATP and microbiome analysis, are suggested to allow for the prediction of filter events. The microbiome diversity analysis showed distinct differences between fresh and old media, and NMF revealed the species biomarkers for regular operations and challenging biofilter events.

Chapter III: Increasing Hydraulic Performance

Sedimentation: Hydraulic improvement of drinking water biofiltration

Leili Abkar, Amina Stoddart, Graham Gagnon

Published in AWWA Water Science, Sep 2019

Sedimentation was proposed as an option for optimizing hydraulic performance in drinking water biofilters. This chapter addresses Hypothesis 2 which evaluates implementing a sedimentation process before biofilters comparing to direct biofiltration. Biological activity monitoring analyses were used to understand the impact of sedimentation, specifically the relationship between hydraulic performance and biological parameters.

Chapter IV: Sources of Head-loss in Direct Biofiltration

In Chapter III, direct biofiltration had significantly higher head-loss accumulation rates compared to sedimentation before biofiltration. Possible root causes for this observation were defined into two hypotheses (see section CI-5.3). An extensive literature review explored the possible toxicity of alum to investigate Hypothesis 3.

Chapter V: Method Development for Microbial Characterization

Leili Abkar, Florentin M. Wilfart, Marta Piercey, Graham A. Gagnon

Peer Reviewed by Letters in Applied Microbiology (LAM); reviewer's comments addressed and will be resubmitted. As the lead author my roles were developing the experimental design and executing the experiments, writing and revising the chapter.

Two high biofilm-producing bacteria were isolated and characterized to investigate Hypothesis 4. A high throughput method was developed to determine their maximum growth rate (as one of their characteristics). Factors listed below were studied to develop a high resolution and reliable method:

- Impact of the inoculation size

- Impact of the OD reading frequency
- Pathlength correction to compare the results between spectrophotometer and microplate reader
- Condensation buildup on the lid

Chapter VI: Nutrient Diffusion Limitation by Floc Accumulation

The impact of P reduction in low nutrient media (minimal media) on the biological response of the isolated bacteria was investigated to address hypothesis 4. The isolated bacteria were identified using 16s rRNA sequencing and submitted to the National Center for Biotechnology Information (NCBI). The biofilm architecture of these bacteria in minimal media was characterized by Scanning Electron Microscopy (SEM) imaging. Various Phosphorus limitation conditions were examined and proved to increase EPS production.

Chapter VII: Conclusions

This chapter summarises the conclusion and results from each chapter also includes the recommendation for future

Chapter II   BIOFILTER MONITORING STRATEGIES

Holistic monitoring strategies to study and predict the biological root causes of drinking water biofilter challenges

Unpublished manuscript

This chapter addresses how microbial communities change in response to variation in water quality and challenging filter events. The microbial community structure of a biofilter is characterized over the course of two years to identify biomarkers corelating with challenging filter events during this time period, understand the microbiome and create a baseline during normal biofilter operation. Events include filter media replacements and diatom algae blooms and their impact on the microbiome and hydraulic performance.

C.II - 1 GRAPHICAL ABSTRACT
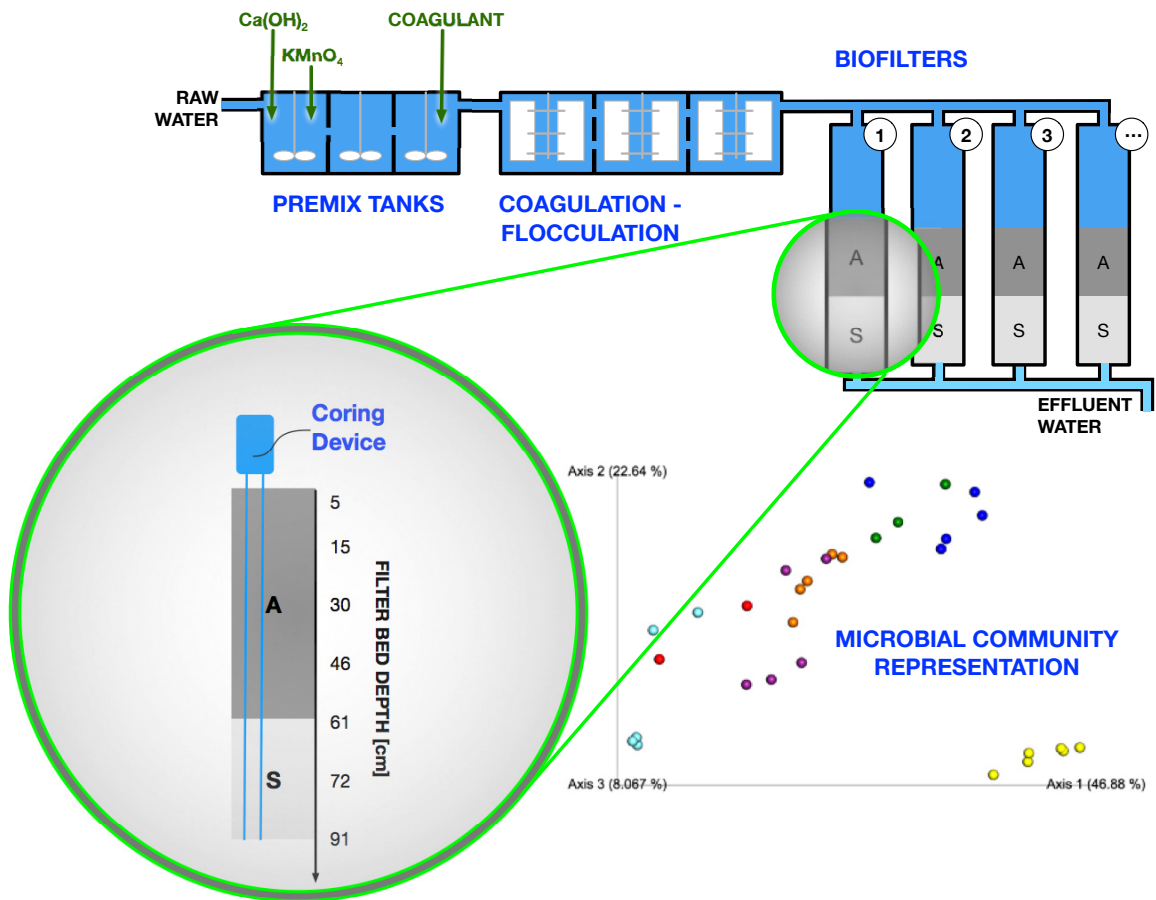
Figure 1   Graphical abstract

C.II - 3 ABSTRACT

The hydraulic performance of drinking water biofilters is a critical factor in their energy consumption and reliability. Hence, there must be an understanding of appropriate monitoring indicators to optimize filter hydraulic performance. Conventional monitoring indicators and new microbiological surrogates were applied to create a holistic approach to monitoring and studying hydraulic biofilter performance. This study was conducted at full-scale biofilters and involved differentiating and challenging events such as a media replacement, diatom bloom and the following chlorination phase. Data were collected in two years and divided into two main categories, conventional monitoring indicators and new microbial community analysis. Conventional monitoring indicators included hydraulic performance surrogates such as head-loss, filter runtime, and filter media analysis covered deposited metals (Al, Ca, Mn), turbidity, and biological activity as measured by Adenosine Triphosphate (ATP). The new microbial community analysis focused on alpha and beta diversity to determine the similarity between the baseline and challenging events. Media samples were collected through depth to observe any spatial variation of biological activity, deposited metals, and microbial community structure. Non-negative matrix factorization (NMF) was applied to determine potential biomarkers, and the correlation between the monitoring indicators examined.

ATP decreased with increasing contact time (i.e., filter depth). No correlation was observed between amplicon sequence variants (ASVs) and ATP levels in various filter depths. A correlation was observed between the ATP and turbidity levels throughout the filter depths with increasing contact time. The highest turbidity accumulation rate, head-loss accumulation rate and shortest filter runtime (FRT) were observed during the diatom bloom event. The fresh media samples were taken after media replacement and showed a distinct microbiome as indicated by beta diversity analysis, using Bray-Curtis and Weighted UniFrac distances.

Chitinophagaceae, and *Rhizobiales*, and *Xanthobacteraceae* were determined as biomarkers for fresh media. *Acetobacteraceae* was observed as the biomarker for the diatom bloom.

Key words: media replacement, microbiome diversity, biofilter surveillance, diatom bloom, chlorination, biomarkers

C.II - 4   ABBREVIATIONS

- Adenosine Triphosphate (ATP)
- Amplicon Sequence Variants (ASVs)
- Non-Negative Matrix Factorization (NMF)
- Divisive Amplicon Denoising Algorithm (DADA)2
- Multiple Alignment Using Fast Fourier Transform (MAFFT)
- Empty Bed Contact Time (EBCT)
- Filter Runtime (FRT)
- Lipopolysaccharide (LPS)
- Extracellular Polymeric Substances (EPS)
- Polymerase Chain Reaction (PCR)

C.II - 5 INTRODUCTION

Many researchers have studied optimizing biofilters using conventional approaches that consider factors such as empty bed contact time (EBCT), raw water temperature [30], type of media, and backwashing techniques [31]. These approaches mostly focused on optimizing the operational and design parameters.

In 2011, Lauderdale introduced the concept of an "engineered biofilter" for drinking water treatment and emphasized biological activity as the critical driver to remove natural organic matter and targeted contaminants like manganese and geosmin[10]. This concept introduced engineered biofiltration methods such as oxidant, hydrogen peroxide[17,32,33], and chlorine addition [34] in order to breakdown NOM to more biodegradable matters and remove excess extracellular polymeric substances (EPS). Nutrient enhancement strategies such as phosphorus and nitrogen addition, were developed for bacterial activity augmentation[17,35].

Organic carbon contaminant removal is driven primarily by biological activity in the biofilter [36]. Biological activity is typically studied by analyzing Adenosine Triphosphate (ATP) and microbial community structure. ATP is the energy carrier in the living cells and has been found to be a quick, straightforward and reliable method over conventional culturing techniques and phospholipid phosphate analysis [37,38]. ATP, by itself, measures the biological activity and does not provide a thorough understanding of a microorganism's role and influence. In other words, ATP is merely a representation of the bacterial activity with no discrimination of species type and bacterial living status. Microbiome studies were introduced to provide insight on the structure and diversity of the microbial community through 16S rRNA genes analysis.

Microbiome community analysis aims to elucidate the role of microbial species inside the biofilter. This knowledge may help to achieve a customized biofilter for targeted contaminant removals and optimizing biofilter performance. Microbial community diversity shows temporal dynamics like seasonality and is affected by design and operational factors such as empty bed contact time (filter depth), type of filter media, and source water quality [13,29]. Source water seeds the biofiltration microbiome; hence any drastic changes in water reservoir microbiota cause alterations in microbial community structure [18].

Algae blooms are one of the drastic changes that may happen in warmer temperatures and high nutrient (N and P) conditions. No studies to the knowledge of the authors were published that investigate the impact of sudden source water changes, such as a diatom bloom, on biofilter microbiota.

The present study focuses on the holistic (conventional and microbiome analysis) monitoring approach of investigating the drinking water biofilter. It considers temporal variation as well as challenging events. This is the first study to investigate the media replacement, diatom bloom and subsequent chlorination via a holistic monitoring approach. Hydraulic performance indicators such as head-loss, filter runtime (FRT) and floc retention are explicitly investigated. Microbiome diversity indices (alpha and beta diversity), biological activity (ATP) and the microbial composition of drinking water biofilters are also examined. More importantly, this study applies a statistical model, non-negative matrix factorization (NMF) to determine biomarkers for regular operation and community transition during challenging events, such as filter media replacement and diatom algae bloom. Finally, the correlation between different monitoring indicators are presented.

C.II - 6   MATERIAL AND METHODS

A series of core samplings were conducted as part of the filter surveillance program in J. D. Kline Water Treatment Facility in Halifax, Nova Scotia, Canada. This facility draws water from the nearby lake, Pockwock Lake. Said samples were taken in two years, 2016 and 2018. Core sampling in 2016 happened in three months of March, April, and May. In 2018, the first set of samples were taken in February. Samples from February 2018 represent old media samples. Media replacement was done in early March 2018; therefore, core samples taken later in March represent the fresh media. The facility faced extremely low filter runtime in July 2018 due to the Lake diatom bloom. Core samples were taken in that month to investigate the impact of diatom bloom on the filter media. The water treatment facility used chlorination to address the drastic decline in filter performance which improved the filter runtime.

C.II - 6.1   Full scale set up and operation

The full-scale J. D. Kline Water Supply Plant is a direct filtration facility (Figure 2). Water from Pockwock Lake is pumped to the three pre-mix tanks where chemicals such as calcium hydroxide, and potassium permanganate are added to adjust pH and oxidizing of iron and manganese. The last pre-mix tank chemical injection includes carbon dioxide to adjust pH to 5.5-6, aluminum sulphate (12 ± 0.5 mg/L) as coagulant and chlorination.

The chlorination step was introduced after the diatom bloom event and was not in-use when the process was on biofiltration mode. Chlorination (at pre-mix tank #3) started with 1.5 mg/L to maintain 0.1- 0.2 mg/L of chlorine on top of the filters [39]. Water then travels to a flocculation step containing four identical trains with each having a three-stage tapered hydraulic flocculation [39]. Each flocculation tank is 5.0 (L)*5.0 (W)*7.8 (D) m with 22 minutes of retention time. The water then travels to seven dual media filters measuring 8.5 by 17.1 m^2

with a height of 3.7 m and dual media containing anthracite (60 cm) on top and sand (30 cm). The sand and anthracite effective sizes are 0.53 and 0.89 mm. The corresponding uniformity coefficients are 1.53 and 1.67 mm, respectively. The plant uses a direct filtration (no sedimentation process) design with an average capacity of 82 ML/day [39]. The schematic of the full-scale setup is represented in Figure 2.
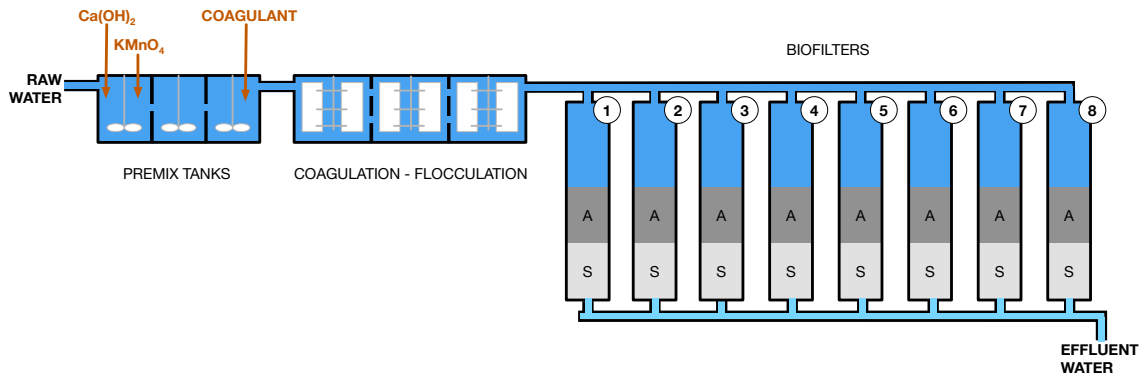
Figure 2   Full-scale drinking water biofilter setup schematic in J. D. Kline Water Treatment Facility.

C.II - 6.2   Source Water Characteristics

The raw water was drawn from the nearby Pockwock Lake, a protected water area. Source water quality in 2016 and 2018 is presented in Table 5.

Table 1   Source water quality average reported by JDK water treatment facility in 2016 and 2018

Year	Alkalinity mg/L as $CaCo_3$	pH	Turbidity [NTU]	TOC [mg/L]	Aluminum mg/L	Manganese mg/L
2016 [40]	<1.0	6.2	0.3	3.0	0.11	0.023
2018 [41]	<5.0	6.5	0.40	3.9	0.10	0.024

C.II - 6.3   Sampling and Analyses

The media filters were sampled using a coring device. Core samples were split at 0-2", 2-6", 6-12", 12-18", 18-24", 24-30", and 30-36" inches resulting in seven cylindrical samples

to represent the whole depth of the filter. 50g and 2g of the sample were used for turbidity and ATP analyses, the rest of the media samples were then transported to the lab and stored at 4°C.

C.II - 6.3.1 _Media Analysis – Floc Retention (turbidity)_

Media turbidity (floc retention profiles) was obtained, as outlined by Booth et al. (Booth, Carlson, & Kawamura, 2006). Media samples were weighed (50 g) and rinsed five times with 100 mL of D.I water and shaken vigorously for 60 seconds. The turbidity of the resultant wash water was taken by a turbidity meter and recorded. Turbidity (NTU/cm^3 of dried media) is normalized by FRT and called turbidity accumulation rate (NTU/cm^3 of dried media/h).

C.II - 6.3.2 _Media Analysis - Metals_

The media samples were dried overnight in a desiccator. 0.5 g of the dried media used for the digestion with nitric acid (purity>99%, sigma-Aldrich, MO, USA) at 95°C based on the EPA method 3050B. Samples were cooled down to room temperature and the supernatants were centrifuged at 3600 rpm for 10 minutes then filtered with a 0.45 μm paper filter (Whatman, GE Healthcare Life Science, Buckinghamshire, UK). Samples were diluted and analyzed by ICP-MS. The metals were reported in μ/L and then converted to $\mu g/cm^3$ of dried media.

C.II - 6.3.3 _Biological Characterization - ATP_

ATP concentration was measured in triplicate on media of each biofilter. Deposit & Surface Analysis ATP kit-DSA test kit (LuminUltra Technologies Ltd., Fredericton, Canada) and Luminometer-PhotonMaster™ (Luminometer, LuminUltra Technologies Ltd., Fredericton, Canada) used to analyze ATP based on the manufacturer instruction. Samples were collected in sterile, 50 mL falcon tubes at different media depths and analyzed. ATP was

reported as per the dry weight of media. The conversion factor was measured by weighing before and after drying the wet media at 105°C for 24h. ATP measurement ($\mu g/cm^3$ of dried media) is normalized by the filter runtime (h) and called the ATP accumulation rate.

C.II - 6.3.4   *Biological Characterization - Microbial Community Characterisation*

Samples were prepared for DNA extraction using DNeasy PowerSoil® (Qiagen, Hilden, Germany) based on the manufacturer's instruction. The extracted samples were then polymerase chain reaction (PCR) amplified applying the high-fidelity Phusion polymerase and "fusion primers" from DNA in duplicate. Amplicon samples were sequenced using Illumina MiSeq, allowing the overlap and stitching of paired amplicon reads into one high-quality, full-length read with primers targeting the V6-V8 region of 16S rRNA [42].

The results were then analyzed using Microbiome Helper Vbox AmpliconV2 (https://github.com/LangilleLab/microbiome_helper.wiki.git)[43]. For the analysis, reads without primers were screened out then the adaptors and primers sequence from high throughput sequencing were removed. This was done using the Cutadapt workflow [44]. Errors and chimeras introduced during the amplicon sequencing were removed using Divisive Amplicon Denoising Algorithm (DADA)2 software package. DADA2 is an improved version of DADA which is a model-based approach for correcting ASVs including the filtering, de-replication, chimera identification, and merging paired-end reads. The results are non-chimeras of the ASVs [45]. Rare ASVs were filtered out and multiple sequence alignment was performed using a Multiple Sequence Alignment Program, MAFFT workflow, to create a de novo multiple-sequence alignment [46]. Rarefaction curves were then generated.

Taxonomy was assigned and taxon tables were generated using Naïve-Bayes approach and SILVA database. Alpha and beta diversity metrics were evaluated using the "diversity

core-metrics-phylogenetic" command. Alpha and beta diversity refer to the diversity within a sample and between the samples, respectively[47]. Alpha diversity indices explored the relative abundance of ASVs, Shannon index, and evenness. Beta diversity was measured by Weighted Unique Fraction metric (UniFrac), Bray-Curtis, and Jaccard distance (APPENDIX A- Figure 40).

Non-negative matrix factorization (NMF) was used to split a dataset of sample taxa abundance into the product of two matrices so that each column of one matrix describes an assemblage of ASVs[48]. The columns of the other matrix contain the weights or proportions of each assemblage corresponding to each sample. In this way, NMF finds a parts-based representation (mixture weights) of the sampled communities. NMF can be supervised by sample class labels [49] and the number of assemblages for each class chosen to best discriminate the separate classes from each other. A sequence of K values in a range from 2 to 10 was used to choose the number of assemblages for each class separately through the cross-validation procedure described in Cai et al. (2017).

C.II - 6.3.5   *Hydraulic Performance Analyses*

Hydraulic performance parameters including head-loss and filter runtime, were measured using inline instruments. The accuracy of the pressure transmitters was reported to be ≤1.0% (including non-linearity, hysteresis, zero point and full-scale error) of an ideal span of 0 to 1 bar. The head-loss data were recorded in the unit of mH_2O. The head-loss accumulation rate was estimated as the deduction of the terminal and clean bed head-loss (mH_2O) divided by the filter runtime (h).

C.II - 7   Results and Discussion

Head-loss is commonly normalized by the filter runtime (FRT) and results in a term called the head-loss accumulation rate [35,38,40,50,51]. ATP and turbidity measured on the filter media was also normalized by FRT to maintain the ability to correlate and compare these parameters. The normalized parameters resulted in two terms called ATP and turbidity accumulation rate.

C.II - 7.1   Why was normalized ATP and turbidity used?

When comparing different indicators in events with varying FRTs, the normalized parameters demonstrate the difference. Figure 3 shows the media turbidity on top in different events and the normalized at the bottom. For example, media turbidity in all filter depth from the diatom bloom event in July 2018 appears to be like the turbidity of April and May 2016. With normalized turbidity (Figure 3-bottom), the difference becomes prominent. These turbidity rates were measured after half the runtime in July 2018 as compared to April and May 2016. The normalized data shows that turbidity on the media was building up at approximately double the rate in July 2018 in comparison to April and May 2016.

The same trend was observed for ATP and ATP accumulation rate. For more detailed information please see the supplemental material.
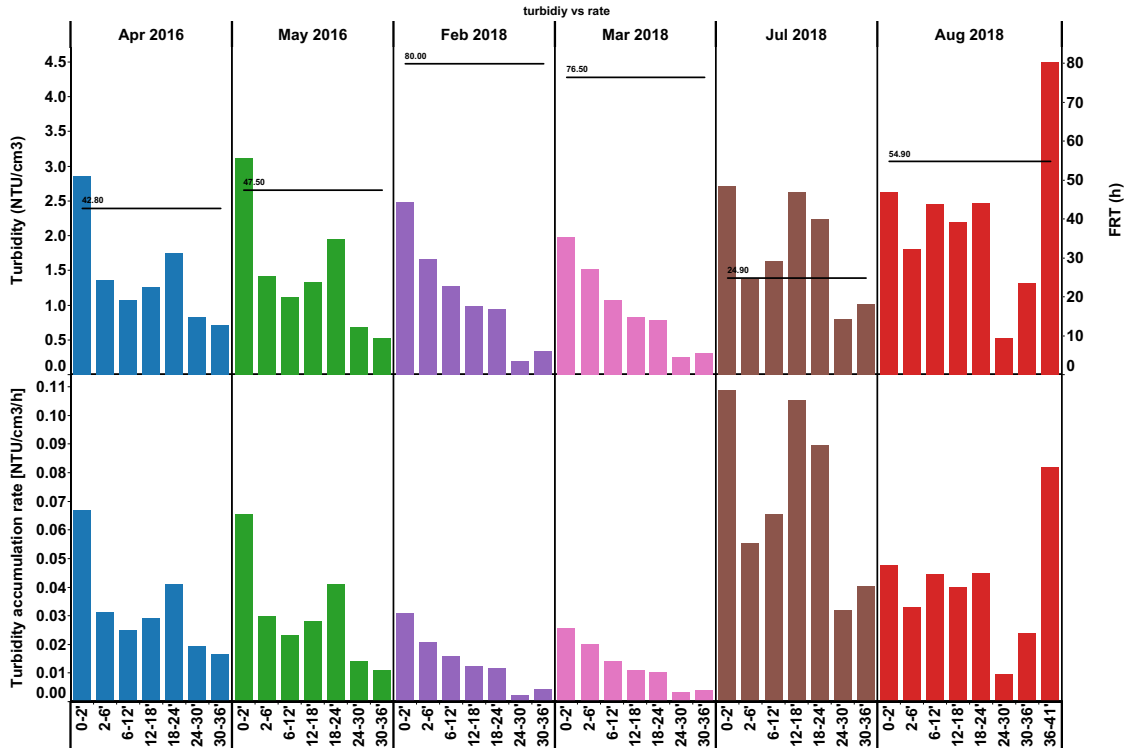
Figure 3   Comparing turbidity and normalized turbidity shows that using turbidity the changes in filter events is not projected in the turbidity while the normalized turbidity can represent the filter challenges. For example, turbidity at top of the filter media in diatom bloom is similar to the Apr and May 2016. This means using the turbidity does not show the real differences between the filter event while comparing the turbidity accumulation rate shows that there is noticeable difference between the July 2018 and other filter events.

C.II - 7.2   How were monitoring indicators changing?

As shown in Figure 4, the top of the biofilter had the highest ATP accumulation rate and turbidity accumulation rate. Both surrogates decreased with increasing empty bed contact time (filter depth). Previous research has also reported this decreasing ATP depth trend [52–54]. Floc retention studies consisting of core sampling of filter depths and analyzing the media turbidity discovered that turbidity decreased with increased filter depths [55,56]. A similar trend was observed in this study. ATP accumulation rate increased with rising seasonal temperatures in both 2016 and 2018. Water temperature at 10°C in 2016 and 18°C in 2018 had the highest amount of ATP accumulation rate at the biofilter top compared to sampling events with lower

water temperature (e.g., 0.4, 2.3, 5.5, and 7.17°C). Declining biomass concentration and bacterial metabolism are associated with low water temperature [30,57–59].

Old media data of Feb 2018 showed media replacement did not largely impact the ATP accumulation rate, head-loss accumulation rate, or turbidity accumulation rate. The lack of impact may be due to the extremely cold-water temperature which causes unnoticeable changes in biological activity (

Figure 4). Both old and fresh media filters had a turbidity accumulation rate of 0.03 [NTU/cm^3/h] at the top of the biofilter. Head-loss accumulation rates for old and fresh media were 0.02 and 0.03 [mH$_2$O/h], respectively.

The diatom bloom event (July 2018) had the highest ATP accumulation rate and turbidity accumulation rate. Tagra 2020, reported that the root cause of high biological activity was due to the enhanced presence of the diatom, *Tabellaria fenestrate*. This specific diatom favours low water turbidity like in Pockwock Lake and has been present throughout the year except for January and February due to very cold-water temperatures. *Tabellaria* has a glue-like wall structure and it sits on the top of biofilters. *Tabellaria* also causes a conglomerate of flocs which become an impermeable surface[39]. This accounts for the increased head-loss accumulation rate and turbidity accumulation rate observed in the July 2018 (diatom bloom) samples. Elevated water temperature and enhanced nutrient levels (nitrogen and phosphorus) are favourable conditions for diatom blooms in a lake. This has caused challenges in water treatment facilities each summer [60].

The lowest ATP accumulation rate in all the filter depths was observed with chlorine addition. This was predicted as chlorine is a biological inhibitor. The ATP level at the top of the biofilter was 0.043 μg/cm^3 dried media. Thus, the chlorinated filter was considered not

biologically active as ATP media did not meet the threshold of 0.1μg/cm^3 [37]. Stoddard et al., (2016) conducted a similar investigation on the biomass media development on a J. D. Kline full-scale biofilter. ATP measurement started after the pre-chlorination process ended. The initial ATP concentration reported was 0.04 μg/cm^3 [61] similar to the chlorination phase ATP values in this study. In the chlorinated filter, the turbidity accumulation rate did not follow the same decreasing trend as other filter events.
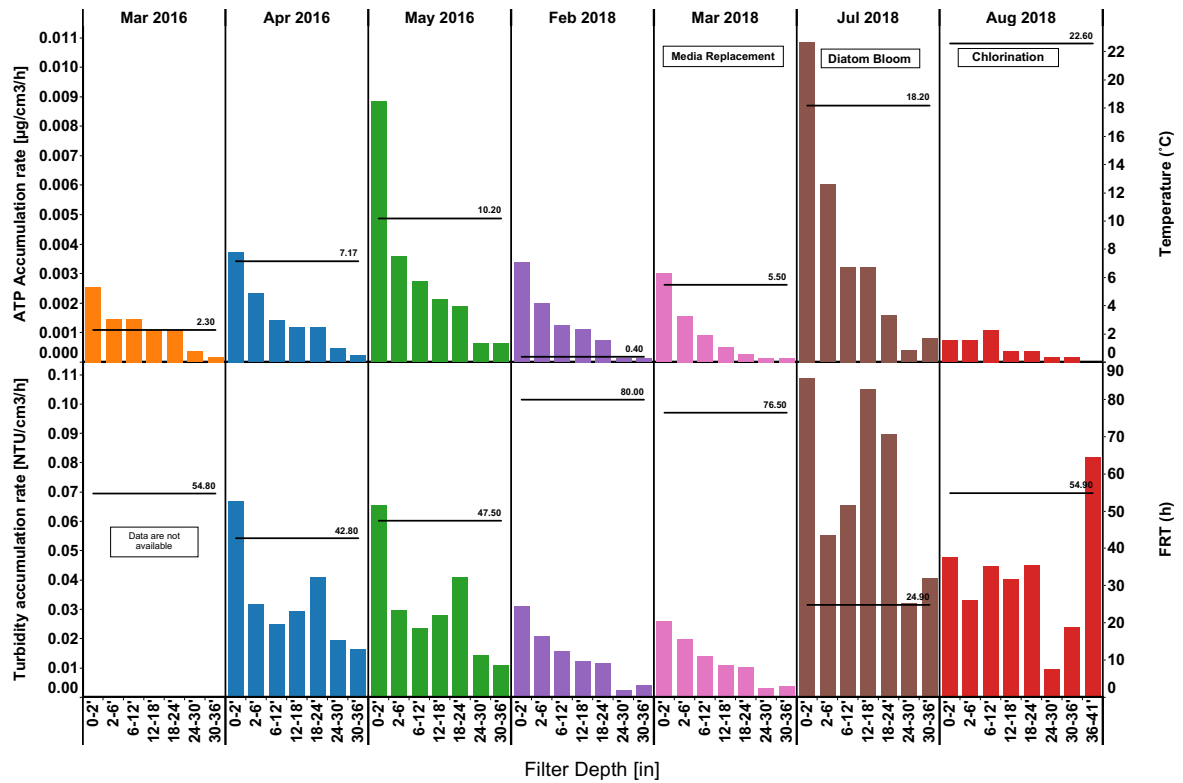
Figure 4   ATP accumulation rate and turbidity accumulation rate in different sampling event in various filter depths. The average raw water temperature in each sampling event is shown (˚C). Filter runtime (h) for each sampling event is illustrated on the rectangular boxes. ATP accumulation rate and turbidity accumulation had the highest value at the top of the biofilters and steadily decreases by the filter depths. The lowest and highest filter runtime occurred in diatom bloom and Feb 2018, respectively. The raw water temperature in Feb-2018 was 0.4 ˚C.

No strong impact of seasonality on FRT or head-loss accumulation rate was observed. The typical filter runtime in the J. D. Kline Water Treatment Plant based on the historical data is reported to be 70±5 hours[39]. The highest FRT (80 h) value was reached on Feb 2018 (water

temperature of 0.4°C). The absence of *Tabellaria* in January and February 2018 in the Pockwock Lake [39] and low biological activity in cold-water temperatures are potential reasons for this. The diatom bloom had the highest head-loss accumulation rate of 0.07 mH$_2$O/h and the lowest FRT of 24.9 hours (Figure 5). As mentioned beforehand, the extreme decline of hydraulic performance was resolved by injecting the chlorine in the biofilter influent. In the chlorinated filter, the Aug 2018 sampling event, the filter head-loss accumulation rate dropped to 0.04 mH$_2$O/h, and FRT increased to 54.9 h.

Based on the operational limit of 80 h for FRT and head-loss of 2.15 mH$_2$O, the head-loss accumulation rate to reach the set limits is approximately 0.03 mH$_2$O/h. As can be seen in Figure 5, when the head-loss accumulation rate was higher than 0.03 mH$_2$O/h, then the facility faced challenging events.
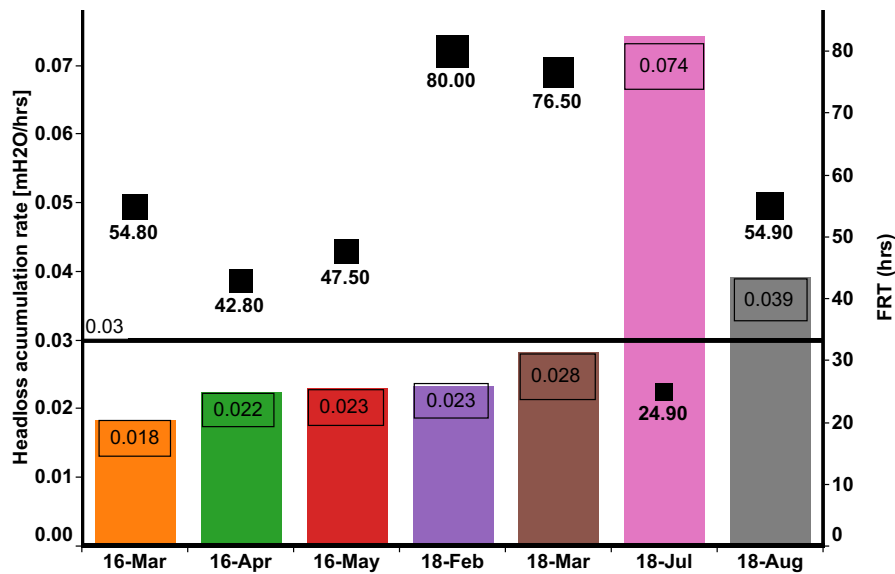
Figure 5   Hydraulic performance parameters including head-loss accumulation rate (first Y-axis) and FRT (second Y-axis) are presented in different sampling events in different colors. Dark square symbols represent FRT in each sampling event. The highest head-loss accumulation rate belongs to the diatom bloom event, July 2018. Chlorination decreased the head-loss accumulatio rate and FRT increased more than twice.

Deposited metals on the filter media such as aluminum, calcium, and manganese versus the filter depth are depicted in Figure 6. Aluminum and calcium are highest and lowest concentrations respectively, on the filter media in all sampling events. Aluminum was added to the influent water as an alum coagulant and manganese as potassium permanganate ($KMnO_4$) to oxidize Mn and Fe in the source water. The metals concentration did not decrease intensely with increasing filter depth and no recognizable pattern were observed in different sampling event. Booth et al. (2006) compared filters in different water utilities with various water treatment processes and alum coagulant doses. In said study, sites with higher alum and permanganate doses had higher deposited media concentrations while metal concentration profile varied depending on the source water quality[62]. No previous studies have addressed the temporal dynamic of metal profiles. This study found no noticeable pattern between water temperature changes and deposited metal concentrations.

Deposited metal concentrations were generally lower in fresh media samples (March 2018) compared to the old media (Feb 2018). Aluminum concentrations in old and fresh media were 9,197 and 1,162 $\mu g/cm^3$, respectively. Mn decreased from 1,732 $\mu g/cm^3$ in old media to 66 in fresh media. The higher metal concentrations in old media demonstrates that backwashing does not entirely remove the metals settled in the filter bed which build up in the filter over time. The operational parameters (e.g. head-loss and turbidity accumulation rate) were not distinctly different, but the deposited metals were lower in fresh media. No statistical conclusion can be made due to the sample size. Thus, deposited metals are not the significant contributor to filter head-loss buildup.

Metals concentrations were higher in the chlorinated filter (Aug 2018) contrasted to the diatom event (July 2018). This could be due to a higher runtime in Aug 2018 that was more than twice in July-2018 filter event. In addition, it is reported that Mn reacts with free chlorine,

and MnOx coats the filter media. Consequently, the autocatalytic metal removal mechanism by the MnOx increases the metals concentration on the filter media [63,64].

Previous studies about biofilter metal profiles during diatom blooms are non-existent. In this study, it was found that the filter runtime profoundly impacted metal concentrations on the media. A correlation between the deposited aluminum at the top of biofilter and filter runtime was found for old media samples (P-Value=0.009- R-squared= 0.99). However, more data are needed to validate the correlation analysis. For further details, see Figure 39 in APPENDIX-A.
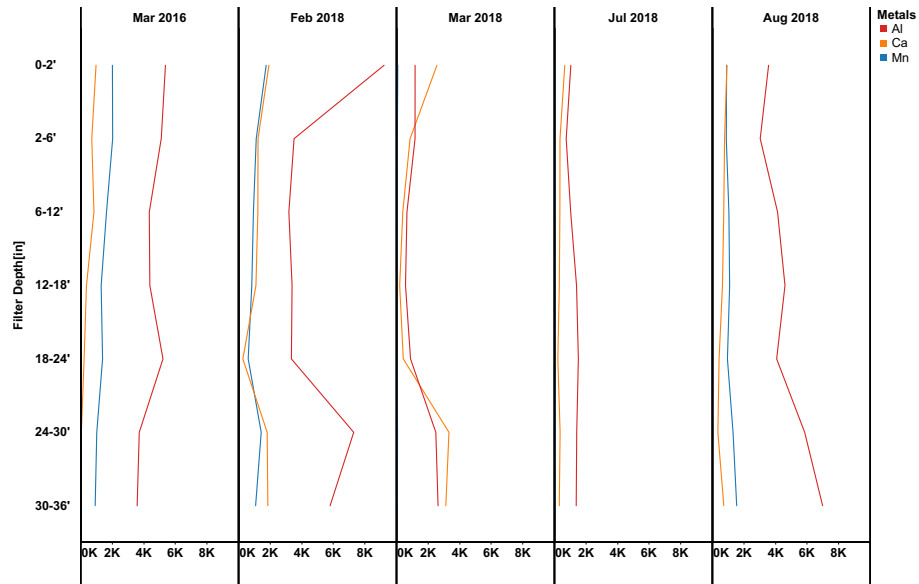
Figure 6   Aluminum, calcium, and mangenese concentration distribution in varying filter depths and different sampling events are graphed. Aluminum had the highest while calcium had the lowest concentration in each sampling event.

C.II - 7.3   How does the microbiome change?

Microbial community analysis has two types of different diversity indices, alpha and beta. Alpha represents the diversity within each sample, while beta explores diversity between samples [65,66]. In this study, alpha diversity was quantified by the number of ASVs, Evenness,

Shannon indices, and relative abundance. Beta diversity was quantified by Bray-Curtis, and Weighted UniFrac.

The data from each biofilter was compositional consisting of overlapping species mixtures. A statistical method called non-negative matrix factorization (NMF) was used to extract four assemblages of taxa as proxies for microbial subcommunities in the filters. The mixture of assemblages as a subcommunity structure and their predominant species helped identify biomarkers for both the baseline filter community and challenging filter events.

C.II - 7.3.1   *Alpha Diversity*

Figure 7 shows the changes in alpha diversity indices (e.g., ASVs, Evenness, and Shannon) with filter depths. Some data for various depths were missing due to the PCR failures.

Biofilter evenness and ASV count richness were relatively high as shown in Figure 7. Both were not impacted by seasonal (temperature) changes and did not significantly differ in different sampling events (Kruskal-Wallis, P-Value=0.4). Dimas, 2016 reported the high richness of the filter media microbiome. He stated that the seasonal fluctuation impacted the microbial community diversity with lower diversity observed in summer[59]. ASVs change had no recognizable patterns with filter depth. Shannon (and evenness) indices changes in different filter depths was insignificant (Kruskal-Wallis, Evenness P-value =0.2, Shannon, P-value=0.7). The results suggest that a filter at steady state would not have alpha diversity variation throughout its depths.

The fresh media microbiome had higher ASVs richness and Shannon index than the old media. The Shannon index increases as both the richness and the evenness of the community increase and higher Shannon indices translate to greater diversity. Thus, fresh media

microbiome had greater overall diversity. The diversity decreased in the aged media microbiome could be due to multiple factors. Selection occurs due to a multitude of factors and could explain the diversity difference between fresh and old filter media's microbiome. Some species that do not stick to the media may have been washed off by backwashing streams[18]. Other bacteria cannot tolerate the oligotrophic biofilter environment.

The PCR process failed for the first three top layers' samples in the diatom bloom event (July 2018) and chlorination phase (Aug 2018). This may be accounted for the diatom presence as some of their related compounds interfere with PCR[67]. As expected, chlorine addition decreased the number of bacteria in the first three top layers, thus no results were extractable. There were not ASV data for all the depths in each sampling event. Therefore, total ASV in each sampling event was divided by the number of depths and the term ASVs/depths was used.
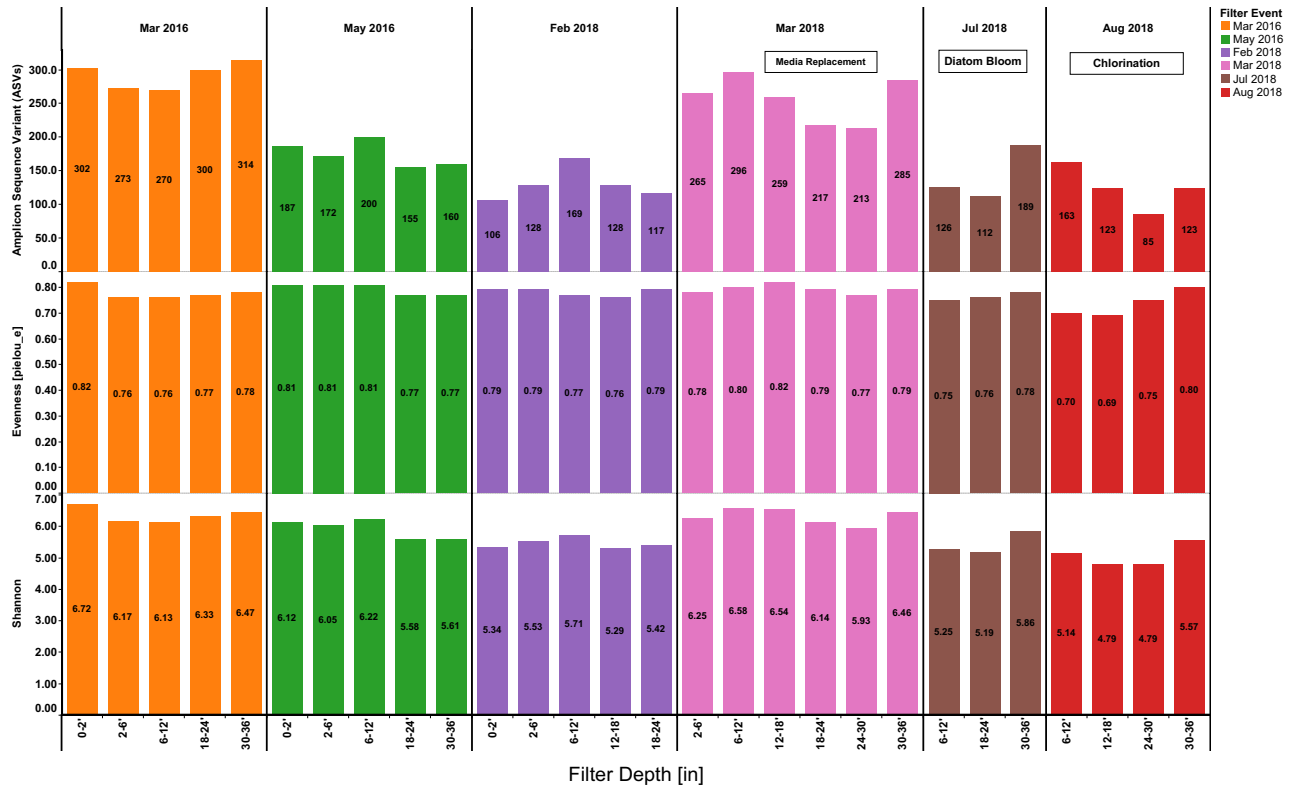
Figure 7   Alpha diversity indices including ASVs, Evenness and Shannon are presented. Shannon and Evenness indices were not different at various filter depths. Thus, a filter at steady state will not have alpha diversity variation throughout its depths. The filter media replacement event increased Shannon and ASVs. This was attributed to microbiome's vulnerability towards environmental challenges.

Media replacement significantly enhanced the ASVs/depth (Table 2) as old media had 129 while fresh media had 255 ASVs/depth (Kruskal-Wallis, P-value= 0.004). Chlorination did not decrease ASV/depths as July and Aug 2018 had 142 and 141, respectively. As filter runtime in July 2018 (Diatom bloom event) was very short (24.9h), there was not as much time for bacterial species to grow and potentially lead to the low ASV count. The DNA extraction method is not sensitive to active/de-active bacteria. Thus, it may have still included already dead bacteria in Aug 2018. Therefore, though the bacteria were not considered to be active anymore due to their lower ATP levels, the ASVs were not significantly different (Kruskal-Wallis, P-value= 0.45).

Table 2   ASV / depth in different sampling event with the corresponding raw water temperature

DATE	Raw water temperature (˚C)	ASV/depth
Feb 2018	0.4	129.6
Mar 2016	2.3	291.8
Mar 2018	5.5	255.83
Apr 2016	7.17	186.5
May 2016	10.2	174.8
Jul 2018	18.2	142.33
Aug 2018	22.6	141

C.II - 7.3.2   *Beta Diversity*

Bray-Curtis and Weighted UniFrac distances were chosen for the microbial community principal coordinate analysis as they covered most of the differences between the data. Bray-Curtis is insensitive to phylogenetic relationships of the microbial community, while Weighted UniFrac considers taxonomy [68,69]. Figure 8 shows the principal coordinate analysis of

microbiome of the baseline and challenging events. The microbial community structure of the fresh media (March-18) was distinct in both Bray-Curtis and Weighted UniFrac PCoA analysis. Fresh media (shown in yellow circle) was illustrated along Axis 1, which covers 43.29% variation in Bray-Curtis distance analysis and 46.8% in Weighted UniFrac. The effluent water quality microbiome is representative of the biofilter microbiota[70] and in a study by Chan et al., (2018) effluent water microbial communities of slow sand filters for new and old media were investigated and proven to be distinct [71]. Their results align with the finding in the current study.
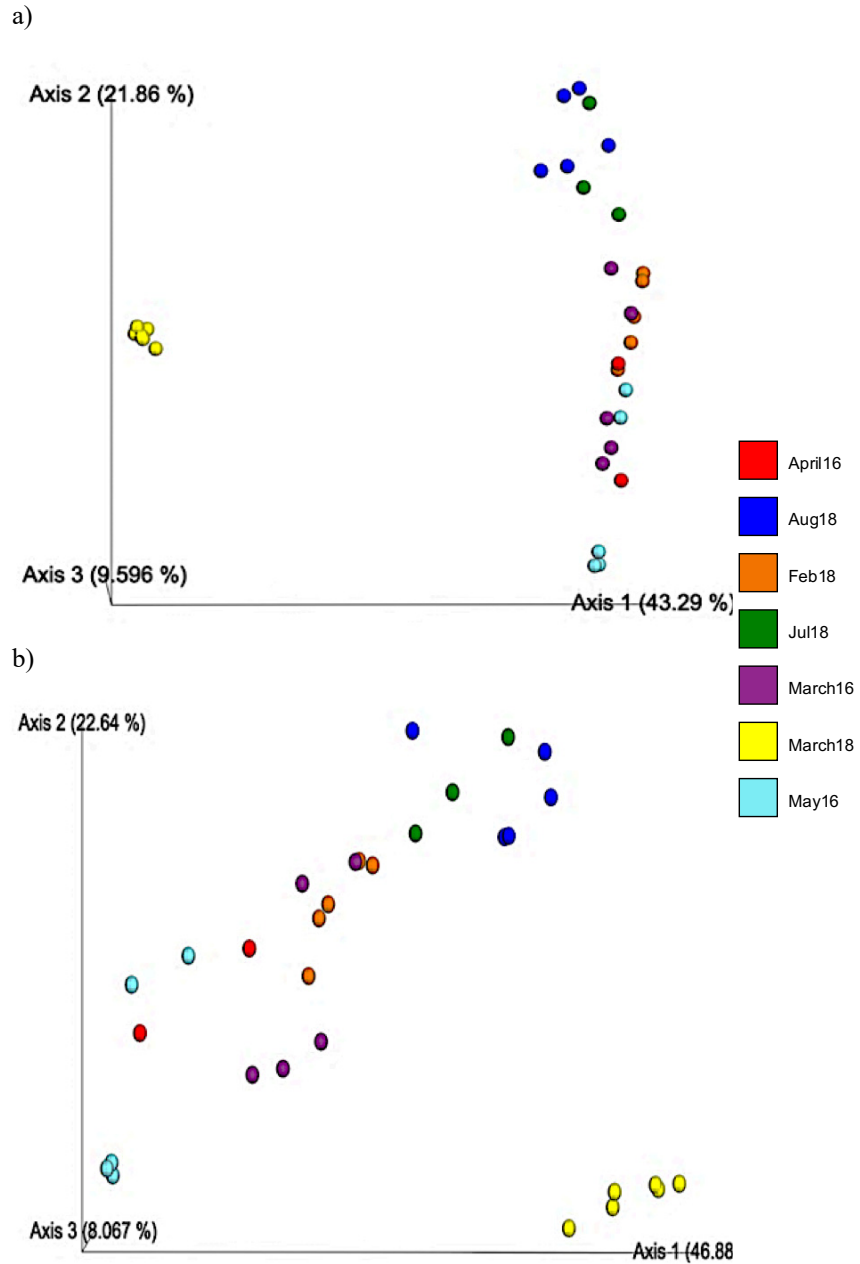
Figure 8   Principal coordinate analysis of drinking water microbiome for the baseline and challenging events are shown with A) Bray-Curtis PCoA, and b) Weighted UniFrac. Both analyses showed that media replacement had a major impact on the microbiome community structure. The diatom bloom and chlorination events did not demonstrate as much difference.

The remaining microbial communities, including the diatom bloom and chlorinated filter, were mostly spread along the Axis 2 in a continuum. Scree plot details are included in

the supplemental material. Bruno e., al., 2018, reported that chlorination does not alter the microbial community structure diversity [72], which supports results observed in this study.

Figure 9 illustrates the PCoA analysis of the filter media microbiome changes in two years, 2016 and 2018.

a)   b)
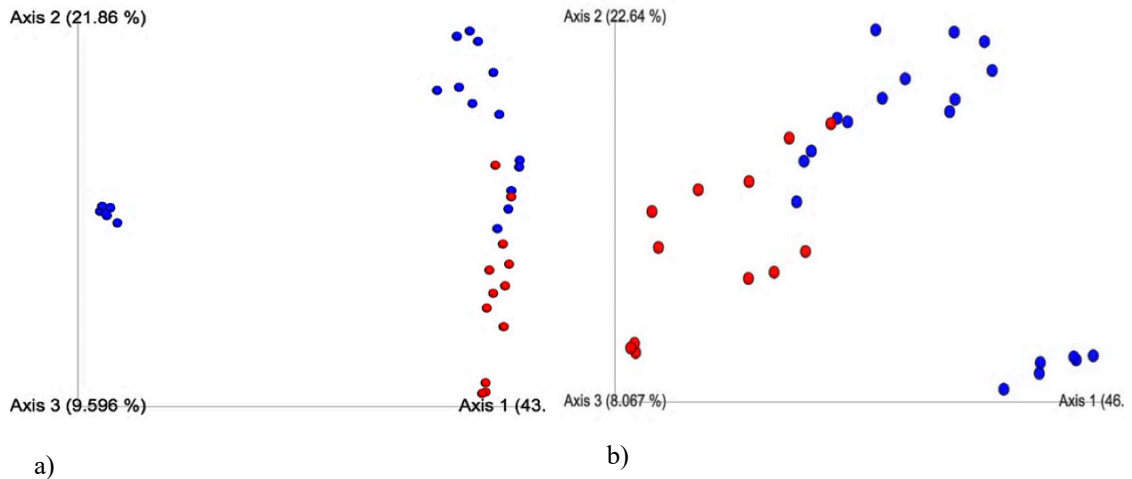
Figure 9   Temporal impact on the microbial community was studied by a) Bray-Curtis and b) Weighted UniFrac PCoA. The red and blue circles represent the microbiome samples form 2016 and 2018.
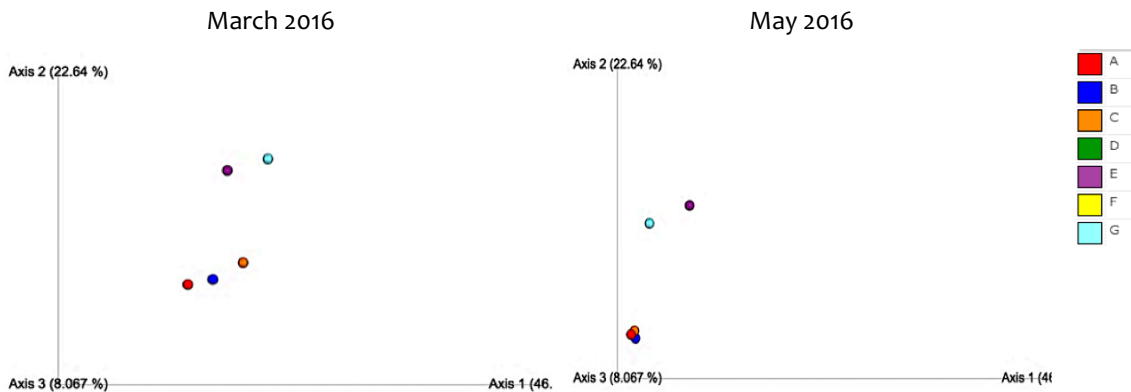
Figure 10   Weighted UniFrac PCoA depicted the dissimilarity between different biofilter depths with different layers are represented in varying color. 0-2" (A) red, 2-6" (B) dark blue, 6-12" (C) orange, 12-18" (D) green, 18-24" (E) purple, 24-30" (F) yellow, 30-36" (G) light blue. The top three layers are closer and consequently have a more similar microbiome structure.

The microbiome of the filter gradually changes from 2016 to 2018 due to the water quality changes, pH and temporal dynamic of the source water microbiota. The temporal

changes in the microbial communities in drinking water distribution system has previously been investigated. There is a consensus in literature that microbial community structure in drinking water distribution system (DWDS) changes with time both in bulk water and biofilm[73–75]. No studies were found for the temporal impact on microbial communities in drinking water biofilters.

The sampling event of March and May 2016 and Feb 2018 had similar PCoA results for microbiome analysis on filter depths. Therefore, only March and May 2016 PCoA are depicted to demonstrate the microbiome changes in different filter depths. As shown in Figure 10, the three top layers A, B and C (0-2" (A), 2-6" (B) and 6-12" (C), respectively) were closer to each other, which exhibited the similarity in microbiota in top three layers of filter media. As can be seen there is a distinct distance between the top layers and bottom layers (18-24" (E) and 30-36" (G)) microbiome. Moll et al. (1998) previously showed that microbial community varies as a function of filter depth [76]. The microbiome analysis of the filter depth in this study found a similar phenomenon.

Beta diversity analysis revealed that temporal variations (data not shown), filter depth (empty bed contact time), diatom bloom and chlorination had a lesser impact on microbial community variation than media replacement.

C.II - 7.3.3   *Bacterial Community Composition*

At phylum level the most common phyla in all the filter events are Proteobacteria, Bacteroidetes, Actinobacter, and Acidobacteria. Verrucomicrobia phyla exists in all the filter events except in the fresh media microbiome. Additional details are in the supplemental material. The core microbiome at phyla level for drinking water is reported to contain

predominantly Alpha- and Beta-proteobacteria, and smaller portions contain Gamma-proteobacteria, Nitrospirae, Planctomycetes, Acidobacteria, Bacteroidetes and Chloroflexi [77].

Studying the biofilter microbiome at high taxonomic level such as phyla, does not capture the differences and characteristics of varying sampling events or even the major challenges (see APPENDIX-A, Figure 43). Hence, lower taxa levels, order and family, were used to analyze the microbiome composition.

Figure 11 shows the relative abundance of bacteria at the family taxonomy level in March, April and May 2016 accounting for baseline events. The six most abundant and common bacterial families were defined as baseline microbiomes. Baseline microbiome includes *Sphingomonadaceae*, *Chintophagaceae*, *Burkholderiaceae*, *SAR11clade III*, *Sporichthyaceae*, and *Acetobacteraceae*. These families consistently made up the majority of the microbiome.

The presence of *Sphingomonadaceae* [10,78], *Burkholderiaceae* [10,79], *SAR 11* [80] and *Acetobacteraceae* [10,81,82] were previously reported in drinking water biofilter. Zhang and Liu, 2019, found the most abundant families to be *Burkholderiaceae*, *Methylophilaceae*, *Comamonadaceae*, and *Rhodocyclaceae* for the Beta-proteobacteria phyla and *Sphingomonadaceae*, *Caulobacteraceae*, and *Methylobacteriaceae* for the Alpha-proteobacteria phyla [77].

Despite the findings in this study, *Bradyrhizobium* and *Nitrospira* have previously been listed as the dominant genus in GAC and sand filters, respectively [83]. Source water, coagulant type, chemical additives and backwashing techniques shapes the microbial community structure in the water treatment systems [72]. A recent study showed that using lime and soda for softening process (reducing water hardness) impacted the water microbiome diversity drastically [84]. Ozonation, a process to breakdown NOMs to low molecular weight compounds, is reported to reduce cell numbers and microbiome diversity [85].
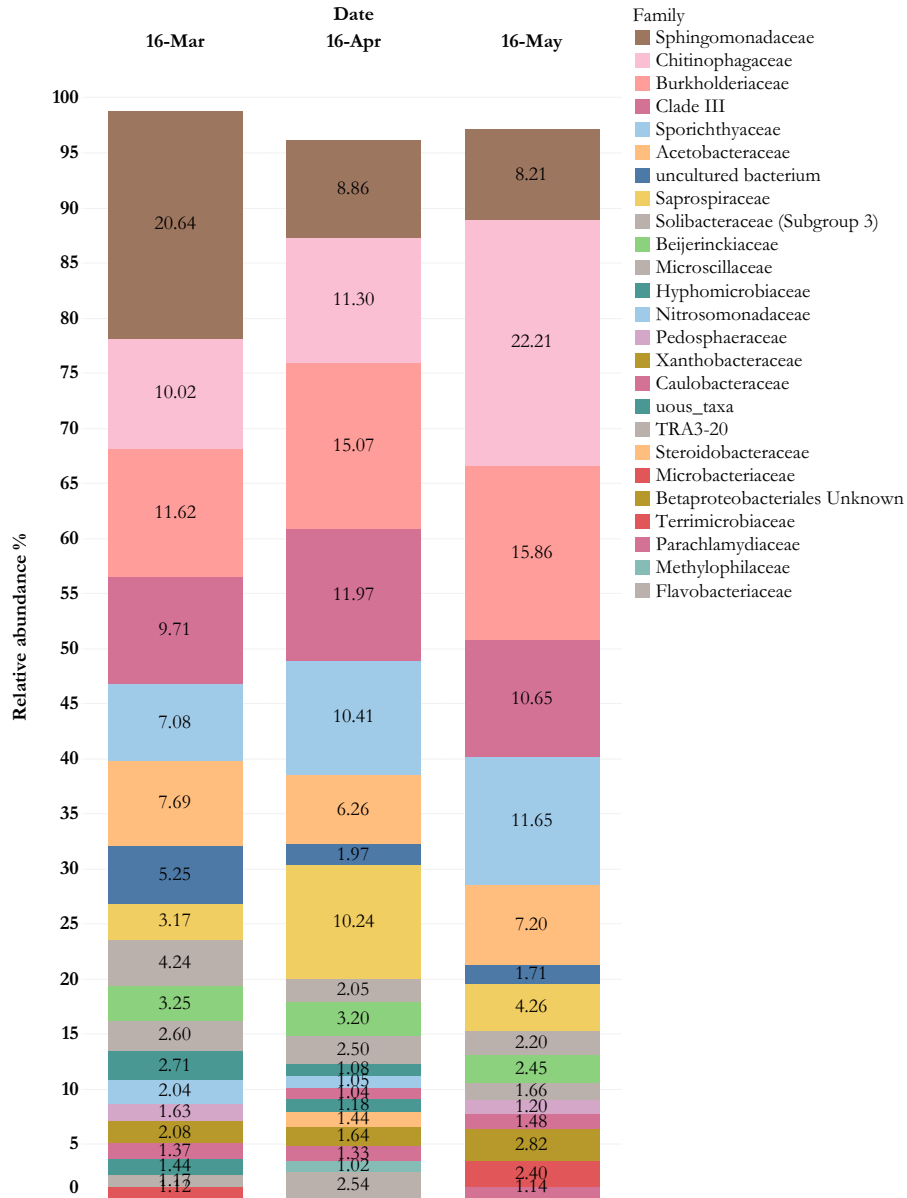
Figure 11   Relative abundance of sampling events in 2016, March, April, and May. Families with less than 1% relative abundance are removed from the bar graph.

The March 2016 filter had the highest proportion of *Sphingomonadaceae*, a type of Bacteroidetes. This family is well known in aquatic environments, activated sludge and Atlantic coastal soils [86]. *Sphingomonadaceae* have both positive and negative characteristics as some species of this family are known to degrade complex aromatics such as hexachlorocyclohexane but also have been identified as EPS producers and linked to the formation of aggregates in

activated sludge [87]. *SAR11clade III* categorizes as Pelagibacterales (order level) and belongs to the class of Alphaproteobacteria [88,89]. Pelagibacterales is found to be a ubiquitous planktonic oligotroph. *Sporichthyaceae* is a common soil bacterium under Frankiales, and Actinobacteria class [90]. It is also been reported to be found as bacterio-plankton in freshwater lakes[89]. *Acetobacteraceae* is an Alphaproteobacteria that includes acetic acid producers bacteria [91]. This family has been previously found in drinking water biofilters [10,92].

The April 2016 filter microbiome is dominated by *Burkholderiaceae*, followed by *Chitinophagaceae*, and *Saprospiraceae* which is within *Sphingobacteriales*, Bacteroidetes. These species are involved in the breakdown and utilization of complex organic carbons; and hence, are common in wastewater sludge[93,94]. *Chitinophagaceae* has been previously reported as the most common Bacteroidetes in drinking water distribution system. It is associated with free living amoebas in purified water[95] and the ability to survive in the contaminated reagent in DNA extraction kit demonstrating their ability to survive in oligotrophic drinking water microbiota [96]. *Chitinophagaceae* is considered to be one of the core families in the activated sludge [97] and also related to high EPS and lipopolysaccharides (LPS) production [98]. *Saprospiraceae* is a filamented bacteria and has the capability of protein hydrolysis specifically complex organic carbons degradation [94]. In one study, an uncultured *Saprospiraceae* was primarily responsible for nitrifying, and phosphorus removal [99].

The May 2016 filter favored *Chintophagaceae* and *Burkholderiaceae* and *Clade III*. The changes in relative abundance could be due to the temperature differences between March (2.3 °C) to May (10.2 °C) [83]. *Burkholderiaceae* are known for degrading dissolved organic matters[79]. This family is very versatile, and the genera found were adaptable to different environment[100]. One species of this family reported to be adaptable to high heavy metals

concentrations [93]. *Burkholderiaceae* family also includes a pathogen species (*Burkholderia pseudomallei*) that are chlorine resistant and is found in northern Australia and south Asia [101].

The old media filter, February 2018, had a similar microbiota with slightly different proportions to the baseline filter microbial compositions. The old media's microbiome was dominated by Clad III (Pelagibacterales) and two complex organic degraders, *Sphingomonadaceae* and *Saprospiraceae* (Figure 12). Freshwater Pelagibacterales tend to dominate with higher inorganic nutrient concentrations [88]. The old media may have been adapted to the biofilter microbiome, while fresh media had a noticeably different microbial structure. This adaptation has been observed in slow-sand filters in other researches [102,103].
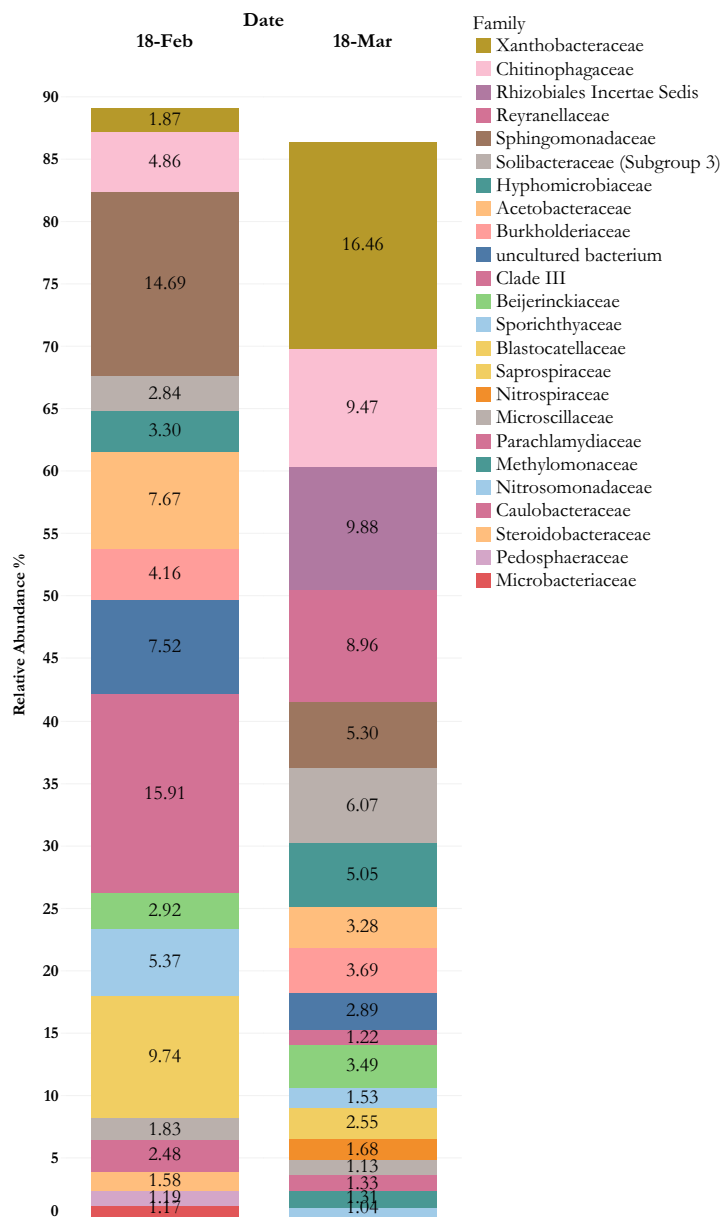
Figure 12   Relative abundance of microbiome sampling event for media replacement. Feb 2018 represents old media and March 2018 represent a fresh media microbiome. Families with less than 1% relative abundance are removed from the bar graph.

The fresh filter media in March 2018 had a vastly different microbiome profile (Figure 12). *Rhizobiales* composed 35% of the total bacterial order (data not shown). *Xanthobacteraceae*, the most abundant family in fresh media, is a family of *Rhizobiales* which includes nitrogen fixers that are symbiotic with plants and make up the most abundant taxa found in fresh media microbiota [104]. *Uncharacterized Rhizobiales (Incertae sedis)* make up the second-highest abundant

bacteria, followed by *Chitinophageceae*. *Reyranellaceae*, the 4th abundant family, is an alphaproteobacterium that seems to be found in water systems [105]. *Hyphomicrobiaceae* had a relative abundance of 5 % in fresh media. This is an oligocarbophilic alphaproteobacterium, which may explain the decrease in relative abundance between the old media (3.3 %) and new [106]. In slow sand biofilters, the microbiome at start-up tends to resemble the source water microbiota while older biofilters have a more distinct microbiota [71]. Biofilters may potentially follow a similar pattern. Factors such as lower nutrient level, aeration, high shear rate of backwashing, and an establishment of an existing biofilm exert selective influences over time, and thus the filter microbiome differs from its seeding source. More research is needed to understand the relationship between the full-scale biofilter microbiome and Pockwock Lake water microbial community as source water.

Uncultured bacteria, *Acetobacteraceae*, *Sphingomonadaceae* and *Xanthobacteraceae* make up a large proportion of July 2018's, diatom bloom, microbiome. Diatom and bacteria have 200 million years of coevolution together, thus also a plethora of different interactions[107]. The phycosphere is a mucus microscale region surrounding a diatom and creates a unique minuscule microbiome as it contains high organic matter and nutrients excreted by said cell. Bacteria inhabit the phycosphere to feed on the nutrients. Bacteria-diatom interactions can be synergistic, mutual, parasitic, or competitive. Mutual interactions can be bacteria producing vitamins and parasitic examples are in the case of algicidal toxins produced by bacteria or competitive cases such as limiting essential nutrients [107,108]. Diatoms have a considerable influence on bacterial diversity, and each species often has distinct associated bacterial phylotypes [109].

Most studies of *Tabellaria fenestrate*, the predominant diatom in the diatom bloom event, are about two decades old, and thus the critical bacterium associated with it has not been

identified. Hence, most bacteria specific to *Tabellaria fenestrate* are uncultured. This may explain the large number of uncultured bacteria from the July 2018 filter microbiome. Likewise, plant growth-promoting bacteria such as Rhizobiales are associated with green algae, a precursor to diatom events [110]. This could also be behind a large proportion of Rhizobiale families found with the diatom event. Lastly, some of the species in *Solibacteraceae* family have an abnormally large genome and diverse metabolic profile[111]. Therefore, it may have been able to adapt to become more competitive in the diatom event.

After chlorination, the filter microbiome showed a unique profile. Chlorination is observed to cause the microbiome to shift down a few layers [112]. Hence the microbial diversity remained the same. *Sphingomonadaceae*, *Acetobacteraceae*, and *Xanthobacteraceae*, and uncultured make the top relative abundance of four bacteria (Figure 13). The absolute and relative abundance of *Sphingomonadaceae* increased, indicated that the population might have grown. Various studies in drinking water systems and dentistry have shown that *Sphingomonadaceae* is relatively chlorine resistant due to its oligotrophic nature and biofilm production [87,113]. This family has also been observed to degrade complex chlorinated substances [114]. *Acetobacteraceae* has had chlorine tolerance in previous studies in drinking water distribution systems, [115] which supports the consistent absolute abundance and increase in relative abundance observed in the chlorinated filter.
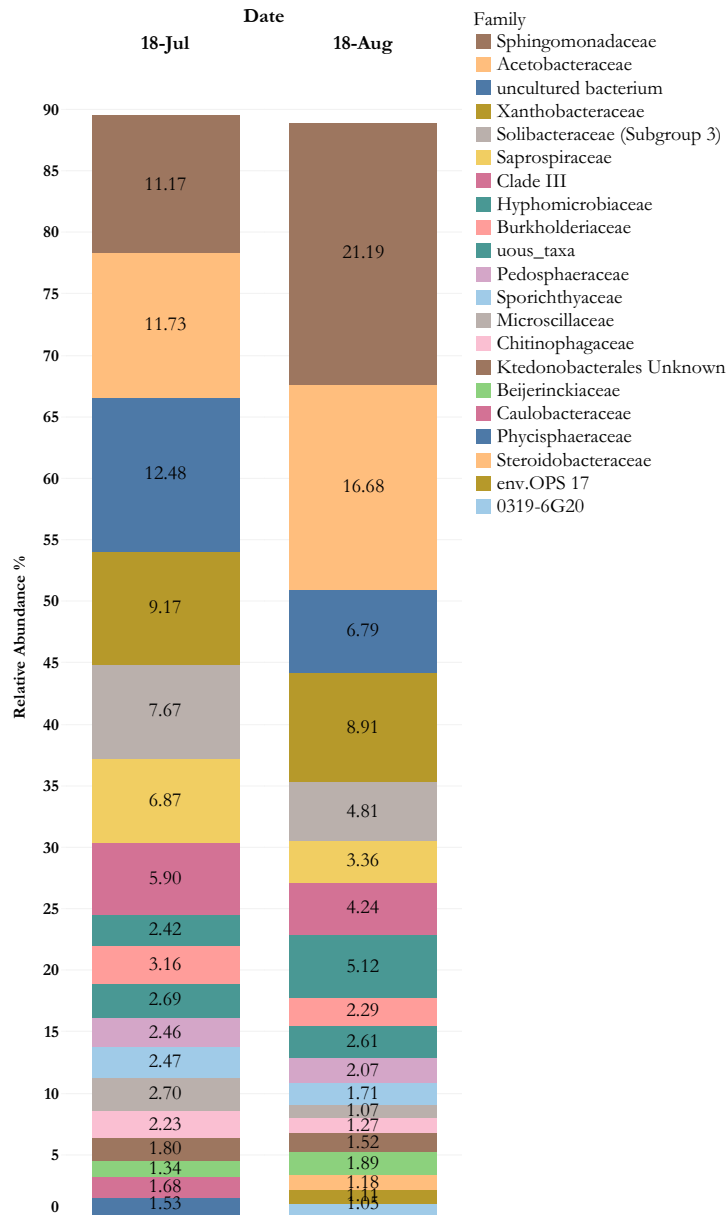
Figure 13   Relative abundance of bacterial families in the diatom bloom (July 2018) and chlorinated filter (Aug. 2018). Families with less than 1% relative abundance are removed from the bar graph.

The lack of diatoms in Aug 2018 samples might have been responsible for the similar absolute abundance of bacteria in July 2018. This could be due to the fact that the stated family was either a competitor or prey for said diatoms [69]. The abundance of uncultured bacteria mostly dropped, indicating that it either was sensitive to chlorine or linked to diatoms. Further research is needed for a more particular answer.

C.II - 7.4   Statistical Modelling

With the statistical method, NMF, the large microbiome dataset was divided into four subcommunities/assemblages, NMFA1-4. Each sample was as a combination of subcommunities/assemblages as depicted in Figure 13. Each ASVs' weight in the corresponding subcommunities/assemblage are presented in Figure 14. The mixture proportion of each ASV was different in subcommunities.

March 2018 microbiome, fresh media microbial community, contained just the NMFA3 which was not present in any other sampling event. As shown the fresh media microbiota was thoroughly different than other's samples. This confirmed the results evaluated from Bray-Curtis and Weighted UniFrac PCoA for fresh media microbiota. The ASVs' weights in NMFA3 assemblage were more spread out compared to the other subcommunities (Figure 15). Four dominant marker species in NMFA3 (fresh media microbiome) consisted of 1) *Chitinophagaceae*, and 2) *Rhizobiales*, 3) *Xanthobacteraceae*, and 4) *Rhizobiales. Incertae. Sedis* which aligns with the relative abundance results mentioned earlier.

NMFA1 dominated the microbiome in the diatom bloom event and the chlorinated filter. *Acetobacteraceae* followed by *Saprospiraceae* has the highest weight and could be considered as the biomarker for the diatom bloom.

Samples from April and May 2016 are dominated by the NMFA2 containing *Burkholderiaceae*, *CladIII*, and *Sporichthyaceae*, and *Chitinophagaceae*. Microbiome from April and May 2016 exemplified the regular operation or baseline microbiome. Hence, the mentioned species may be representative biomarkers for baseline microbiota biofilters.

No difference in assemblages was observed in different depth of biofilter for fresh media. Top three layers seemed to be very similar in the mixing portion of the assemblages which aligns with the finding of beta diversity analysis.
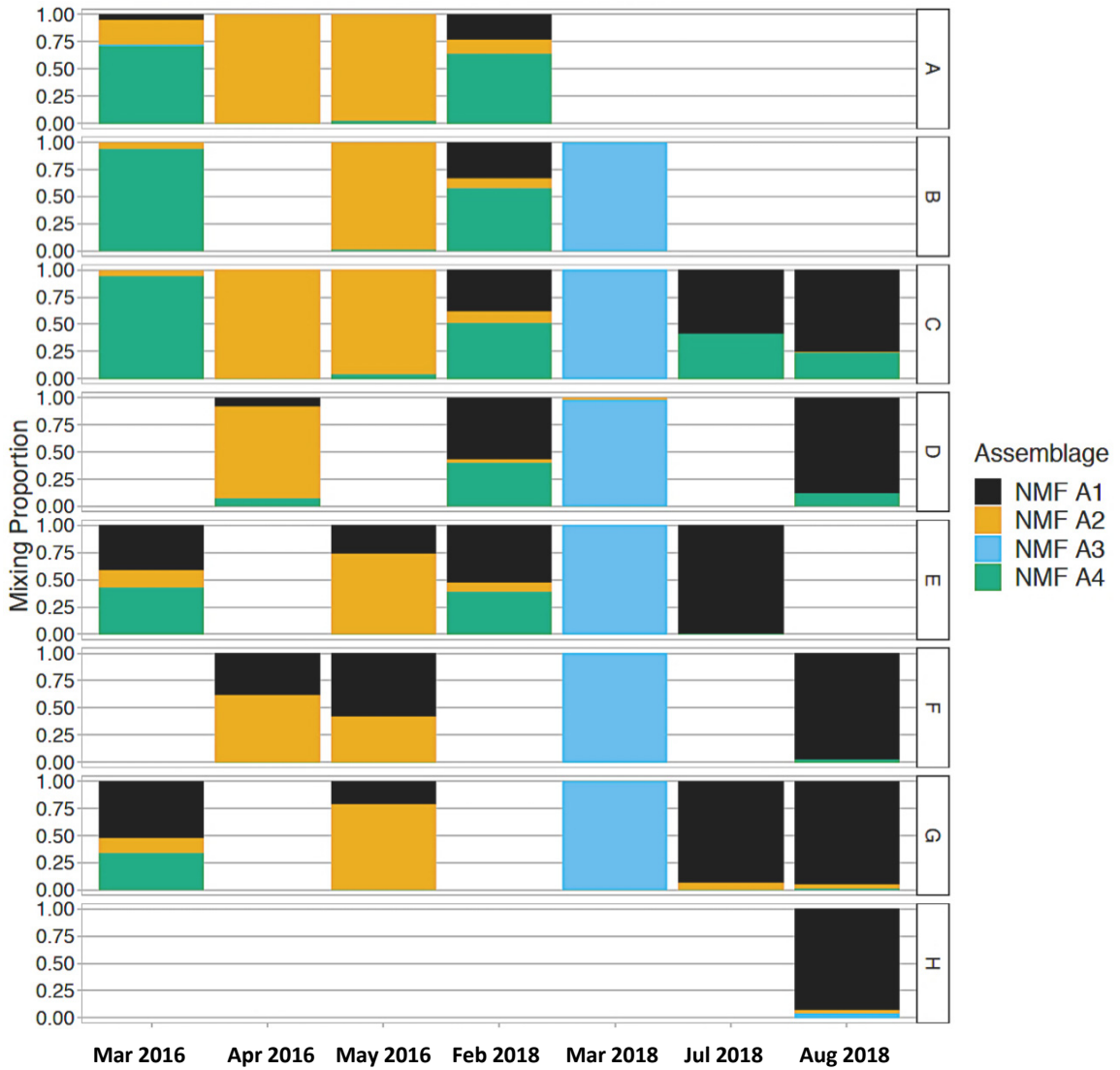
Figure 14   Sampling events as a combination of subcommunities/assemblages in different depth. A-H represent different depth of the filter. Fresh media community contained only the NMF A3 which was not presented in any other sampling event showing that the microbial community of fresh media was distinctly different than other biofilter sampling events.
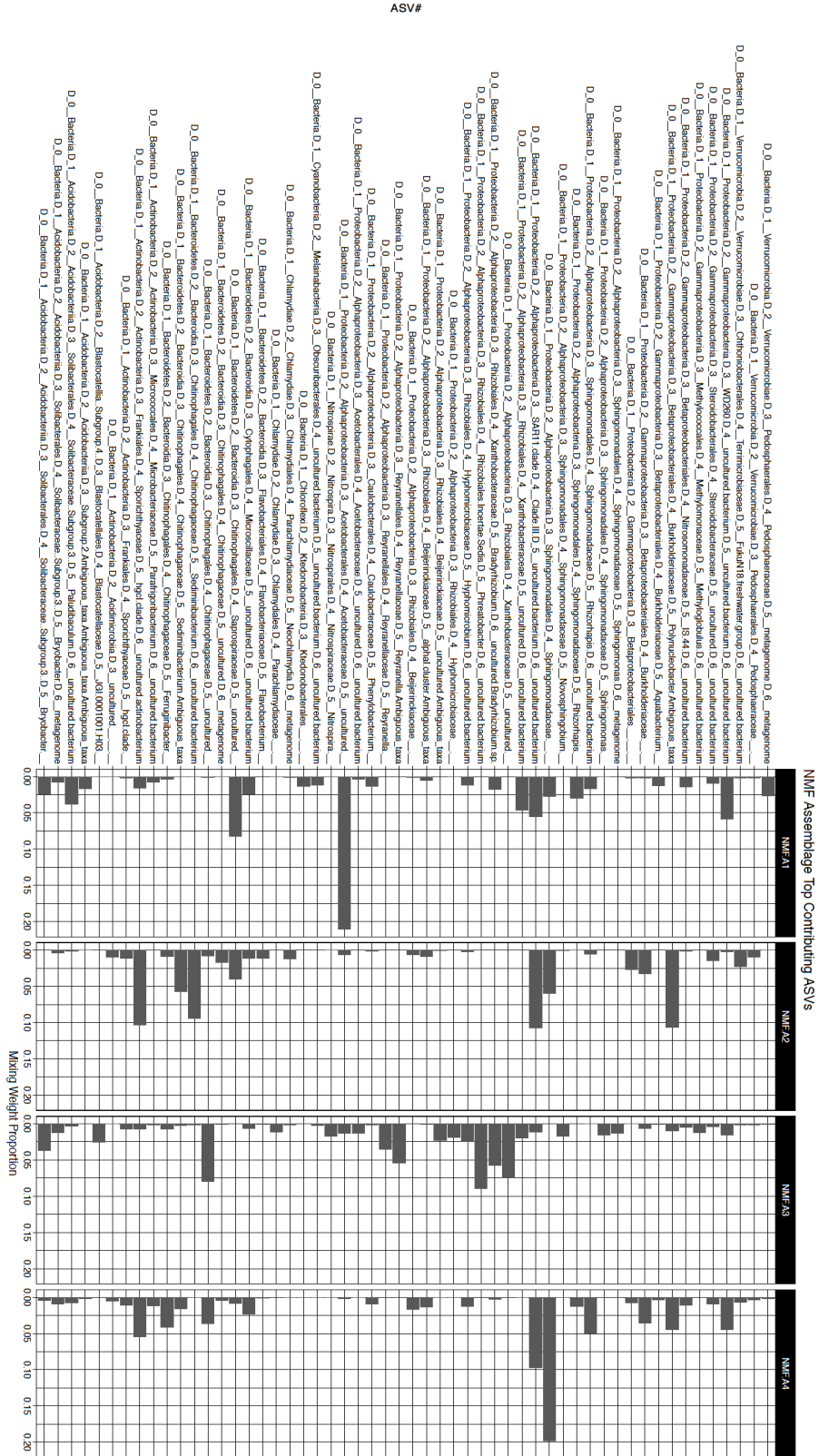
Figure 15   NMF divided the microbiome community into 4 subcommunities/assemblages. The weight proportion is assigned for the each ASVs in different subcommunities

C.II - 7.5 How do they correlate to each other?

The correlations between various biological monitoring indicators such as ATP accumulation rate, and microbiome diversity indices (ASV, Shannon and Evenness), and conventional monitoring surrogates (e.g., head-loss accumulation rate, turbidity accumulation rate and FRT) were investigated.

FRT was correlated against the previously listed factors. No significant correlation was observed for FRT with the head-loss accumulation rate and ATP accumulation rate. Nor were any significant correlated factors detected for FRT and microbiome diversity indices.

A strong correlation between FRT and turbidity accumulation rate (at the top of biofilter media) was detected. The equation is presented in Figure 16 with R-squared of 0.95 and P-value of 0.004). It can be concluded that the established method of measuring media turbidity from top of biofilter is an excellent surrogate to spot and predict performance challenges. This process can be done before and after backwash with sampling from the top of biofilter. Note that establishing and setting the turbidity accumulation rate limit is plant-specific and must be defined based on the specific conditions and historical data.
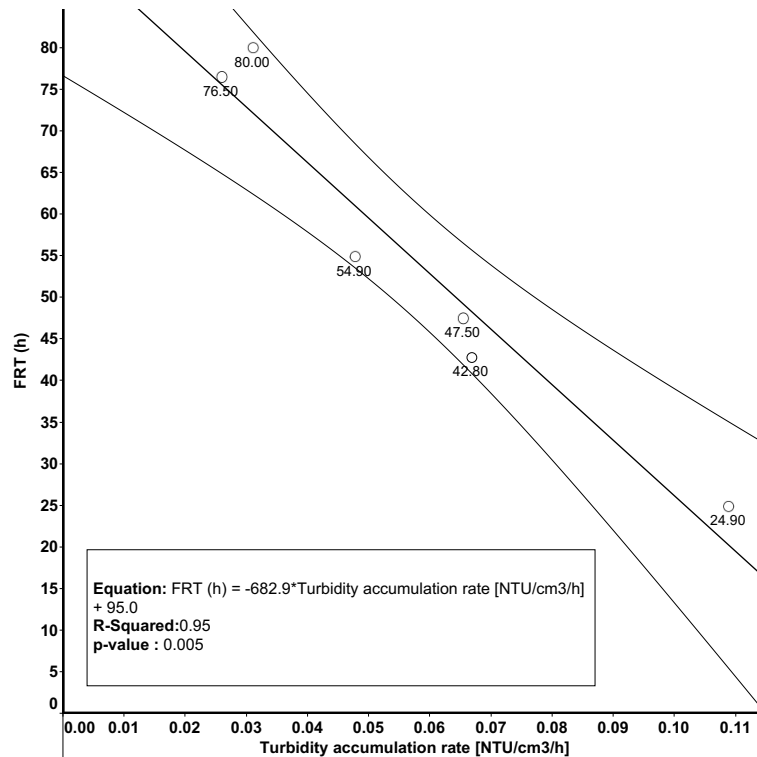
Figure 16   Correlation between the FRT and turbidity accumulation rate (at the top of biofilter media). The results are statistically significant.

Head-loss is monitored and recorded online. Understanding it as a response variable regarding other parameters changes could help to notice system challenges. However, no correlation was found for the head-loss accumulation rate with the other listed parameters, including biological and microbiome indices. It is recommended to further explore the relationship between the extracellular polymeric substances (EPS) and head-loss to create the baseline dataset. Literature suggests there is a correlation between these two parameters [50,116–120]. However, this study did not collect EPS data.

Although there was a linear relationship between turbidity accumulation rate and ATP accumulation rate at the top of biofilter (excluding the chlorinated filter), no significant correlation for 95% confidence intervals (alpha=0.05) were detected (Figure 17). As calculated P-value of 0.06 is very close to the alpha of 0.05, higher sample number may change the statistical significance. Therefore, it is suggested to collect more data for future studies.

The correlation between turbidity accumulation rate and the ATP accumulation rate at different filter depths is presented in Table 3. Although slopes and intercepts are event-specific, the results suggest a robust linear dependency between turbidity and ATP accumulation rates within each biofilter's depths. The P-value for diatom bloom and chlorination (which is not a biofilter) were not statistically significant.

There was no correlation detected between the ATP ($\mu g/cm^3$dried media) and other microbiome surrogates such as ASVs, Shannon, and Evenness. The ASVs and raw water temperature showed no significant correlation. This could be because DNA analysis is insensitive to dead/live bacteria.

Note that although the correlation was observed between some parameters, to ensure of the validity of the proposed equation higher sample size is required.

Table 3   R-squared and P-value related to the correlation of ATP level and turbidity accumulation rate in filter depth

Date	R-squared	P-value
Apr 2016	0.79	0.007
May 2016	0.82	0.005
Feb 2018	0.98	<0.0001
Mar 2018	0.90	0.0011
Jul 2018 (Diatom bloom)	0.33	0.17
Aug 2018 (Chlorination)	0.32	0.17
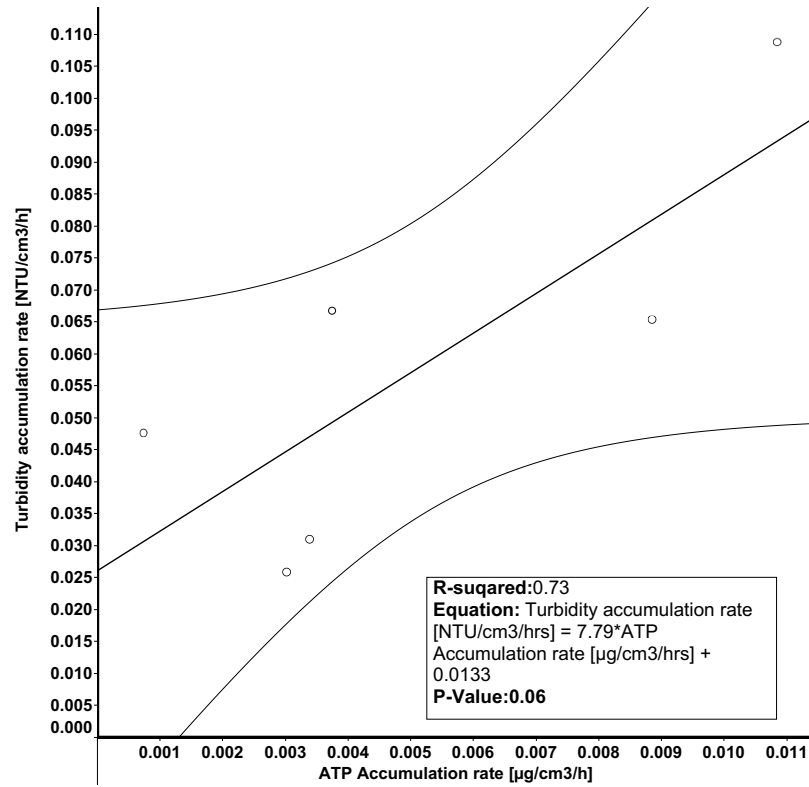
Figure 17   Although there is a linear trend between ATP accumulation rate [μg/cm³/h] shown in X-axis and turbidity accumulation rate [NTU/cm³/h] shown in Y-axis, no significant correlation was observed between them. (°) shows the collected data from the top of biofilter media, (–) depicts the linear correlation, the upper and lower bound are 95% confidence intervals. P-value >0.05 shows that the correlation is not statistically significant.

C.II - 8   IMPLICATIONS, APPLICATIONS AND CHALLENGES

When defining the maximum limit for the monitoring indicators, it is crucial to consider the physical characteristic of the filter (e.g. the head-loss must be $<=$ 2.15 [mH₂O]). To diagnose and predict the potential operational issues and consequently to optimize the performance, determining the duration in which the biofilter/filter reached the set limit is crucial. This was why the head-loss and turbidity accumulation rates were used as performance monitoring indicators in this study.

For future research, it is suggested that the media samples be taken in weekly intervals from the top of the biofilters and in between runs (after backwashing and before starting the new run) and analyze the media for turbidity, ATP, EPS, microbial community structure and

microbiome diversity indices. There is a consensus in the literature that the top layer, schmutzdecke layer, has the highest biological activity.

The final head-loss, raw water temperature, and FRT are usually recorded online. Documenting suggested parameters regularly will lead to set a baseline, which includes performance and biological indicators to assist with timely detection of any drastic changes leading to long shut offs.

Using statistical models such as NMF on the microbiome analysis results, will assist to create a baseline microbial community composition, core microbiome. The variation from the core will benefit utilities diagnose problems promptly. For example, it may be possible to notice an increase relative abundance of EPS producing bacteria and begin an initial investigation for the root cause and create a well-informed solution for the ongoing problem.

C.II - 9   CONCLUSIONS

Raw water temperature increased the biological activity as measured by ATP accumulation rate, turbidity accumulation rate and subsequently, head-loss accumulation rate. The deposited metals on the media was lowered after media replacement. However, the head-loss accumulation, turbidity and ATP accumulation rate did not have a noticeable variation. This shows that the small proportion of head-loss and media turbidity may be attributed to the concentration of the deposited metals. It also demonstrates that the hydraulic performance of the biofilter is highly influenced by raw water temperature and quality rather than the media lifetime. The sharp changes in hydraulic performance indicators and biological parameters in the July 2018 diatom bloom event confirm this strong dependency. The diatom bloom was observed to have the lowest filter runtime, highest head-loss accumulation rate, and ATP

accumulation rate. Noticeable changes were observed in the biofilter microbiome, such as changing evenness, ASVs and Shannon indices.

PCoA analysis indicated that the biofilter microbiome was influenced by media lifetime, filter depth and time with the primary one as the most substantial influence. The fresh media microbiome was different from other sampling events, confirmed by both PCoA and NMF analysis. Although source water seeds biofilter media, microbial composition is the result of the conditional and situational environment in biofilter rather than a mere voyage of the bacteria from the source water to filter media. Microbiota alterations happen due to the shear stress of backwashing, predation from other microbes, and nutrient/oxygen gradient in the filter.

In conclusion, this study provided a comprehensive insight to the challenging event in drinking water operation including media replacement and diatom bloom in the source water. For the first time using a statistical model biomarkers species, for the baseline and challenging filter events in biofilter operations were determined. This study specifically investigated the interrelationship and correlation between typical operational, hydraulic parameters, and the biological indicators. This study could be used as an example for water utilities operating biofiltration to improve the monitoring strategies and root cause investigation of drastic performance changes.

Chapter III   INCREASING HYDRAULIC PERFORMANCE

Sedimentation: hydraulic improvement of drinking water biofiltration

Leili Abkar, Amina Stoddart, Graham Gagnon

Awarded with the author highlight

The impact of sedimentation on hydraulic performance is investigated in this chapter. In addition to hydraulic parameters, the impact on biological performance is also investigated.

C.III - 1 ABBREVIATIONS

- Natural Organic Matter (NOM),
- Dissolved Organic Matter (DOC),
- Photoelectrochemical Oxygen Demand (peCOD),
- Adenosine Triphosphate (ATP),
- Extracellular Polymeric Substances (EPS),
- UV absorbance measurements at 254 nm (UV254),
- Total Organic Carbon (TOC),
- Trihalomethanes (THMs),
- Haloacetic acids (HAAs),
- Filter Runtime (FRT),
- Coagulation-Flocculation (C-F),
- Coagulation-Flocculation-Sedimentation (C-F-S)

C.III - 2 HIGHLIGHTS

- Implementing sedimentation after coagulation and flocculation improves filter runtime in dual-media (sand/anthracite) and tri-media (add granular activated carbon) biofilters by 18-30% and 8% respectively and decreases head-loss accumulation rate by an average of 34%.
- Sedimentation does not impact the natural organic matter removal rate, as measured in the biofilter effluent by dissolved organic carbon, photoelectrochemical oxygen demand, and UV absorbance at 254 nm.
- Sedimentation does not impact natural organic matter as measured by humic-, fulvic, and protein-like substances.
- Sedimentation does not impact adenosine triphosphate values but decreases extracellular polymeric substances by 35%.
- Implementation of sedimentation offers a reliable and robust optimization approach for biofilter performance.

C.III – 3 **ABSTRACT**

The performance of drinking water biofiltration systems is commonly measured by the effluent water quality and filter runtime (FRT). At constant flow rates, lower FRTs increase backwashing frequencies and hence, lower water recovery and increase the water production cost.

This study was conducted on a pilot-scale in two parallel trains, one included sedimentation and one did not. Both trains have three matched filter columns. Sedimentation improved FRT up to 30%, reduced head-loss and head-loss accumulation rate up to 29% and 35%, respectively. NOM removal remained unchanged. ATP levels did not differ, while EPS was reduced by 36%.

In conclusion, sedimentation increased long-term stability and reliability while reducing the backwash frequency, offering a robust approach for optimizing biofiltration performance. Potential operating cost savings have to be weighed versus the capital costs of retrofitting sedimentation in future studies.

Keywords: Sedimentation Process, Drinking Water Biofilter, Biofilter Performance, Biofilter optimization, Filter Runtime.

C.III - 4 INTRODUCTION

Drinking water biofiltration has recently been gaining attention because of its low energy consumption, its potential for decreasing disinfectant by-product (DBP) formation, and high water recovery [121]. Biofilters are common in North America, with different designs, configurations, and process combinations [12]. This drives a fast-growing interest in optimizing the process performance of these filters, resulting in "engineered biofilters" [119]. In engineered biofilters, the focus is on increasing and balancing the biological activity to increase system efficiency, stability, and robustness while simultaneously lowering the operational costs and improving water quality [34]. However, there is currently no consensus on optimization approaches (e.g. oxidant addition, nutrient supplementation and clarification process addition).

One optimization approach is the inclusion of a clarification step, such as sedimentation, after coagulation and flocculation. Coagulation is a well-known process to remove NOM from water, especially the hydrophobic, high molecular weight fraction, which is associated with humic-like substances [122–127]. Flocculation provides a gentle mixing step for the flocs to develop and reach their optimum size. Then, the volume is ready to be sent to a sedimentation stage [128]. Without sedimentation, flocs formed during coagulation and flocculation mostly carryover and penetrate the depth of the biofilter column. Floc carryover into the biofilter was hypothesized to cause early clogging which is measured by head-loss. Accordingly, flocs build up in the biofilters can result in channeling in the filter bed, leading to uneven flow and nutrition distribution. In addition, floc carryover can cause higher shear stress in the channel areas [129]. A 2016 survey by Brown et al. reported a total of 8% of all facilities in the United States and Ontario still use coagulation-flocculation (direct filtration), without sedimentation or other clarifiers in the process. Although floc carryover can cause challenges from an

operational standpoint, retrofitting sedimentation tanks in existing facilities can be a significant endeavor, and the benefits have not been formally and statistically explored.

The objective of this study was to investigate the inclusion of a sedimentation tank in direct biofiltration (coagulation-flocculation- biofiltration) and its influence on effluent water quality and hydraulics of the biofilter. Specifically, this work evaluates the impact of sedimentation on effluent water turbidity, and DBP precursors such as DOC, UV_{254}, peCOD, and fEEM parameters (humic-, fulvic-, and protein-like substances). The biological stability of the biofilter media was assessed as adenosine triphosphate (cellular activity) and extracellular polymeric substances (EPS). EPS is a matrix produced by cellular activity and its excess productions leads in clogging biofilter [116]. It was hypothesized that hydraulic conditions (higher FRT and lower head-loss accumulation rate) will be improved during biological filtration through the addition of a clarification process after coagulation without negatively impacting effluent water quality.

C.III - 5 MATERIAL AND METHODS

This study was conducted in collaboration with Halifax Water at the automated pilot plant (Intuitech Inc., Salt Lake City, Utah, USA) in the J.D. Kline Water Treatment facility, which treats water from Pockwock Lake and serves peninsular Halifax, Nova Scotia, Canada. This custom pilot plant aims to foster the understanding of how to optimize the current treatment practices at the full-scale plant.

C.III - 5.1 Pilot Plant Design
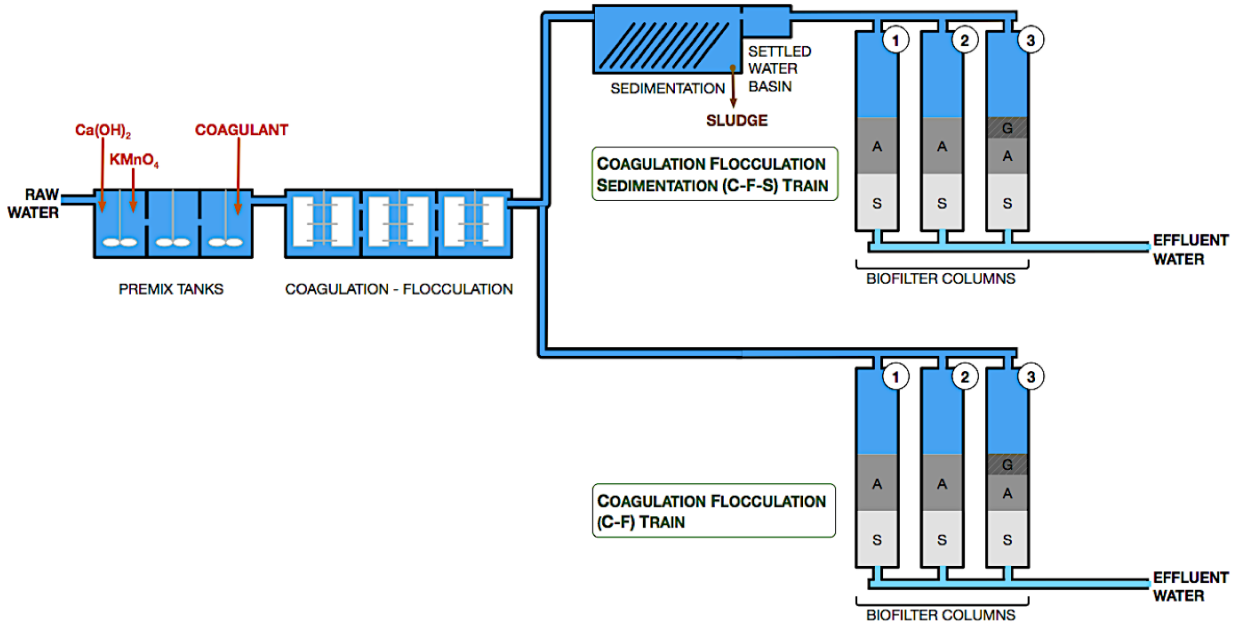
Figure 18   Schematic of the custom-designed pilot plant system (Intuitech Inc., Salt Lake City, Utah, USA) used in this study

Water from Pockwock Lake entered the pilot plant (Figure 1) through the premix tank, which was separated into three compartments, at a flow rate of 10 L/min. Chemicals, such as lime, potassium permanganate ($KMnO_4$, 0.15 mg/L), and coagulant (aluminum sulfate, 12 mg/L) were added at different stages of the premix tank to adjust the pH, oxidize NOM and mix the coagulant, respectively. The retention time for each premix tank was approximately 1 minute. The water then continued to the flocculation tank at different G-values of 30 s^{-1}, 20 s^{-1}, 10 s^{-1}, in three stages; the retention time for each stage of flocculation tank varied from 16-19 minutes. An optional sedimentation tank was available on both trains with a capacity of 330 L and 30 adjustable plates (each with an area of 0.1 m^2) [130]. In these tanks, water passed over the plates, and resulting clarified water flowed to biofilters. Sludge collected at the bottom of the basin was pumped to waste [131].

In the current study, one of the trains used sedimentation (C-F-S) while the other one bypassed it (C-F). The influent water from each respective train entered three biofilter columns (I.D. 200 mm) in each skid. Each train employed equal media bed packing for biofilters 1 and 2 (Table 4), where biofilters 3 were also matched but differed from biofilters 1 and 2 by the inclusion of a granular activated carbon (GAC) cap (see Figure 18).

Table 4   The biofilter media bed design in each train

	Filter Media	Depth cm [ft]	Effective Size mm [in]	Uniformity Coefficient	L/D	Total L/D
Biofilters 1 & 2	Anthracite	61.0 [2]	0.89[0.03]	1.67	685	1225
	Sand	30.5 [1]	0.52 [0.02]	1.53	540	
Biofilter 3	Anthracite	45.0 [1.5]	0.89 [0.03]	1.67	506	1219
	Sand	30.0[1]	0.52 [0.02]	1.53	577	
	GAC	15.0[0.5]	1.10 [0.04]	1.40	136	

Biofilters 1 and 2 on each train had dual media: 61.0 cm (2 ft) of anthracite and 30.5 cm (1 ft) of sand, and biofilter 3 consisted of three media: 15 cm (0.5 ft) of GAC over 45 cm (1.5 ft) of anthracite and 30 cm (1ft) of sand. Each biofilter was designed to simulate full-scale depth. The effective sizes of anthracite, sand, and GAC were 0.89 mm (0.03 in), 0.52 mm (0.02 in) and 1.10 mm (0.04 in), respectively. Uniformity coefficients were 1.67 for anthracite, 1.53 for sand and 1.40 for GAC. The pilot plant worked under a filter loading rate of 4.4 m/h (1.80 gpm·ft^{-2}) and an empty bed contact time of 12.5 minutes [132]. The biofilters were operating for more than 24 months before the current experiments. The pilot plant was fully automated with the capability to change operating variables. Biofilters were backwashed at the end of each cycle with the collected effluent water from biofilters. Each backwash included three phases: (i) air scour phase, (ii) combined air and water wash, and (iii) three water washes.

C.III - 5.2 Source Water Characteristics

Pockwock Lake in Halifax, Nova Scotia, Canada provided the source water to both the pilot and the full-scale plant. Pockwock Lake is a protected area, and it is characterized by low alkalinity, pH, and low organic carbon, as shown in Table 5. Raw water temperature changes during this study were plotted and shown in Figure 19.

Table 5   Source water quality

Alkalinity[2] [mg/L] as $CaCO_3$			pH[1]			Turbidity [NTU]			TOC [mg/L]		
Mean±SD	Min	Max	Mean±SD	Min	Max	Mean±SD	Min	Max	Mean±SD	Min	Max
<1 [38]			5.67±0.14	5.47	6.31	0.43±0.10	0.24	1.79	3.23±0.23	2.8	3.71

[1] Measured using Fisherbrand™ accumet™ pH Benchtop Meter
[2] Alkalinity was measured based on Standard method 2320, Titration
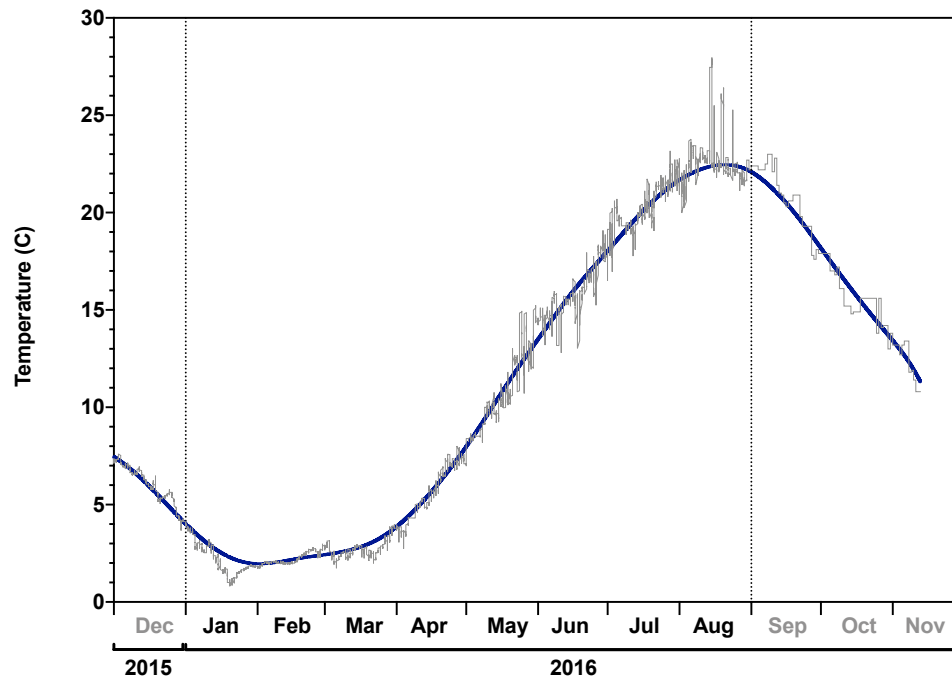
Figure 19   Raw water temperature variations in 2016. The study was conducted from January to August 2016.

C.III - 5.3 Experimental Schedule.

The experiments were conducted for eight months. During the experimental phase, both trains went through some additional treatments such as increasing the $KMnO_4$ dose and adding hydrogen peroxide and pre-chlorine. However, the only difference between the two trains was the inclusion of a sedimentation tank. The raw water flow rate to the pilot plant was 10.02 L/min $\pm$ 0.11, and to each biofilter was 2.38 L/min $\pm$ 0.12. The common raw water source provided the same temperature and other seasonal effects for both trains.

C.III - 5.4 Methods of Measurement.

Water samples were taken from raw water entering the pilot plant and in the biofilter effluent stream. To assess the biomass activity, media samples were taken from the top of the biofilters in sterilized 50 mL falcon tubes and transferred overnight to the lab.

C.III - 5.5 Dissolved Organic Carbon.

DOC samples were collected headspace-free, in 40-mL glass vials. The samples were acidified with phosphoric acid to a pH < 2, stored at 4 °C before analyzing them with a TOC-V CPH analyzer (Shimadzu Corp., Kyoto, Japan) in duplicate. DOC samples were filtered with primed 0.45-µm Polyethersulfone filter membranes (Ultrasep, GVS Filtration, Findlay, Ohio, USA).

C.III - 5.6 Fluorescence Spectroscopy (i.e., Humic-, Fulvic-, Protein-like Substances)

Fluorescence Excitation-Emission Matrix (fEEM) spectroscopy was conducted on an Aqualog® fluorometer (HORIBA Scientific, Kyoto, Japan) varying the excitation wavelengths from 200 to 400 nm and the emission wavelength from 200 to 500 nm. Samples were collected in a headspace-free, 40 mL borosilicate glass vials and preserved at 4 °C. To run the samples through the fluorometer, samples were brought to room temperature. Processing the raw data

included first-order and second-order Rayleigh masking. Inner-filter effects and normalization were then conducted. Fractional regional integration (FRI) was the result of the fluorescence spectroscopy data collected in the study. Integration bounds were applied to the humic-like, fulvic-like, and protein-like regions described by Markechova et al., 2013.

C.III - 5.7 Photoelectrochemical Oxygen Demand Analysis (peCOD).

For peCOD analysis, samples were collected headspace-free in organic-free 40-mL glass vials and analyzed using a COD analyzer based on standard method SM 5910B. This analyzer calculates a detection limit of 0.5 mg/L. When adjusting pH to < 3, the holding time is 14 days. The analyzer measures the current generated from the photocatalytic oxidation of organic matter using a titanium dioxide catalyst irradiated with UV light from a light-emitting diode. The analyzer performs a direct count of the electrons transferred during the oxidation of the sample [134].

C.III - 5.8 UV Absorbance at 254 nm.

UV254 was measured using a spectrophotometer (DR4000, Hach, Loveland, Colorado, USA) after filtering the samples through 0.45-µm filter membranes.

C.III - 5.9 Biological Activity.

Biological activity was measured as adenosine triphosphate (ATP) and extracellular polymeric substances (EPS). ATP concentration, as an indicator of biological activity, was measured in triplicate on media samples from each biofilter. Deposit & Surface Analysis ATP kit-DSA test kit (LuminUltra Technologies Ltd., Fredericton, New Brunswick, Canada) and a PhotonMaster™ (Luminometer, LuminUltra Technologies Ltd., Fredericton, New Brunswick, Canada) were used to analyze the ATP following the manufacturer's instructions. Samples were collected in sterile, 50-mL falcon tubes at a media depth of 15 cm (6 in) and

analyzed immediately after collection. ATP is reported as per dry weight of media, using a conversion factor of dry to wet media. The conversion factor was measured by weighing the wet media before and after drying it at 105 °C for 24 h. EPS was measured as polysaccharides and protein at the University of Texas at Austin as part of Water Research Foundation (WRF) Project 4555. Polysaccharides were quantified with a phenol-sulfuric acid assay by Dubois and co-workers [135]. Protein was measured using a modified Lowry assay. EPS results are reported as total EPS, which is the summation of BSA protein and polysaccharides [17].

C.III - 5.10 Hydraulic Performance.

Hydraulic performance parameters, including head-loss, FRT, and flow rate, were measured using the following inline instruments. The accuracy of the pressure transmitters (WIKA Instruments Ltd., Edmonton, Alberta, Canada) was reported as ≤1.0% (including non-linearity, hysteresis, zero points, and full-scale error) at 0 to 1 bar. The head-loss data were recorded in mH_2O and the analysis in this paper was based on the head-loss accumulation rate and hourly recorded head-loss. The head-loss accumulation rate was estimated as the deduction of the terminal and clean bed head-loss (mH_2O) divided by the filter runtime (hours). Flowrate was monitored with GF Signet 2551 Magmeter flow meter (Georg Fischer Signet LLC, El Monte, CA, USA).

FRTs for organic cycles (no manual shut off) were selected for this study. The organic cycles allow the biofilters to reach a specific limit of turbidity or head-loss, or filter runtime. The limits were defined to simulate the full-scale plant including a turbidity limit of 0.2 NTU, a head-loss limit of 2.15 m (7 ft) or FRT limit of 80 hours. In case where a biofilter reached one of the limits, the filter run was ended, and a backwash was initiated. When a filter run ended for reasons other than the criteria mentioned above, the data were not considered.

Unit filter run volume (UFRV) (gal/ft^2) was calculated for the corresponding filter run time of organic cycles as the product of filter load rate (gpm/ft^2) and FRT (minutes).

C.III - 5.11 Disinfection By-Product Formation Potential

DBP, including trihalomethanes (THMs) and haloacetic acid (HAAs) formation potential, were determined using uniform formation conditions as described by [136]. THMs and HAAs were collected in 20-mL glass vials that were baked for 24 hours at 100 °C. Samples for DBPf were collected at each stages of treatment process including raw water, influent and effluent of biofilters. Gas chromatography with electron capture (CP-3800 Gas Chromatograph, Varian, Inc., Walnut Creek, California) was used to analyze THMs and HAAs according to US EPA methods 551.1 and 552.2, respectively.

C.III - 6 RESULTS

In general, the results are structured into three major sections: (1) water quality, (2) biological activity, and (3) hydraulic performance. Water quality parameters include NOM (i.e., DOC, peCOD, UV$_{254}$, humic-like and fulvic-like and protein-like substances) and turbidity. Biological activity indicators include ATP and EPS. Biofilter hydraulic performance parameters were evaluated by FRT, and head-loss and head-loss accumulation rate.

C.III - 6.1 Effect of Sedimentation on Effluent Water Quality

The influence of sedimentation on NOM in the effluent water streams was assessed as percent removal from raw water NOM levels and analyzed as paired data over time for biofilters 1, 2, and 3. DOC, UV$_{254}$, and peCOD have been selected as NOM parameters (see Table 6).

Table 6 NOM removal in C-F versus C-F-S train in biofilters 1, 2, and 3. No significant difference was found between the trains for either NOM.

		DOC [ppm]		UV$_{254}$ [cm^{-1}]		peCOD [ppm]	
		mean ± SD	n	mean ± SD	n	mean ± SD	n
Biofilter 1	**C-F**	0.33 ±0.07	39	0.61 ± 0.08	27	37.56 ± 17.61	16
	C-F-S	0.34 ± 0.06	39	0.60 ± 0.07	27	43.31 ± 13.89	16
	P-value	>0.9999 (ns)		0.6487 (ns)		>0.9999 (ns)	
Biofilter 2	**C-F**	0.34 ± 0.07	39	0.61 ± 0.07	27	35.50 ± 16.44	16
	C-F-S	0.34 ± 0.05	39	0.60 ± 0.07	27	37.75 ± 19.58	16
	P-value	>0.9999 (ns)		0.2830 (ns)		0.8959 (ns)	
Biofilter 3	**C-F**	0.34 ± 0.07	39	0.61 ± 0.08	27	34.69 ± 14.50	16
	C-F-S	0.33 ± 0.06	39	0.61 ± 0.07	27	37.31 ± 22.74	16
	P-value	0.4648 (ns)		0.6487 (ns)		>0.9999 (ns)	

Values calculated as (raw-effluent)/raw, n: number of samples, P-values (Kruskal-Wallis) were adjusted for multiple comparison (Dunn's), ns : not significant at P-value>0.05, * at P-value≤0.05, ** at P-value≤0.01, *** at P-value≤0.001, **** at P-value≤0.0001.

The data were collected from January to August 2016. Throughout this time, seasonal changes on temperature and water quality were observed. However, no significant differences between both trains (C-F and C-F-S) for biofilters 1, 2, or 3 as measured by DOC, UV$_{254}$, and peCOD were observed (non-significant, ns, describes P>0.05) in the effluent water. NOM removal was also evaluated by fEEM, as measured by fulvic-like, humic-like, and protein-like substances. The results showed that sedimentation does not significantly impact the removal of fEEM parameters in both trains (see Table 7). Values represented in the Table 7 are the differences between raw water and biofilter effluent normalized by raw water ± standard deviation).

Table 7 fEEM parameters values reported for three biofilters in two trains. No significant difference was found between the trains for either fEEM parameters.

		Fulvic-like [μg/L]		Protein-like [μg/L]		Humic-like [μg/L]	
		mean ± SD	n	mean ± SD	n	mean ± SD	n
Biofilter 1	**C-F**	0.46 ± 0.15	16	0.28 ± 0.18	11	0.48 ± 0.16	15
	C-F-S	0.48 ± 0.12	16	0.30 ± 0.11	11	0.50 ± 0.11	15
	P-value	0.5576 (ns)		>0.9999 (ns)		>0.9999 (ns)	
Biofilter 2	**C-F**	0.46 ± 0.13	16	0.29 ± 0.16	11	0.47 ± 0.16	15
	C-F-S	0.49 ± 0.10	16	0.33 ± 0.15	11	0.50 ± 0.11	15
	P-value	>0.9999 (ns)		>0.9999 (ns)		>0.9999 (ns)	
Biofilter 3	**C-F**	0.49 ± 0.14	16	0.37 ± 0.18	11	0.51 ± 0.15	15
	C-F-S	0.50 ± 0.10	16	0.34 ± 0.12	11	0.51 ± 0.11	15
	P-value	>0.9999 (ns)		>0.9999 (ns)		>0.9999 (ns)	

Values calculated as (raw- effluent)/raw, n: number of samples. P-values (Kruskal-Wallis) were adjusted for multiple comparison (Dunn's), ns : not significant at P-value>0.05, * at P-value≤0.05, ** at P-value≤0.01, *** at P-value≤0.001, **** at P-value≤0.0001.

C.III - 6.2 DBP formation potential.

Formation potential of DBPs were measured as THMs and HAAs. Dibromochloromethane (THM), Bromoform (THM), Bromoacetic Acid (HAA), Dibromoacetic Acid (HAA), Chlorodibromoacetic Acid (HAA), Tribromoacetic Acid (HAA) were consistently less than their detection limits.

Other DBPs, as shown in Table 8, are not significantly different between the two trains. In other words, the inclusion of the sedimentation process did not significantly impact the removal of DBPs in the duration of the study. The results did not change with temperature variation during this study.

Table 8   DBPs values (mean ± standard deviation) in two trains in biofilters 1, 2, and 3. No significant difference was found between the trains for DBPs.

		THMs (µg/L)			HAAs(µg/L)		
		Chloroform	Dichlorobromo methane	TTHM	Dichloro acetic acid	Trichloro acetic acid	Bromochloroac etic acid
Biofilter 1	**C-F**	0.61 ± 0.11	0.16 ± 0.12	0.64 ± 0.05	0.57 ± 0.12	0.55 ± 0.14	9.63 ± 8.71
	C-F-S	0.68 ± 0.14	0.09 ± 0.06	0.60 ± 0.07	0.57 ± 0.09	0.55 ± 0.13	11.00 ± 5.66
	P-value	>0.9999 (ns)	0.9315 (ns)	>0.9999 (ns)	>0.9999 (ns)	>0.9999 (ns)	>0.9999 (ns)
Biofilter 2	**C-F**	0.59 ± 0.08	0.11 ± 0.11	0.60 ± 0.05	0.59 ± 0.05	0.55 ± 0.13	10.60 ± 5.05
	C-F-S	0.64 ± 0.14	0.21 ± 0.13	0.68 ± 0.06	0.52 ± 0.10	0.52 ± 0.16	11.00 ± 4.17
	P-value	0.9315 (ns)	0.5289 (ns)	0.3246 (ns)	0.3685 (ns)	>0.9999 (ns)	0.9783 (ns)
Biofilter 3	**C-F**	0.64 ± 0.06	0.10 ± 0.09	0.63 ± 0.07	0.58 ± 0.11	0.58 ± 0.14	10.80 ± 4.25
	C-F-S	0.64 ± 0.09	0.14 ± 0.10	0.62 ± 0.10	0.52 ± 0.11	0.56 ± 0.16	11.00 ± 4.17
	P-value	>0.9999 (ns)	0.7102 (ns)	>0.9999 (ns)	0.2689 (ns)	>0.9999 (ns)	>0.9999 (ns)

Values calculated as (raw-effluent)/raw, P-values (Kruskal-Wallis) were adjusted for multiple comparison (Dunn's), ns at P-value>0.05, * at P-value≤0.05, ** at P-value≤0.01, *** at P-value≤0.001, **** at P-value≤0.0001. number of samples in each column is 5.

C.III - 6.3 Turbidity

Turbidity levels were measured in the effluent water from the biofilters. Figure 20 shows that the turbidity levels in the C-F biofilters were significantly higher (P<0.0001) and fluctuated more than the C-F-S biofilters. In summary, applying the sedimentation process decreased the turbidity level and range.
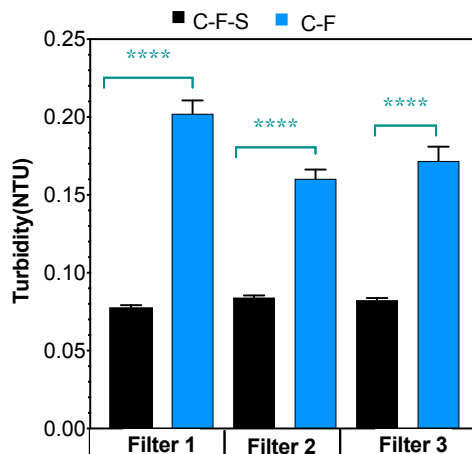
Figure 20   Effluent water turbidity from each biofilter at two trains. The biofilters in C-F had higher turbidity level in comparison to the biofilter in C-F-S train. Each point shows the mean and error bars represent 95%CI.

C.III - 6.4 Effect of Sedimentation on Biological Activity.

As microorganism are the main building blocks in biofiltration, studying their activity level is essential. ATP is an indicator of cellular activity. The comparison of cellular activity, as measured by ATP between two trains, showed no significant differences in all three biofilters (see Table 9).

Table 9   ATP value (mean ± SD) in the C-F and C-F-S trains for biofilter 1,2,3. No significant difference was observed in the biofilters between two trains.

		ATP [pg/g]
Biofilter 1	**C-F**	59630 ± 19278
	C-F-S	71657 ± 22606
	P-value	0.7102
Biofilter 2	**C-F**	101301 ± 55454
	C-F-S	64903 ± 30239
	P-value	0.1276
Biofilter 3	**C-F**	80582 ± 25678
	C-F-S	110141 ± 36739
	P-value	0.1276

C-F and C-F-S as absolute measures, P-values (Kruskal-Wallis) were adjusted for multiple comparisons (Dunn's), ns : not significant at P-value>0.05, * at P-value≤0.05, ** at P-value≤0.01, *** at P-value≤0.001, **** at P-value≤0.0001.number of samples is 5.

However, the EPS showed different results, representing a different aspect of bacterial behavior. Higher level of EPS is not desirable in the biofilter as this material accumulates and results in clogging in the filter bed [118]. As shown in Figure 21, total EPS (summation of EPS-Protein and EPS-Carbohydrate) in the C-F biofilters are significantly higher (35%, p-Value<0.001) than in the C-F-S biofilters.
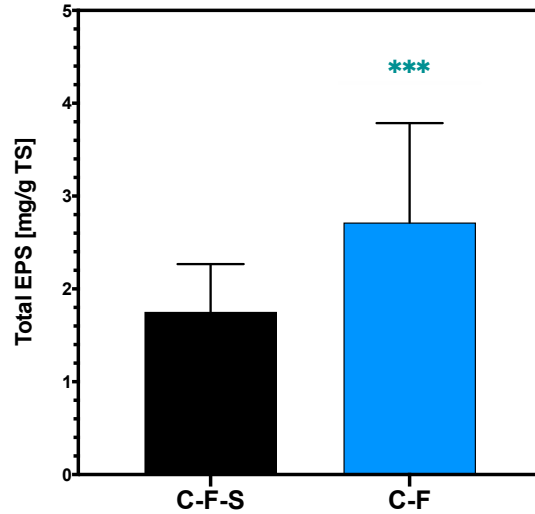
Figure 21   Comparing total EPS production in biofilters in both trains representing the higher production of EPS in C-F train. P-values (Wilcoxon matched-pairs signed-rank test), ***** significant at P-value <0.033, ****** significant at P-value<0.003, ******* significant at P-value <0.001. Error bars represent the standard deviation. (EPS Raw Data Source: Water Research Foundation Project 4555).

C.III - 6.5 Effect of Sedimentation on Hydraulic Performance.

C.III - 6.5.1   *Head-Loss*

All the biofilters in the C-F train showed significantly higher head-loss (P<0.05) compared to the C-F-S train (see Figure 22).
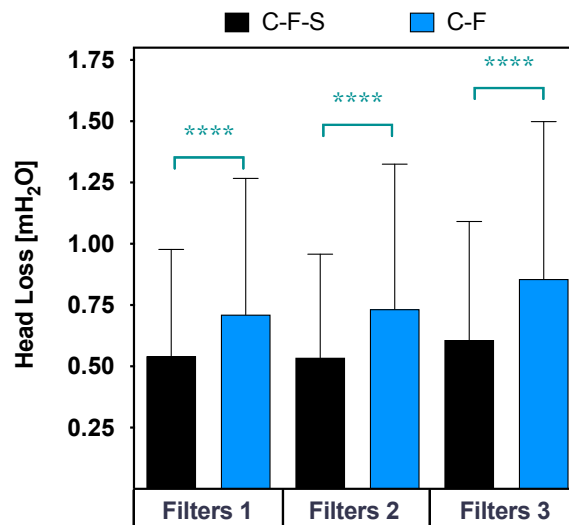
Figure 22   Comparing head-loss in two trains, C-F-S: Coagulation-Flocculation-Sedimentation. C-F: Coagulation-Flocculation. ******** shows a statistically significant difference. P values (Kruskal-Wallis) are adjusted for multiple comparisons (Dunn's), (P-value<0.05). Error bars representing standard deviation.

Compared to C-F, using sedimentation, the average head-loss in all biofilters decreased by 24%, 27%, and 29% for biofilter 1, biofilter 2, and biofilter 3, respectively. Also, the head-loss accumulation rate, calculated by ~~peak~~ FRT divided by the corresponding head-loss, is on average 34% (P<0.001) higher in all C-F biofilters compared to C-F-S (see Figure 23).
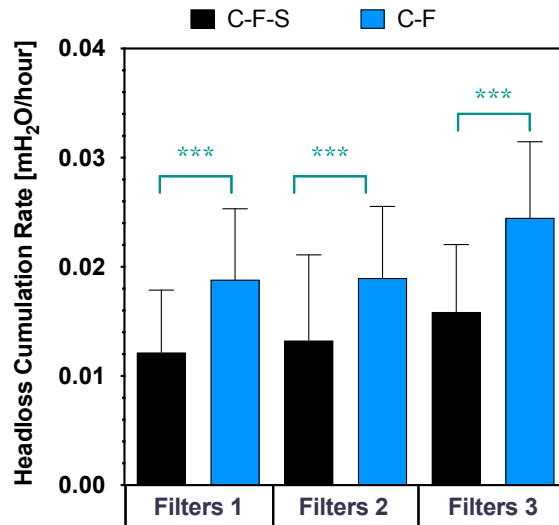
Figure 23   Head-loss accumulation rate was significantly reduced by 35% (P-value<0.001, ***), 30% (P-value <0.001, ***) and 35% (P-value <0.001, ***) in the C-F-S train for biofilters 1, 2 and 3 respectively. P values (Kruskal-Wallis) were adjusted for multiple comparisons (Dunn's). Error bars represent the standard deviation.

Temperature variation was observed during this study due to seasonality, but the differences between the trains were maintained overall. The C-F-S train showed consistently less head-loss and head-loss accumulation rate in comparison to the C-F train. As discussed previously, the C-F-S train also had lower EPS and while EPS alone may not be the only reason it does illustrate the broad accumulation of excess material accumulating in the C-F train.

C.III - 6.5.2   *FRT and UFRV.*

FRT was significantly higher by 11.9 hours (30%) (P-value <0.001, ***) and 7.6 hours (18%) (P-value=0.007, **) in the C-F-S train biofilters 1 and 2, respectively. While FRT in biofilter 3 showed no statistically significant differences (P = 0.52, ns), it was higher by 3.7 hours (8%). In general, FRT was improved in the C-F-S train compared to the C-F train (see Figure 24).
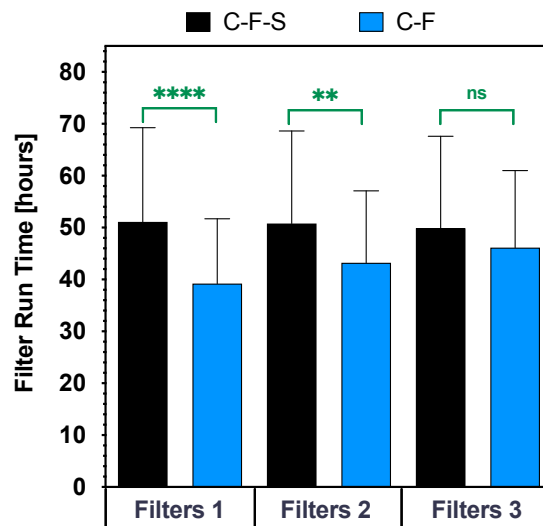
Figure 24   FRT in biofilter 1,2,3 in both trains. FRT was significantly higher by 11.91 hours (30%) (P-value <0.001, ***) and 7.58 hours (18%) (P-value=0.007, **) in the C-F-S train biofilters 1 and 2, respectively. Although FRT of biofilter 3 in C-F-S was higher by 3.74 hours (8%), it did not show any statistical significance (P-value =0.52, ns). Error bars represent the standard deviation.

UFRV, calculated from FRT and a constant biofilter loading rate, has the same trend as FRT. UFRV in biofilter 1 and 2 in C-F-S is significantly higher than in C-F (P<0.05), while biofilters 3 did not differ statistically (P=0.17, ns). In C-F-S train biofilters 1, 2, and 3, the UFRV is 30%, 18%, and 8% higher, respectively.

C.III - 7 DISCUSSION

In the C-F-S train, the sedimentation tank removed a large portion of the flocculated matter, resulting in fewer flocs carried over into the biofilters. In the C-F train, however, all flocs were carried over. As flocs tend to accumulate on the upper layers of biofilters, higher head-loss accumulation rate and shortened biofilter run times can be expected [34,137]. Grace et al. 2016, studied the clogging mechanism in slow sand biofilters and concluded that the organic matter builds up mostly occurs in the upper layers [137]. This is in agreement with the findings of the higher head-loss accumulation rate and shorter FRT not using sedimentation in this study. The changes in FRT and UFRV followed the same trend in all biofilters. However, there was no statistical significance observed for the tri-media biofilters.

However, secondary effects likely occur when the bacteria get exposed to floc carry over and flow channeling effects that may lead to increased EPS production, adding to the clogging of the biofilter. Specifically, the coagulants used during this study were alum based (trihydrate and bauxite alum). Therefore, floc carried over to the biofilters contained aluminum. Aluminum is a toxic ion with no nutritional benefit to the cell. Presence of aluminum can potentially damage the cell and impact its activity through different pathways such as binding to phospholipids or membrane transport proteins (damaging the membrane transport) and interacting with enzyme-phosphatases [138]. Exposure to toxic substances can cause stress on bacteria and induce SOS responses. SOS response in bacteria persuade DNA repair system that bacteria choose in abrupt DNA damage situation [139,140]. Pursuing the bacteria to SOS responses include increased biofilms formation [141]. This could explain the higher EPS formation observed in the C-F biofilters. Guzzo et al. (1991) showed that aluminum stimulates the flagellin (fliC) genes expression. Flagellin is part of the system that can help the bacteria move away from toxic environments toward more nutritious conditions [142]. The gene fliC is

correlated with biofilm formation ability in *Pseudomonas aeruginosa* isolates in a clinical study [143]. This could also be an explanation for the higher EPS production observed in the C-F biofilters, which are exposed to a higher level of floc carryover. Bacterial EPS and humics in the water influent have the ability to form a hydrophilic gel matrix with high water content and low density [144,145], potentially further explaining the effects of higher EPS production in the C-F biofilters.

Overall, organic removal in both trains and none of the NOM surrogate in water quality parameters showed a significant difference. Possibly, the relatively low organics removals rate may not be sensitive enough to show statistical differences. The system was operating with mean total biomass of ATP 1×10^5 pg /g, and the dissolved oxygen consumption was lower than 0.1 mg/L (data not shown) demonstrating low biological activity. The ATP level did not differ between the two trains. The bio-available organic compounds in the floc may be bound in the floc in such way, that they are not available to bacteria. This may explain why the amount of floc in the biofilter does not affect ATP levels in two trains.

The sample size is too small to draw a statistical conclusion on EPS correlation with head-loss. However, the levels of EPS in C-F are higher than in C-F-S. Mauclaire et al. studied the clogging reasons for biological slow sand filtration as the final step in a water treatment facility to treat water from Lake Zurich. They stated that the significant reason for clogging is EPS buildup [120]. Their findings are in agreement with the current study results.

C.III - 8 CONCLUSIONS

Findings of this study suggest implementing a sedimentation tank decreases the head-loss accumulation rate, effluent water turbidity, and increases the FRT regardless of seasonal variations. It is worth to mention that in tri-media biofilters the FRT differences were not statistically significant. Employing sedimentation process would offer a reliable and robust optimization approach for biofiltration performance.

However, further studies should be done to investigate the biofilter clogging mechanism for different water resources and process combinations. Also, understanding the mechanism of coagulant and floc interaction with bacteria when floc is carried to biofilters is of crucial importance. Future work should also compare the savings in operational cost from less frequent backwashing to the capital cost of retrofitting a sedimentation tank. Backwashing can have significant environmental and cost implications for the total operating cost of a drinking water biofiltration plant [34].

C.III - 9 ACKNOWLEDGMENTS

Chapter IV SOURCES OF HEAD-LOSS IN DIRECT BIOFILTRATION

In Chapter III, direct biofiltration had significantly higher head-loss accumulation rates compared to sedimentation before biofiltration. Possible root causes for this observation are investigated through literature review and discussed in the context.

The experimental part of this section was not possible due to Covid-19 halting laboratory experiments in the Summer of 2020.

C.IV - 1   Introduction

As shown in chapter 3, the biofilters after the sedimentation tank had lower EPS levels and less head-loss accumulation and, consequently, higher filter runtime than the direct biofilters. As mentioned, the sample number was too low to make a solid conclusion about the linearity of the relationship between the head-loss and EPS. However, in general, the trend showed that direct biofiltration had higher EPS levels.

This chapter further investigates possible causes for higher EPS levels observed in the direct biofilters. Hypotheses are as follows:

1. Toxicity of alum (aluminum sulphate) triggering the EPS pathway in bacteria. Floc carryover is causing more EPS production due to alum toxicity.

2. The floc carryovers hinder the diffusion of the nutrients to the bacteria. The low nutrient condition causes stress and forming more EPS.

3. Flocs are the source of the differences in the higher EPS measurement. As alum flocculate particulate matter, viruses, and bacteria, there is a possibility that the flocs carry the microorganisms and related EPS to the direct biofilter.

4. As flocs contain the Al residuals the interaction between Al and bacteria (EPS) must be further investigated.

C.IV - 2   Aluminum toxicity

Alum (aluminum sulphate) is one of the most common coagulants used in conventional water treatment systems [146]. The hydrolysis of alum in water depends on pH and temperature and produces varying aluminum hydroxyl complexes, $Al_x(OH)_y^+$ [147,148]. Alum reacts in two different ways to achieve coagulation: 1) at a low dose (<5 mg/L) the primary mechanism is

destabilizing the particles through charge neutralization 2) at higher dosages the common mechanism is believed to be entrapment where the aluminum hydroxide as "sweepfloc" attracts the suspended solids in the water and creates the flocs.

The pH is adjusted to 5.5-6 in a direct filtration system to achieve optimum coagulation. Therefore, it is possible that the coagulation-flocculation process's pH is playing a role in bacteria selection and could explain the microbiome differences between the source water and biofilters.

The health impact of alum was studied extensively [149–155], the regulatory agencies set the maximum concentration of aluminum in drinking water.

The Health Canada guideline suggests a maximum acceptable concentration (MAC) of 2.9 mg/L (2900 µg/L) for total aluminum in drinking water considering the 12-month running average of a minimum of quarterly samples taken in the distribution system. The operational guideline value is proposed to be less than 0.050 mg/L (50 µg/L) for total aluminum to optimize water treatment and distribution systems [156]. The US.EPA, European Union, and Australia's National Health and Medical Research Council set the operational guidance (OG) values for aluminum in the range of 0.050 mg/L to 0.20 mg/L considering the aesthetic or operational concerns.

Understanding how alum impacts the microbiota in the water treatment systems is crucial as it affects the microbiome health in biofiltration, specifically direct biofiltration.

The alum toxicity impact on microorganisms is of scholars' interest since the 1950s. Sheets stated that 18 mg/L of alum caused a 50% reduction in BOD of sewage sludge due to the microbial activity reduction [157]. YuV (1987) showed that the negative effect of aluminum sulphate on bacteria starts to be noticed at 1 mg/L. He reported a 60% reduction in natural

bacteria at 10 mg/L of alum [158]. Zwarun et al. (1971) showed that *Bacillus* sp is resistant up to 80 mg/L of alum. However, for the bacterium, *Pseudomonas stutzeri* at pH 4.5, adding 10 mg/L of aluminum reduced the number of bacteria significantly while the concentration of 80 mg/L was lethal [159]. The impact of aluminum sulphate on fungi species was studied in the range of 0-500 mg/L. No growth was observed for *Thelephora terrestris* at 150 mg/L and higher concentrations (ranked as the most sensitive one). Other species of fungi, *Cenococcum graniforme, Suillus luteus,* and three isolates of *Pisolithus tinctorius* were sensitive to alum at all the concentration (showed growth reduction) [160]. Ali (2018) has studied the antibacterial impact of potassium alum on six bacteria (*S. aureus, K. pneumoniae, P. vulgaris, P. aeruginosa, P. fluorescens,* and *E. coli*) and one yeast (*C. albicans*). The inhibition zone used as a measure for antibacterial sensitivity and reported that all of the bacteria were sensitive at 20% of alum concentration while *C. albicans* showed more sensitivity even at the lower concentration of 8% (8.09 g/L of aluminum) [161]. In another study, to prolong the flower vase life, alum was added to the water at different concentrations (100, 200, and 300 mg/L) [162]. It is reported that at 100 mg/L of alum, no bacterial growth was observed as measured by CFU counts until day 4. No pH data was reported [162]. Investigating the impact of alum on bacterial and fungal population in poultry litter showed that 10% alum addition decreased the bacterial populations by 50%. It has been hypothesized that the decrease in pH by alum addition caused a decrease in the bacterial population[163].

It has to be noted that the pH impacts the aluminum availability in the water [164,165], and care must be taken to interpret the aluminum toxicity level [166].

The mechanism of alum toxicity on the bacterial cells is not very well elucidated. Some scholars hypothesized that pH reduction and alum addition could cause cell deterioration and consequently negatively affect the bacterial cell wall [167]. However, some researchers have

shown that Al deteriorates the cell wall membrane even in the alkaline condition, [168] further explaining the water uptake changes by disturbing the osmo-regulatory reaction of the cell membrane [169]. Also, it has been described that aluminum binds to the DNA and consequently influences the synthesize of DNA. [170].

Al can substitute Fe, an essential micronutrient; however, Al cannot undergo the rest of the Fe metabolic pathway. Hence, it creates a dangerous situation inside the cells called oxidative environment leading to a dysfunctional cell by interfering with tricarboxylic acid (TCA) cycle [171]. There are some species tolerant to the presence of Al; some of the bacteria can shift in their metabolic pathway in a way that can survive aluminum toxicity; This mechanism is explained for *Pseudomonas fluorescens* survival at 15 mM of Al [171].

Microbiome in the biofilters often faces P-limitation. Applying alum as coagulant prior to biofilter in conventional water treatment systems reduces P availability. In addition, Al residuals from the coagulation-flocculation process are transferred to the biofilters. In a recent study, Barra et al., (2018), investigated the impact of P-limitation and Al-toxicity on growth and performance of the soil bacteria, *Klebsiella* sp. RC3, *Stenotrophomonas* sp. RC5, *Klebsiella sp. RCJ4, Serratia* sp. RCJ6, and *Enterobacter* sp. RJAL6. These bacteria are known to be resilient to a high concentration of Al and P-scarcity. They studied bacterial response in two phosphorus and aluminum levels. Phosphorus was added at high and low concentrations (1.4, and 0.05 mM as KH_2PO_4), and Al was added (0, and 10 mM as $AlCl_3 \times 6H_2O$). It is reported that 10mM is the maximum Al tolerable concentration for the mentioned species [172]. The bacterial growth was reduced by 50% at 0.05 mM of KH_2PO_4 and at 0.003 mM was almost completely inhibited. Decreased growth rate after 24h was determined at high Al concentration and triggered a stationary phase growth. The results showed that *mdh* gene expression was significantly up–regulated under conditions of Al toxicity, P-limitation and

combination of both by the strains *Klebsiella*, *Stenotrophomonas*, and *Serratia* [168]. The *mdh* gene expression has been linked to biofilm formation. This gene encodes the proteins that have been related to adhesion and biofilm formation. An *E.coli* mutated species, *mdh* gene deleted, showed the inability to form biofilm [173]. The phosphorus limitation and Al presence in this study are similar to the condition in the biofilter. Therefore, this could explain why direct biofilters with higher alum dose had higher EPS. It is suggested to examine the *mdh gene expression* in isolated bacteria in the presence of alum and phosphorus limitation condition to explore this hypothesis further.

Cui et al., 2018, studied impact of low concentrations of Al (III) at 0.6 and 2.0 mg/L on biofilm formation. They showed that aluminum residuals stimulated bacterial growth and EPS production due to hormesis. Hormesis is defined as stimulation in bacterial cell caused by lower doses of toxic substances [174]. Also, hydrolysis of membrane outer layer of bacteria cells in presence of Al led to Al- protein bound and created a double layer structure of biofilm hence a thicker biofilm was created [175]. Al (III) induces the ion-bridging in EPS and causes the aggregation of biofilm leading to bio-clogging [176].

C.IV - 3 FLOC INHIBITS NUTRIENT DIFFUSION

Floc, an accumulation and agglomeration of particulate matters, natural organic matter and suspended solids get transferred to the biofilters. These agglomerations can spread non-uniformly and cause a stressed situation, such as blocking nutrient diffusion to the bacteria, in different parts of the biofilter, thus producing more biofilm/EPS.

The various phosphorus limitations levels were investigated, and it was shown that a P limitation can cause higher EPS production. These results prove that in case the uniformity of floc spreading on the top of biofilter causes nutrient diffusing hindrance. EPS production will

be higher in the direct biofiltration compared to the sedimentation- biofilters with fewer floc carryovers.

This hypothesis was assessed by the two isolated bacteria from full-scale drinking water biofilters. Details for this study are presented in Chapter VI.

C.IV - 4   MICROBIAL ACTIVITIES IN FLOC

The last hypothesis is that floc are aggregates of bacteria and suspended solids. In direct biofiltration, more flocs are carried over. Therefore, the concentration of bacteria and their survival in and potential release from the alum complex are of interest to direct biofiltration. It is essential to know the kinetics of bacteria die-off and whether they are released into the biofilter. Bulson et al. (1984) studied bacterial removal during the alum treatment of recreational lake. They studied the fecal coliform (FC), fecal streptococci (FS) and chromogen differences at the surface, mid-layers and bottom of the lake before and after alum treatment and in the different time frames. The significant decrease in the FC and FS and chromogens at the surface and concomitant increase at the bottom 72 hours after alum treatment was observed. Further, it was shown that *E. coli* survived in the flocs. Hence suggested that ingesting flocs by swimmers in the lake may impose a risk to their health, and care must be taken to the die-off bacteria in the flocs [177]. This study triggers the following questions regarding direct biofiltration:

1. Are bacteria in floc contributing to the biological activity in direct biofiltration? This can be measured by ATP, cell count, and EPS.

2. Are bacteria entrapped in floc released into the biofilter? Or how long does it take for floc de-stabilization?

3. What is the kinetic of bacteria die-off in flocs? Understanding the biological activity response versus time.

Chapter V METHOD DEVELOPMENT FOR MICROBIAL CHARACTERIZATION

Development of a high-throughput method with a simplified inoculation and pathlength correction to determine microbial growth rates

Leili Abkar, Florentin M. Wilfart, Marta Piercey, Graham A. Gagnon

Addressing Hypothesis 4, two high biofilm-producing bacteria were isolated from a full-scale drinking water biofilter and identified. Growth curve and maximum growth rates were examined to characterize them. Working with high biofilm-producing bacteria using a microplate reader for characterizing their growth comes with challenges. This chapter identifies and addresses key challenges and verifies the presented solutions. As a result, the two isolated species have successfully been characterized for their growth behaviour. A detailed protocol is presented in Appendix C.

C.V - 1   HIGHLIGHTS

- Developed a high-throughput procedure to obtain bacterial growth curves.
- Verified OD600 readings from microplate reader with spectrophotometer by applying the pathlength correction factor post-hoc.
- Verified repeatability of the protocol to determine reliable maximum growth rates.
- Compared the OD600 reading time intervals and inoculum method for the bacteria investigated.

C.V - 2   GRAPHICAL ABSTRACT
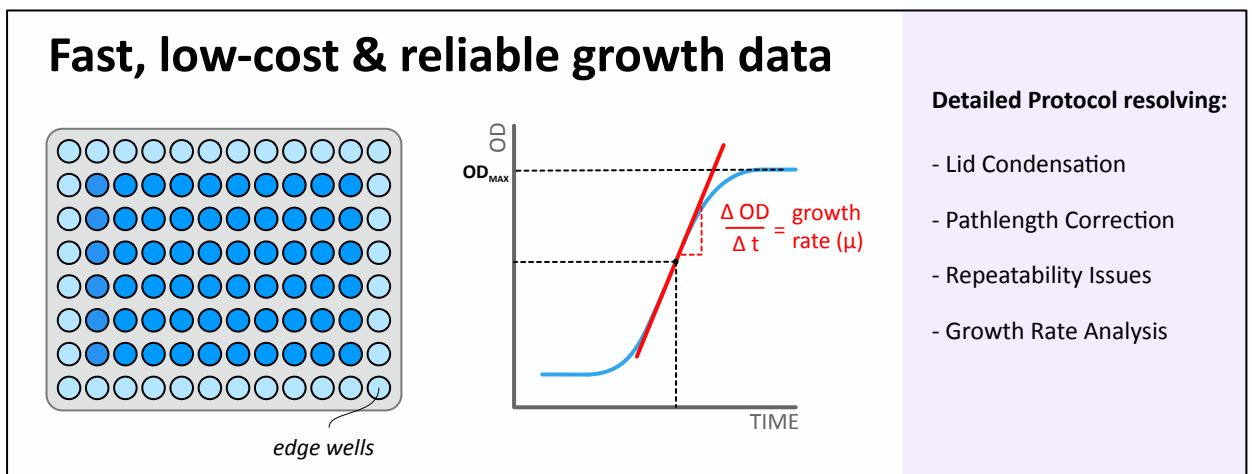
Figure 25   Graphical abstract: Fast, Low-cost & reliable growth data

C.V - 3 SIGNIFICANCE AND IMPACT OF THE STUDY

The importance of lid warming, pathlength correction, and the inoculation method for obtaining reliable, accurate and reproducible data on microplate readers has been shown in detail. The protocol was developed and verified on biofilm producing bacteria. The result of this study can be expanded to other methods using microplate readers and high-throughput protocols.

C.V - 4 ABSTRACT

This study aimed to develop a simple, reliable, and high-throughput protocol for monitoring bacterial growth curves in 96-well plates and analyzing the maximum growth rate. The growth curves and specific growth rates of two isolated bacteria from full-scale drinking water biofilter were determined. In this study, issues including (i) lid condensation, (ii) pathlength correction, (iii) inoculation method, and (iv) sampling time interval were investigated. Ultimately, a rapid, high-throughput protocol to determine maximum growth rates (h^{-1}) of *Bacillus mycoides* (0.99 $\pm$ 0.03) and *Paenibacillus tundrae* (0.85 $\pm$ 0.025) was successfully developed and verified. This protocol and its verification steps can easily be adapted to other instruments and help to determine the run-to-run variation, and most appropriate inoculation size for the system used.

Keywords: High-throughput, bacterial growth curve, maximum growth rate, microplate reader, biofilm-producing bacteria

C.V - 5   INTRODUCTION

Developing interest in multi-omics manipulation, including mechanism and metabolic studies of bacteria, highlights the importance of high-throughput and automated recording of growth data [178,179]. Growth data, including kinetic parameters such as specific growth rates, helps to characterize bacterial responses to different physical, chemical, and antibacterial conditions. Growth rate data are a standard response variable utilized to uncover potential genotype-phenotypes linkages [178], or indicate the microbial safety and the shelf life of produce [180,181]. Techniques such as adaptive laboratory evolution (Choe *et al.*, 2019, Dykhuizen and Dean, 1990; McDonald, 2019), genome-wide screening, some chemical assays [183], and various forward genetic screens [184] rely on growth rates to evaluate the results.

C.V - 5.1   Optical Density as Measure of Bacterial Growth

Optical Density (OD) measurements of bacterial cultures are a standard microbiological method to monitor bacterial growth. OD measurements are often recorded at a wavelength of 600 nm, relying on light scattering related to the cell density based on the Beer-Lambert law [185,186]. The Beer-Lambert law explains the dependency of the OD values to the concentration (i.e., cell density, cell number), pathlength, and absorptivity coefficient. The geometry and optical system of a spectrophotometer influence the OD readings [186].

C.V - 5.2   Microplate Readers for Automated Optical Density Measurements

Classical methods of OD measurements can be very time and labor-intensive, and the data can carry a variety of human errors. Using a microplate reader can decrease analyst time [187,188] and also exposure time for samples to be biologically contaminated. High-throughput analysis using microplate readers is already broadly applied in the screening of biofilm-

producing bacteria [189,190], bacterial growth inhibition [191], yeast cell growth [192], determination of antifungal susceptibility [193], and toxicity screening of nanomaterials [194].

While few researchers have published protocols to determine specific bacterial growth rates using a microplate reader [187,195,196], the ability of a protocol to cope with bacterial species that can be difficult to assay or other factors remains of interest to many. Factors such as sealing tapes may impact the repeatability due to oxygen transfer inadequacy in a 96-well plate [197,198] or the type of species may produce relatively noisy data [199–201]. However, factors such as condensation on the lid, inoculation size, pathlength correction in combination with sampling time interval are not fully investigated in sensitive bacteria such as biofilm producing bacteria.

C.V - 5.3 Aim of this Study

This study presents a protocol for monitoring bacterial growth and measuring specific growth rates using a microplate reader. The protocol is verified with two recently isolated biofilm-producing bacteria from a full-scale drinking water biofilter. These species were used as their fast growth and biofilm-producing character traditionally proof to be challenging in both manual and automated approaches. Key factors influencing data quality and repeatability are studied, including (i) importance of pathlength correction by comparison to a spectrophotometer data, (ii) avoidance of noise and data fluctuation caused by the lid condensation, (iii) the inoculum preparation method and (iv) OD600 readings time interval.

C.V - 6 MATERIALS AND METHODS

C.V - 6.1 Bacterial Strain Isolation and Identification

Two bacterial species were isolated from full-scale drinking water biofiltration. These biofilters are located in JD Kline water treatment facility, Halifax, NS treating the water from nearby lake. Pockwock lake is characterized as a low alkalinity, low turbidity and low organic carbon water resource[40]. Species were isolated from the filter media, anthracite, for their ability to produce biofilm. The bacterial species were then identified by full-length16S rRNA compared to the BLAST data base as *Bacillus mycoides* (SAMN10518261) and *Paenibacillus tundrae* (SAMN10452279).

C.V - 6.2 Microplate Reader Settings

Using the embedded software, Gen5 (version 3.08, BioTek Instruments Inc., Winooski, VT, US), a protocol was created in which temperature, runtime intervals and OD600 reading were set at 30°C, 24 hours, and 30 minutes, respectively. Continuous shaking in the protocol was set at frequency of 9.45 Hz. The temperature gradient was set at 1°C higher than the plate which provided the lid warming. Non inoculated media used as control samples to measure the background OD and deducted from the reported OD600.

C.V - 7   PROTOCOL VERIFICATION

C.V - 7.1   Determination of Pathlength Correction Factor

To verify the OD600 readings from the microplate reader (Synergy H1, BioTek Instruments Inc., Winooski, VT, US), a culture of *Bacillus mycoides* in TSB was used (Method 2). The culture was incubated in the benchtop shaker incubator as explained below. Culture samples were taken from flasks to be read by the microplate using a 96 well plate and a UV fused quartz cuvette (1cm pathlength) in a spectrophotometer (DR 5000TM UV-Vis, Hach, Loveland, Colorado, US) at 600 nm.

A pathlength correction factor was determined, following the manufacturer's instructions (BioTek Instruments Inc.,): The 200μL of DI water was transferred to a 96-wellplate (Polystyrene, flat bottom, clear, sterile, Corning® Coastar®, New York, US) to fill up the non-edge wells with a transparent lid (Polystyrene, clear, sterile, Corning® Coastar®, New York, US). The absorbance was measured using the microplate reader at 977 nm and 900 nm and then subtracted (A977-A900). The determined value was then divided by the reference value of water (0.18 for A977-A900, at 23°C). The average result of all non-edge wells was the pathlength correction factor. It was applied to all the OD measurements (dividing all the OD values by correction factor) for monitoring growth curves obtained from the microplate reader.

C.V - 7.2   Resolution of Lid Condensation

Lid condensation was observed during an earlier version of this protocol not including lid warming and was observed causing data fluctuations and unreliable results. To inhibit this phenomenon, which happens due to the temperature difference between the top and bottom of the well plate, the lid temperature was set 1°C above the incubation temperature. The

growth data presented is based on the final protocol including the lid warming to reduce condensation. Temperature changes in the microplate reader were measured for 92 hours incubation as 30.03 ± 0.04 (mean $\pm$ SD) and data is shown in supplementary data Figure 24.

C.V - 7.3 Inoculum Preparation and Culture Conditions

Two inoculum methods were compared as follows.

C.V - 7.3.1   *Inoculum method 1*

50 μL of glycerol stock were added to 10 mL of fresh Tryptic Soy Broth (TSB) in a 15 mL centrifuge tube and incubated overnight at 30°C and 150 rpm. Then, 500 μL of overnight culture were transferred to fresh TSB and incubated in a shaker incubator (Innova 40, New Brunswick Scientific Co., Edison, NJ, USA) at 150 rpm and 30°C to mid exponential phase. Cells were harvested and the bacterial suspension adjusted to an OD600 of 0.6 ± 0.05 and was adjusted to a 5% (v/v) inoculum to transfer to the 96-well plates.

In flask studies, for comparing the results in spectrophotometer and microplate reader, Method 1 (5%) was used. A large volume of inoculated TSB (5% v/v) was prepared, with 100 mL volumes transferred into 250 mL flasks, in triplicate. Flasks were incubated with shaking at (150 rpm) at 30°C.

C.V - 7.3.2   *Inoculum method 2*

50μL of glycerol stock were added to 10 mL of fresh Tryptic Soy Broth (TSB) in a 15 mL centrifuge tube and incubated overnight (15-16hrs) at 30°C without shaking. The OD600 of the overnight culture was 0.65±0.05 for *P. tundrae* and 0.96 ± 0.05 for *B. mycoides*. 100μL of the overnight culture were then transferred to 10 mL fresh TSB (1% inoculum size).

For 96-well plates (Polystyrene, flat bottom, clear, sterile, Corning® Coastar®, New York, US), 200 µL of inoculated TSB was transferred to twelve non-edge wells in the microplate. Each well represents a microbiological replication. The wells located on the edges were filled with the same volume of distilled water as the sample volume, to reduce evaporation. A column in the micro-plate consisting of 6 wells was loaded with the TSB not inoculated as blank samples. A transparent lid (Polystyrene, clear, sterile, Corning® Coastar®, New York, US) was placed before loading the well plate in the reader.

C.V - 7.4 Sample Reading Time Intervals

Different time intervals of as 30 min and 1 hour were examined by changing the set time in the protocol to study the impact of the reading interval frequency on the growth rate estimation.

C.V - 8 GROWTH DATA RECORDING AND ANALYSIS

Growth rates were determined using the equation below:

$$\mu = \left. ln \frac{OD_i}{OD_{i-1}} \middle/ (t_i - t_{i-1}) \right. \tag{1.}$$

In which µ is growth rate, OD_i is the OD600 in each time point, OD_{i-1} is the initial OD600 value in last time point, t_i, t_{i-1} are times differences between two points. The mean of five consecutive growth rates was determined then the greatest mean was evaluated which is the maximum growth rate (μ_m) [195].

C.V - 9 STATISTICAL ANALYSES

The outliers in maximum growth rates were determined and removed based on ± 1.5 times the inter quartile range of each run. Data were tested for normality using the Shapiro-Wilk test. The non-parametric analysis of variance (ANOVA, $\alpha = 0.05$) was performed to determine the differences between the runs in a 96-well plate. A post-hoc test, Dunn's multiple comparison, identified which means were different. To detect the growth rate differences between two isolated species, all the measured growth rates were pooled together ($\sim$n = 36) and a non- parametric Mann-Whitney test ($\alpha = 0.05$) with two-tailed P-value calculation was used. All statistical analyses were performed using Microsoft Excel and Graph-Pad Prism Version 8.4.2 for Mac (GraphPad Software, San Diego, CA, USA, www.graphpad.com).

The term repeatability is defined as the deviation of the results in the replications on the same measurements. Repeatability refers to measuring the same subject under same condition, same apparatus with same operator. Normally is demonstrated by the standard deviation [202]

The sample size of 12 for growth rate data in three separate technical runs resulted in a high statistical power of 0.9.

C.V - 10 RESULTS AND DISCUSSION

C.V - 10.1 Protocol Verification Results

C.V - 10.1.1   *Impact of Pathlength Correction*

Split samples of *B. mycoides* culture were taken at different time points and measured by both, the microplate reader and the spectrophotometer (Figure 1a).

The obtained OD600 data did not match between the two devices (Figure 1a). However, the OD readings from the two instruments correlated well. The correlation was linear with a slope of 0.55, (95% CI:0.53-0.58) and $r^2= 0.99$. The goodness of fit test evaluated the Root Mean Square Error (RMSE) and standard error of estimate (Sy.x) to be 0.01 proving the high accuracy of predicting the correlation line. The correlation (linear regression) indicated (Figure 1b) that there is a constant offset (slope) between two instruments.
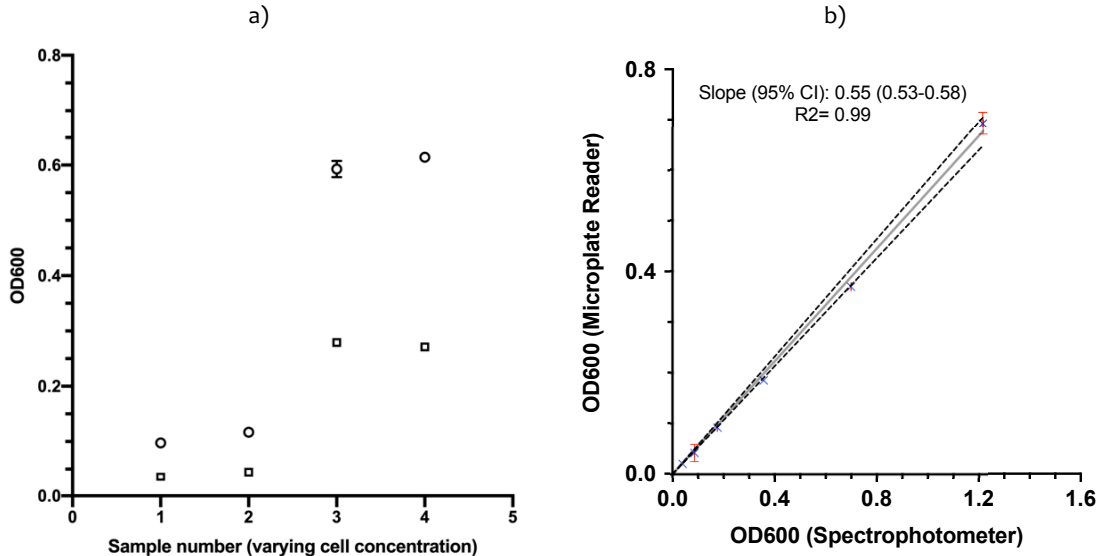
Figure 26   a) Comparing OD600 data from the microplate reader ( ) and spectrophotometer (O) for the split samples. b) correlation between the two instruments. The dashed line shows the 95% confidence interval for the correlation line.

Investigating this issue further, missing pathlength correction was identified as the root cause of the offset. The pathlength correction factor was then determined as explained in the material and methods to be 0.54 ± 0.01 (mean $\pm$ SD) for the specific sample volume, plate, and lid type used. As shown, the offset or slope (0.55) and the measured pathlength correction factor (0.54 ± 0.01) matched. Not only does this show the absolute necessity to use the pathlength correction step to obtain correct OD readings, but also that the factor can be applied retrospectively to achieve correct results.

Spectrophotometers perform based on horizontal photometry, which depends on the physical geometry of the cuvette, as opposed to vertical photometry in the microplate readers, which varies based on the volume and therefore height of the solution in each well. The volume used in each well in this study was 200 μL and the pathlength of the spectrophotometer cuvette is 1 cm. The microplate reader required a pathlength correction to produce comparable results, which is consistent with the literature (Matlock et al., 2011). Uncorrected data from the microplate reader would lead in OD600 values that result in underestimated maximum growth rate and maximum OD600 values. The sample volume directly impacts the light pathlength based on Beer Lambert Law. Therefore, factors such as evaporation with impact on the solution height and consequently the pathlength in each well must be considered. Using continues shaking in microplate reader, the evaporation rate demonstrated no significant impact on the bacterial growth[203]. In this protocol continues shaking was applied.

C.V - 10.1.2 *Impact of Lid Condensation*

Another issue encountered, was condensation buildup on the 96-well plate lid. Lid warming of 1°C above the sample temperature (30°C) resulted in a substantial reduction of noise in the recorded data (see Figure 27a). Significant condensation buildup is visible after 24h without lid warming as depicted in Figure 27b compared to Figure 27c using lid warming step included in the protocol.
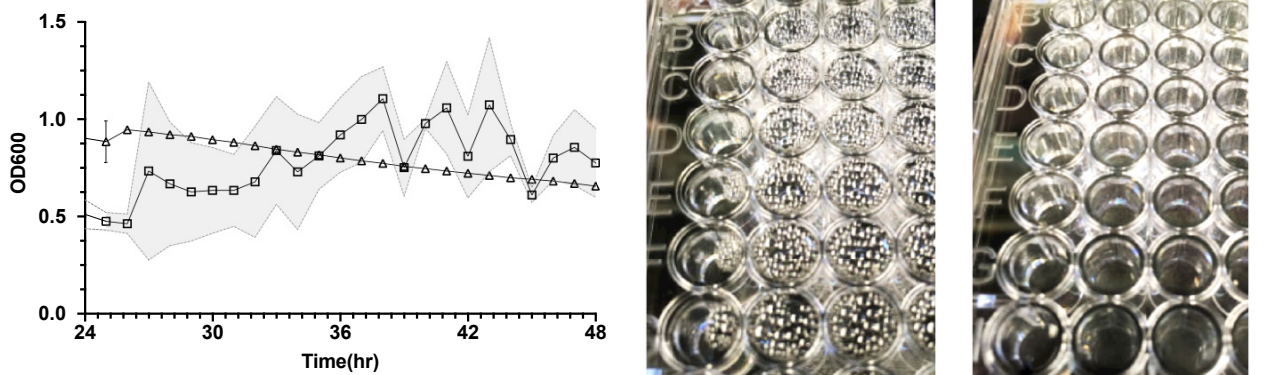
Figure 27   (a) Sample data representing the OD600 readings with lid condensation buildup ( ) and after including the lid warming step (△). Standard deviation is shown as band on ( ) and as error bars on (△).

(b) Condensation buildup on the lid during incubation in 24h.

(c) No condensation when using a temperature gradient of 1°C in 24h on the lid.

Hart et al., (2019) also observed heavy condensation using a 96-well microplate to study time-lapse fluorescence microscopy, despite a temperature-controlled environment. They resolved the condensation with warming the lid by 0.68 ± 0.44 °C above sample temperature using an additional heating plate [204].

The lid warming step, temperature graduation of 1°C, in the current study inhibited the condensation accumulation on the lid during the growth curve data collection.

C.V - 10.1.3 *Impact of the Inoculation Method*

The inoculation method used directly impacted the standard deviation, standard error and fluctuation between OD600 readings. As observed the fluctuation is higher at the end of log phase and stationary phase for both species (Figure 28). It was concluded that using method 2 reduced the OD600 data noise.

(a)

(b)

(c)

(d)
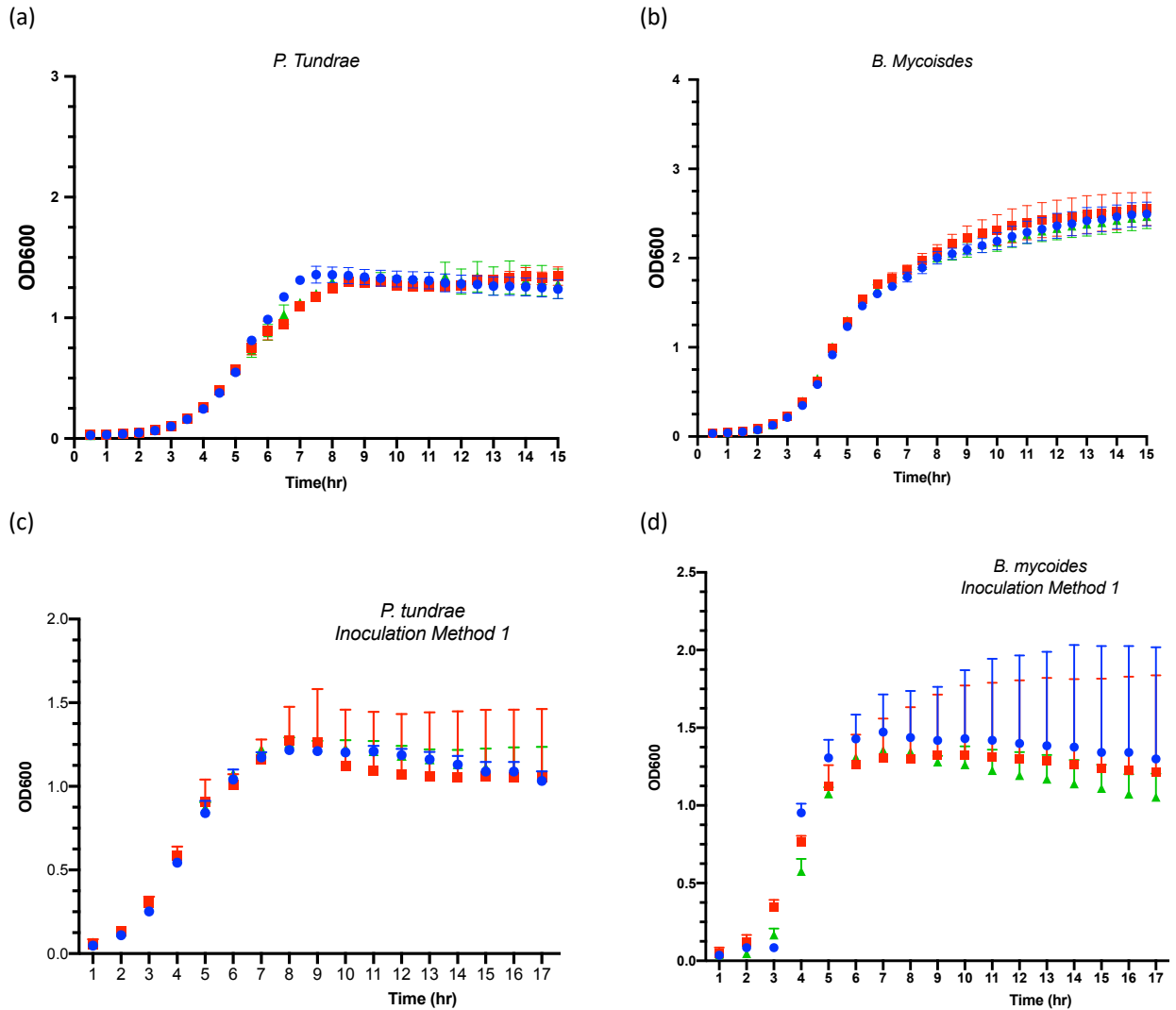
Figure 28   Growth curves for two species in (a) *P. tundrae* and (b) *B. mycoides* with 1% inoculation and a 30-minute sampling time interval (c) *P. tundrae* and (b) *B. mycoides* with 5% inoculation and one-hour time interval. Three runs including run1 (○), run2 ( ), and run3 (Δ) represent separate technical replication. The x-axis shows growth time in hours and the y-axis represents OD values at 600 nm. Each point is an average of at least 6 measurements for (a) and (b). Error bars represent the standard deviation. The growth curves with 1% inoculation have lesser standard deviation and each point falling within the standard deviation.

Using method 1 (5% inoculation size) and the affinity of the bacteria to produce biofilm could result in dense biofilm clusters falsely reflecting on the sample OD. The OD readings may become unreliable, as cells can agglomerate, resulting in highly noisy data. Method 2 (1% inoculation size) resolved this issue and was used for the remainder of the experiments (Figure 28 a and b).

C.V - 10.1.4 *Impact of Sample Reading Interval*

The method chosen for growth rate calculation in this study uses the maximum average slope of five consecutive time points in the log phase.

To ensure reliable results, a high enough temporal resolution is required. Reading intervals have to be set in a way that the log phase readings include more than five timepoints. As shown in Figure 28 c and d, one-hour reading intervals barely contain five timepoints in the log phases for both species while thirty-minutes time interval provide sufficient timepoints to identify the highest slope in the log phase. One-hour reading interval underestimates the specific growth rate as it cannot capture the highest slope in the log phase. The maximum growth rate for *B. mycoides* with one hour and 30 minutes sampling interval is 0.66 and 1.03, respectively. For detailed results please see "Supplemental material- Table 11"

C.V - 10.2 Growth Data

Applying pathlength correction, lid heating, inoculation method 2, and 30-minute reading intervals, the growth curves for *B. mycoides* and *P. tundrae* were recorded.

The results are depicted in Figure 28a and b. The X-axis shows time (hr) and the Y-axis shows OD600 values collected automatically by the microplate reader. Each of the three runs represents a technical replication on a different date.

Growth rates of the two species in each run were calculated and presented in Figure 29a and 29b. To assess the repeatability between runs, the growth rates in the three separate technical runs were compared and found to be not significantly different (non-parametric ANOVA, Kruskal-Wallis, P > 0.05). A post-hoc Dunn test also showed no significant difference between any two runs.
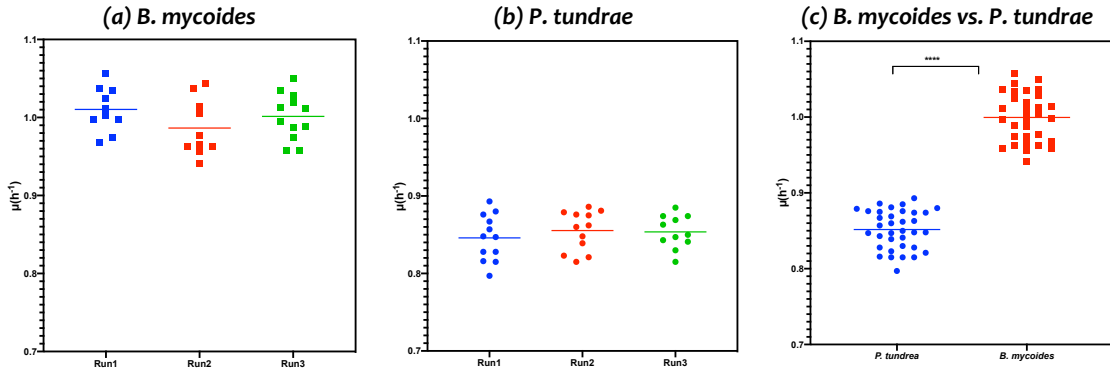
Figure 29   Maximum growth rate (h^{-1}) in three separate runs for (a) *B. mycoides* and (b) *P. tundrae*. The maximum growth rate for each run represented as mean (± SD) and [95% CI]. Comparing the maximum growth rates in different technical runs and for both species using Kruskal-Wallis test (B. mycoides P-value: 0.29, *P. tundrae* P-value: 0.69) demonstrated repeatability between the runs. (c) Growth rates (h^{-1}) for *P. tundrae* (○) and *B. mycoides* ( ) are significantly different (Mann-Whitney, P< 0.0001).

This demonstrates the repeatability and accuracy of the protocol to obtain reliable results for high biofilm-producing bacteria. Additionally, a standard deviation of the growth rate for each run is 0.03 further showing the repeatability of this protocol. For detailed results, please see Supplemental material – Table 12-15.

Pooling all growth rate data for each bacterium, resulted in a maximum growth rate (h^{-1}) of 0.99 ± 0.03 for *B. mycoides* and 0.85 ± 0.025 for *P. tundrae*. These results align with a maximum growth rate of 1.08 h^{-1} for *B. mycoides* (30 °C, nutrient rich medium) in the literature [205].

The maximum growth rates for the two species were confirmed to be significantly different (Mann-Whitney, P< 0.0001) (Figure 29c). This illustrated the ability of the protocol

to differentiate the bacterial growth rates for various biofilm producing species with a high sensitivity.

As represented in Figure 28 a and b, the obtained growth curves in three separate runs using method 2 inoculum are fairly similar and lay within their collective standard deviation for both bacterial species. Researchers investigated the impact of the preparation procedure of the inoculum and the variability of growth rate in separate trials [187]. Hall et al., suggests a variability of ± 2.5% for 6-12 replicates per experimental run as reasonable which aligns with the variability in this study. Mira et al. (2017), suggests a V-factor of less than 0.053 as acceptable variability in an individual trial. They define the V-factor as standard error of mean divided by the mean. A lower V-factor reflects a low variability within a run (Mira *et al.*, 2017).

Although no significant differences were observed between the runs for the method 2 inoculum preparation, it is recommended to repeat the technical runs for growth data to assure of the microplate reader noise, fluctuation, inoculum size, and human errors involved in the process are captured.

C.V - 11 CONCLUSIONS

Microplate readers allow for obtaining consistent and repeatable growth rates. This technology minimizes human error and enables high-throughput sampling. The small amount of culture required per sample, makes this approach an attractive, low cost alternative to direct cell counts, using flasks or test tubes.

This article presents a detailed protocol for measurement and analysis of growth data. The protocol was verified with *B. mycoides* and *P. tundrae*. These bacteria were isolated from a full-scale drinking water biofilter for their ability to produce biofilm, making it more challenging to assess them with a microplate reader.

Four major sources of error for reliable and accurate measurements were identified: Lid condensation, pathlength correction, inoculum size and reading interval with major impact on the results.

1. Lid condensation during data collection leads to erroneous and noisy results and was resolved by raising the lid temperature $1°C$ above the incubation temperature.

2. Light pathlength correction is of essential importance for accurate results and can be determined and applied automatically or retrospectively. Data was verified by cross-calibrating with a spectrophotometer and showed the importance of pathlength correction for a specific sample volume, lid, and well-plate type used.

3. It is important, while using this protocol, to consider the inoculum size, as too large inoculum sizes can lead to erratic reading results when the density increases too rapidly and unevenly during incubation.

4. Reading intervals impact the growth rate calculation based on the methods applied for the calculation. When using the numerical method described, the reading intervals need to be frequent enough to capture numerous data points in the log phase as otherwise the resultant growth rate will be underestimated and inaccurate.

Microplate readers provide the opportunity of having large sample size which can increases the statistical power and subsequently reliable growth rate calculations while cost and labor remain low.

Although repeatability of data in different runs were investigated and showed no significant differences for growth rates, it is worthwhile to re-run the experiments to account for the between run variations.

One of the advantages of this protocol is that the method of calculating growth rate could be adjusted with the data collection frequency. It is highly recommended to try higher time interval frequencies (e.g., 30, 10 minutes) when using numerical growth rate models to capture changes with higher resolution and eliminate the risk of under sampling.

C.V - 12 ACKNOWLEDGMENTS

C.V - 13 SUPPLEMENTAL MATERIAL FOR CHAPTER V

The results of the statistical comparison between the runs for maximum growth rates are shown in Table 12 and 13. Pair wise comparison and descriptive analysis are shown in Table 12- 15.

Table 10   Growth rate for two isolated species with two different sampling time intervals

	B. mycoides		P. tundrae	
Time interval	One hour	30 minutes	One hour	30 minutes
Growth rate (average± SD)	0.66 ± 0.03	1.01±0.03	0.58 ±0.03	0.85 ±0.03

Table 11   Post-hoc multiple comparison for *B. mycoides* in three separate runs with 1% inoculum and sampling time interval of 30 minutes

Dunn's multiple comparisons test	Significant?	Adjusted P Value
Run 1 vs. Run 2	No	0.35
Run 1 vs. Run 3	No	>0.99
Run 2 vs. Run 3	No	>0.99

Table 12   Post-hoc multiple comparison for *P. tundrae* in in three separate runs with 1% inoculum and sampling time interval of 30 minutes

Dunn's multiple comparisons test	Significant?	Adjusted P Value
Run 1 vs. Run 2	No	>0.99
Run 1 vs. Run 3	No	>0.99
Run 2 vs. Run 3	No	>0.99

Table 13   Descriptive analysis of growth rate for different runs *P. tundrae* with 1% inoculum and sampling time interval of 30 minutes

Run	Run 1	Run 2	Run 3
Minimum	0.79	0.81	0.81
25% Percentile	0.82	0.83	0.84
Median	0.85	0.86	0.85
75% Percentile	0.87	0.88	0.87
Maximum	0.89	0.88	0.88
Mean	0.85	0.85	0.85
Sd. Deviation	0.03	0.02	0.02
Sd. Error of Mean	0.008	0.007	0.006
Lower 95% CI	0.83	0.84	0.84
Upper 95% CI	0.87	0.87	0.87

Table 14   Descriptive analysis for growth rate *B. mycoides* with 1% inoculum and sampling time interval of 30 minutes

Run	Run 1	Run 2	Run 3
Minimum	0.97	0.94	0.96
25% Percentile	0.99	0.96	0.97
Median	1.01	0.97	1.00
75% Percentile	1.03	1.02	1.03
Maximum	1.06	1.04	1.05
Mean	1.01	0.98	1.00
Sd. Deviation	0.03	0.03	0.03
Sd. Error of Mean	0.008	0.01	0.008
Lower 95% CI	0.99	0.96	0.98
Upper 95% CI	1.03	1.01	1.02

Table 15   Growth rate measured for each species in three separate runs in two forms of mean [95% confidence interval] and mean (± standard deviation) using inoculum method 2 and 30 minutes OD reading time interval.

	B. mycoides **[95% CI] (± SD)**	*P. tundrae* **[95% CI] (± SD)**
Run 1	1.01 [0.99-1.03] (± 0.03)	0.85 [0.83-0.87] (± 0.03)
Run 2	0.99 [0.96-1.01] (± 0.03)	0.85 [0.84-0.87] (± 0.03)
Run 3	1.00 [0.98-1.02] (± 0.03)	0.85 [0.84-0.87] (± 0.02)

Table 16   Temperature changes inside the microplate reader for 92 hours incubation at 30 °C

Time	T°	Time	T°	Time	T°
0:59:10	30	31:59:10	30.1	62:59:10	30.1
1:59:10	30.1	32:59:10	30	63:59:10	30
2:59:10	30	33:59:10	30	64:59:10	30
3:59:10	30	34:59:10	30	65:59:10	30
4:59:10	30	35:59:10	30	66:59:10	30
5:59:10	30	36:59:10	30	67:59:10	30
6:59:10	30	37:59:10	30	68:59:10	30
7:59:10	30	38:59:10	30	69:59:10	30
8:59:10	30	39:59:10	30.1	70:59:10	30.1
9:59:10	30.1	40:59:10	30	71:59:10	30
10:59:10	30.1	41:59:10	30	72:59:10	30
11:59:10	30	42:59:10	30.1	73:59:10	30
12:59:10	30	43:59:10	30	74:59:10	30
13:59:10	30	44:59:10	30	75:59:10	30
14:59:10	30	45:59:10	30.1	76:59:10	30
15:59:10	30.1	46:59:10	30	77:59:10	30
16:59:10	30	47:59:10	30	78:59:10	30
17:59:10	30	48:59:10	30.1	79:59:10	30
18:59:10	30.1	49:59:10	30.1	80:59:10	30.1
19:59:10	30.1	50:59:10	30.1	81:59:10	30
20:59:10	30	51:59:10	30	82:59:10	30
21:59:10	30	52:59:10	30	83:59:10	30.1
22:59:10	30	53:59:10	30.1	84:59:10	30.1
23:59:10	30.1	54:59:10	30	85:59:10	30
24:59:10	30.1	55:59:10	30	86:59:10	30.1
25:59:10	30	56:59:10	30	87:59:10	30
26:59:10	30.1	57:59:10	30.1	88:59:10	30
27:59:10	30	58:59:10	30.1	89:59:10	30.1
28:59:10	30	59:59:10	30.1	90:59:10	30.1
29:59:10	30	60:59:10	30	91:59:10	30
30:59:10	30.1	61:59:10	30	92:59:10	30.1

Chapter VI NUTRIENT DIFFUSION LIMITATION BY FLOC ACCUMULATION

Isolation, and characterization of biofilm-producing bacteria from drinking water biofilter; P limitation impact on biological responses

Unpublished Manuscript

Chapter III established that sedimentation reduced EPS levels and head-loss accumulation rates for biofilters, leading to higher filter runtime in comparison to direct biofiltration. This chapter investigates the root-causes for this observation.

The following hypothesis was tested:

Floc carryover reduces the diffusion of nutrients to bacteria. Low nutrient conditions cause stress leading to an increased formation of EPS.

C.VI - 1 ABSTRACT

In direct biofiltration due to the absence of a clarification step, a large portion of formed flocs get transferred to the biofilter. In Chapter III, sedimentation deployment showed improvement in hydraulic performance and lowered extracellular polymeric substances (EPS). It is hypothesized that the accumulation of flocs on top of the biofilters may cause inhibition of nutrient diffusion to the bacteria in formed biofilm on media, consequently creating a nutrient-limited environment. To investigate the impact of nutrient limitation, P as an essential macronutrient for bacteria was selected. A minimal medium (M63) with specific components was chosen to simulate the low nutrient condition in drinking water. The minimal media provided the possibility of adjusting the P levels and control the availability of other constituents. Two of the most biofilm-producing bacteria were isolated from a full-scale biofilter, provided the opportunity to study the indigenous biofilter bacteria. The isolated bacteria were identified using full-length 16S rRNA and characterized. The biological behavior of the species of P was studied under different P-limited conditions. Results showed that carbohydrate and protein-EPS were increased when decreasing the available P in the medium while the ATP level decreased and reached a plateau. It can be concluded that the possible nutrient inhibition due to floc buildup can led to excess EPS formation.

Keywords: EPS production, Phosphorus limitation, *B. mycoides*, *P. tundrae*, biofilm architecture

C.VI - 2 HIGHLIGHTS

- Two cultivable, and highest biofilm producing bacteria were isolated from drinking water biofilter successfully.
- Isolated bacteria were identified based on full-length 16srRNA.
- The biofilm architecture of *B. mycoides* and *P. tundrae* was studied.
- The biofilm related genes were identified through extensive literature search and compared and identified to the genome maps of two isolated species. The isolated bacteria possess the 140 genes responsible for biofilm production.
- Extracellular Polymeric Substances chemically characterized with carbohydrate, protein, and extracellular DNA.
- Phosphorus limitation influence on biological behavior, ATP and EPS was studied.

C.VI - 3 ABBREVIATIONS

- Natural Organic Matter (NOM)
- Dissolved Organic Carbon (DOC)
- Extracellular Polymeric Substances (EPS)
- Optical Density (OD)
- Tryptic Soy Agar (TSA)
- Tryptic Soy Broth (TSB)
- Phosphate-buffered Saline (PBS)
- Crystal Violet (CV)
- Ribosomal Database Project (RDP)
- National Center for Biotechnology Information (NCBI)
- Molecular Evolutionary Genetics Analysis (MEGA)
- Critical Drying Point (CDP)
- Adenosine Triphosphate (ATP)
- Extracellular DNA (e-DNA)
- National Center for Biotechnology Information (NCBI)

C.VI - 4 **RATIONALE**

Flocs are an accumulation and agglomeration of particulate matter, natural organic matter, and suspended solids that are largely transferred to the biofilter when no clarification/sedimentation is present. Flocs can accumulate non-uniformly and cause varying levels of nutrient limitation for the microorganisms in different parts of the biofilter. Nutrient limitation has been shown to cause an increased EPS production, suggesting non-uniformly spread floc on the top of the filter media as a possible root-cause for increased EPS in direct biofiltration compared to biofilters with sedimentation.

C.VI - 5 **INTRODUCTION**

Bacteria in biofilters remove natural organic matter (NOM) and other contaminants in the source water through their metabolism, thus treating water [206]. However, under stressful conditions such as a low nutrient environment, oxidant addition (i.e., chlorine, hydrogen peroxide, ozone, etc.,), and high shear stress excess EPS is produced by bacteria (Evans, 2013; Fang et al., 2009; Liu et al., 2006). Excess EPS is reported to be linked with the accelerated head-loss accumulation rate and consequently shorter filter runtime in biofilters [120].

In conventional drinking water treatment systems, coagulation and flocculation is a common method to aggregate the fine particles to form larger, settleable flocs prior to a sedimentation, clarification, or filtration process [209]. Coagulation partially removes the NOMs, mostly the dissolved organic carbon (DOC) [210], inorganic material (iron and phosphorus), viruses, and bacteria [211]. Coagulation specifically has been used to remove P in discharge from municipal and industrial wastewater treatment plants [212,213]. Alum (aluminum sulfate), a coagulant, has been widely used to control the P release of the lake sediment since the 1970s [214]. Therefore, using alum in water treatment facilities can unintendedly lead to the reduction

of already low P level in drinking water biofilters. As P is an essential nutrient for microbe growth, its removal by chemical coagulation may subsequently impact the biological behavior of drinking water biofilters microbiome negatively. Also, it is hypothesized that the physical clogging by the flocs carried over to the biofilters may cause the nutrient diffusion limitation to the biofilm bacteria.

The relationship between the nutrient limitation and reduction, and consequently the bacterial biological activity, is not very well understood.

Lack of essential nutrient, starvation, showed to co-regulate with the quorum-sensing pathways and led to the production of biomolecules which are involved in the surface's attachment in stationary phase [215]. Thompson et al. (2006), reported lower biofilm cell counts at lower nutrient concentrations. They studied four different nutrient ratios (C:N:P) and concluded that the ratio is influential on biofilm formation. They observed no statistically significant differences by the phosphorus level changes. However, varying nitrogen concentration showed significant differences [216]. A C:N:P ratio of 100:10:1 is the most referenced ratio to achieve optimum growth and inhibit the excess EPS production in drinking water [53,217–219].

Wong (2015) stated that the so called optimum nutrient ratio of (C:N:P) 100:10:1 is "ill-suited" (p-23) and evaluated the nutrient amendment strategies described by Lauderdale et al., 2012 were invalid as they could not be reproduced by the other researchers [58,206,220–222].

In this study, we focused on investigating the P limitation/reduction, as an essential macronutrient, and its impact on the biological activities. Most of the P limitation studies were done on the mixed culture of either drinking water distribution or biofilter microbiome.

Effective P level reduction in drinking water distribution systems (DWDS) was found to be influential in restricting the microbial re-growth [223,224]. In biofiltration, the P limited condition was reported to cause higher production of EPS that negatively impacted the biofiltration performance [117,225].

While few researches studied the P limitation on pure culture, none of them used the bacterial species isolated from drinking water biofilters.

In the current study, two of the most biofilm-producing bacteria were isolated from full-scale drinking water biofilter and characterized. The bacteria were identified using the 16s rRNA genes sequencing and submitted to the National Center for Biotechnology Information (NCBI). Biofilm architecture of these bacteria in the minimal media were characterized. Biofilm related genes were identified in their genome maps. The impact of the P reduction in the low nutrient media (minimal media) on the biological responses of the isolated bacteria was investigated.

C.VI - 6 Materials and Methods

C.VI - 6.1 Sample Collection

Samples were collected in 50 mL pasteurized tubes from the media on the top of a full-scale drinking water biofilter and topped up with the water from the biofilter. Biofilters are located at the J. D. Kline Water treatment facility, Halifax, Nova Scotia, Canada which drew the water from the nearby lake. Pockwock Lake is characterized as low organic carbon, turbidity, and alkalinity water resource [38,131,226]. Biofilters are dual media and include anthracite (60 cm) on top and sand (30 cm) at the bottom. This plant is a direct biofiltration containing eight biofilters 8.5 ×17.1 × 3.7 (m) [L × W × H] with an average capacity of 82 ML/day [39].

C.VI - 6.2 Biofilm Bacteria Extraction

Upon the collection, samples were stored at 4 °C and transferred to the lab. Water on top of the samples were decanted and then media were washed three times with sterilized phosphate-buffered saline (PBS) (pH7.4 Bioreagent, Biotech Performance Certified, Sigma-Aldrich, MO, USA) in a sterilized environment. Two grams of the media were suspended in 10 mL of PBS, then submerged in a sonicated bath (Fisher Scientific Ultrasoni, FS30D, PA, USA) for one minute, put on ice for one minute, and vortexed vigorously for five seconds. This procedure was repeated five times to extract the bacteria in the biofilm from the anthracite [10].

C.VI - 6.3 Isolating Biofilm-Producing Bacteria

Bacterial isolation was done using the dilution streaking method on tryptic soya agar (TSA) (BD Difco™, Becton, Dickinson and Company, NJ, USA) plates. All the plates were incubated at 30ºC for 48 hours [10] providing enough time for environmental bacteria to grow on the agar plates. Five colonies were selected based on the visually distinguishable morphologies. Their viability was screened in TSB (BD Difco™, Becton, Dickinson and Company, NJ, USA) media. The selected bacteria were stored on TSA plates at 4°C and in 2 mL sterile vials with 20% glycerol (>99.5%, Fisher Chemicals, NJ, USA) in a -80°C freezer (Ultra-Low Temperature Freezers Innova, U101-86, New Brunswick Scientific Co., Inc., CT, USA).

Selected colonies then went through a screening process to select the most biofilm producing bacteria. The biofilm production ability was further evaluated by microtiter biofilm formation assay explained in detail in section C.VI - 6.5.

C.VI - 6.4 Minimal Media Preparation

The minimal media used was based on the recipe of the M63 containing 3g KH_2PO_4 (>99%, Fisher Chemicals, NJ, USA), 7g K_2HPO_4 (>99%, Fisher Chemicals, NJ, USA) and 2g $(NH_4)_2SO_4$ (>99%, Fisher Chemicals, NJ, USA) in 1 L of D.I. water. Magnesium sulfate (>99%, Fisher Chemicals, NJ, USA) (1mM), Glucose (>99%, Fisher Chemicals, NJ, USA) (0.2%) and L-arginine hydrochloride (MP Biomedicals, LLC, OH, USA) (0.4%) and $FeSO_4.7H_2O$ (>99%, Fisher Chemicals, NJ, USA) (0.5 mg/L) were added [190]. The minimal media was chosen to provide a well-defined constituents medium facilitating to adjust the components and concentration for the P reduction experiments.

C.VI - 6.5 Screening of Biofilm-Producing Bacteria

The biofilm production ability of the five selected colonies were measured and compared using the microtiter biofilm formation assay [190]. Inoculum with Optical Density (OD) of 0.6±0.05 was added to the fresh TSB and vortexed for 10 seconds. 100 μL of the inoculated TSB was then transferred to a 96-well plate reader with 6 replications for each species. The 96-well plate was incubated at 30 °C for 24 h. After incubation, the planktonic cells were removed, and the microplate was gently submerged twice in a small water tub to reduce the background staining.125 μL of 0.1% crystal violet (CV) (>95%, Alfa Aesar, MA, USA) was added to each cell and then incubated for 15 minutes at in room temperature. The plates were washed 3 times in a small water tub and airdried overnight. To quantify the CV staining, a 125 μL of 30% acetic acid (99.7%, BDH, London, UK) was added to each well and incubated for 15 minutes. Then the solubilized CV was transferred with a pipet to a new 96-well plate (Polystyrene, flat bottom, clear, sterile, Corning® Coastar®, NY, US). The absorbance was quantified at OD_{550} nm by microplate reader (Synergy H1, BioTek Instruments

Inc., VT, US) and reported as biofilm production [190]. Two bacteria with higher OD_{550} nm were selected.

C.VI - 6.6 Bacterial Identification

The bacterial identification was performed based on the full-length 16S rRNA sequences. The isolated bacteria were sent to the Integrated Microbiome Resources (IMR) lab (Halifax, NS, Canada) for DNA extraction, amplification and whole genome sequencing. The sequence data were compiled based on the full-length16S rRNA and were examined for sequence homology with the archived 16S rRNA sequences from GenBank employing BLASTN (https://blast.ncbi.nlm.nih.gov). The identification was based on the highest query cover and identity percentage. The results from BLASTN were then compared with Ribosomal Database Project (RDP) (http://rdp.cme.msu.edu), and EZ-Biocloud (https://www.ezbiocloud.net) to confirm the correct identification of the isolated bacteria.

The whole genome sequence of two bacterial isolates were submitted to the National Center for Biotechnology Information (NCBI) GenBank and the accession numbers were assigned.

Phylogenetic trees, evolutionary relationships of taxa, were constructed using neighbor-joining DNA distance algorithm [227] using Molecular Evolutionary Genetics Analysis (MEGA) software version 7.0 [228]. The bootstrap consensus tree was inferred from 500 replicates [229]. Branches corresponding to partitions reproduced in less than 50% bootstrap replicates are collapsed. The evolutionary distances were computed using the Kimura 2-parameter method [230] and are in the units of the number of base substitutions per site. The rate variation among sites was modeled with a gamma distribution (shape parameter = 2). The analysis involved 10 nucleotide sequences. Codon positions included were 1st+2nd+3rd+Noncoding. All

positions containing gaps and missing data were eliminated. There were a total of 1481 positions in the final dataset. Evolutionary analyses were conducted in MEGA7 [228].

The final step to confirm the biofilm production ability of isolated bacteria was spotting the genes related to EPS/biofilm production in isolated species genome map. The genes tables were reported along with the sequencing data from IMR lab. A literature review on the genes related to the EPS/biofilm production in *Bacillus* sp. was performed. The genes related to the EPS/biofilm production were spotted in both isolated bacteria.

C.VI - 6.7 Investigation of Biofilm Architecture

The polycarbonate disc (1 cm radius) were used as the substratum for biofilm formation to study the biofilm architecture of the isolated bacteria. One sterilized polycarbonate disc was put in the sterilized tube and topped with 10 mL of minimal media and 0.5 mL of the inoculant was added. The tubes were incubated in static condition at 30 °C for 72 hours. The 5 mL of the broth was gently replaced (to ensure not disturbing the formed biofilm) with fresh broth to provide enough nutrients during the incubation.

The discs went through primary fixation with 2.5% glutaraldehyde (Grade I, 25% in H_2O specially purified for use as an electron microscopy fixative, Sigma, Darmstadt, Germany), and secondary fixation of 1% osmium tetroxide (for electron microscopy, 4% in H_2O, Sigma, Darmstadt, Germany). Between the fixation process, samples were washed with distilled water for three times. Samples went through dehydration process with varying ethanol concentration of 25%, 50%, 75%, 90% and 100%. The residence time in each step was 5 minutes. These steps were done in sequence with no time gap in between. The critical drying point (CDP) (EM CPD 300, Lecia microsystem, ON, Canada), was final dehydration step. The CDP was used to replace water in the sample with CO_2 gas. Each sample was then coated with

a layer of gold palladium (thickness of 20 nm) for 260 seconds in a Vacuum sputter (EM ACE200, Lecia microsystem, ON, Canada).

The fixated, and dehydrated samples then were observed under a cold field emission scanning electron microscopy (S-4700, Hitachi High Technologies America Inc., SC, USA) with different magnifications.

C.VI - 6.8 Biological Activities under Phosphorus Limitation

The biofilm formation was investigated under different P levels. The M63 recipe was used for P limitation experiments. The C:P ratio in M63 was 1:1. The glucose and nitrogen concentrations were kept constant while the P concentration decreased to create different C:P molar ratios specifically 1:0.1, 1:0.01, and 1:0.001.

The prepared media was added to the 50 mL volumetric flask including 2 g of 3 mm borosilicate glass beads (Aldrich, CA, USA) in a sterilized environment. The OD of the inoculant was adjusted to 0.6± 0.05 and added at 5% (v/v) to the media. Each flask was incubated for 72 h at 30°C and 150 rpm in a shaker incubator (Innova 40, New Brunswick Scientific Co., Edison, NJ, USA). After incubation, the spent medium was discarded, and the glass beads were processed for ATP and EPS measurements. Note that for each C:P ratio and analysis (ATP and EPS) samples were prepared in triplicates.

C.VI - 6.8.1   *ATP Analysis*

Adenosine Triphosphate (ATP) of biofilm formed on glass beads was measured in triplicate. Deposit & Surface Analysis ATP kit, DSA™ test kit, (LuminUltra Technologies Ltd., NB, Canada) and Luminometer-PhotonMaster™ (Luminometer, LuminUltra Technologies Ltd., NB, Canada) were applied. Glass beads were transferred to a sterile, 50 mL falcon tubes

and analyzed as soon as the samples were collected. ATP reported as per dry weight of glass beads which represent the dry weight of media.

C.VI - 6.8.2   *EPS Extraction*

For EPS extraction from glass beads, samples were incubated at 35°C and 200 rpm in a benchtop shaker incubator (Innova 40, New Brunswick Scientific Co., Edison, NJ, USA) for 4 hours using an extraction buffer (10 mM Tris, 10 mM EDTA, 2.5% NaCl, pH 8). The samples were centrifuged (IEC Centra-CL2, Thermo Electron Co., Needham, MA) at 3600g for 10 minutes. The resulting supernatants were then filtered through 0.45 µm cellulose nitrate membrane filters (Whatman, GE Healthcare Life Science, Buckinghamshire, UK). The filtrate is the EPS in aqueous solution [35].

C.VI - 6.8.3   *Chemical analysis of EPS*

The EPS solution was further analyzed for protein, carbohydrate, and extracellular DNA (e-DNA). Carbohydrate-EPS quantified using phenol sulfuric acid assay based on Dubois method [135]. Protein-EPS was measured using a modified Lowry assay by a Micro BCA™ Protein Assay Kit (Thermo Fisher Scientific, IL, USA). The absorbance of the EPS solution were measured in a microplate reader at 260 nm and reported as e-DNA [17].

C.VI - 7 RESULTS AND DISCUSSION

C.VI - 7.1 Bacterial Identification

The five distinguishable colonies were further purified with the streak plate method to ensure the purity of the selected colony. The biofilm production ability of five bacteria were compared and evaluated using the microtiter biofilm assay in a 96-well plate and microplate reader (Figure 30). Among them the two bacteria (#1 and #3) that produced most biofilm were selected and stored in both agar plates and 2 mL vials in a freezer at -80 °C (Figure 31).
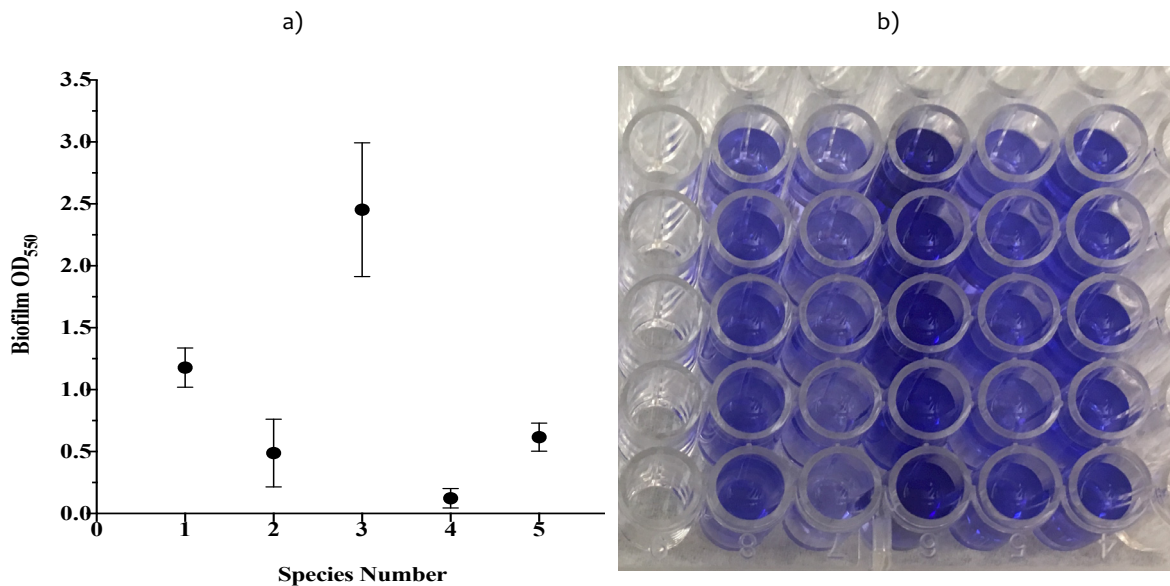
Figure 30   Biofilm development in a 96-well plate. a) Biofilm measured using the microtiter biofilm formation assay at 550 nm; data are average of 5 replicates and the error bars are standard deviations. b) shows the solubilized crystal violet in acetic acid transferred into a fresh 96-well plate for reading OD550 in a microplate reader. The color intensity displays the higher biofilm formation.

The full-length 16S rRNA gene sequence was used to identify the most biofilm forming bacteria as *Bacillus mycoides* and *Paenibacillus tundrae* with NCBI accession number of *SAMN10518261* and *SAMN10452279,* respectively.
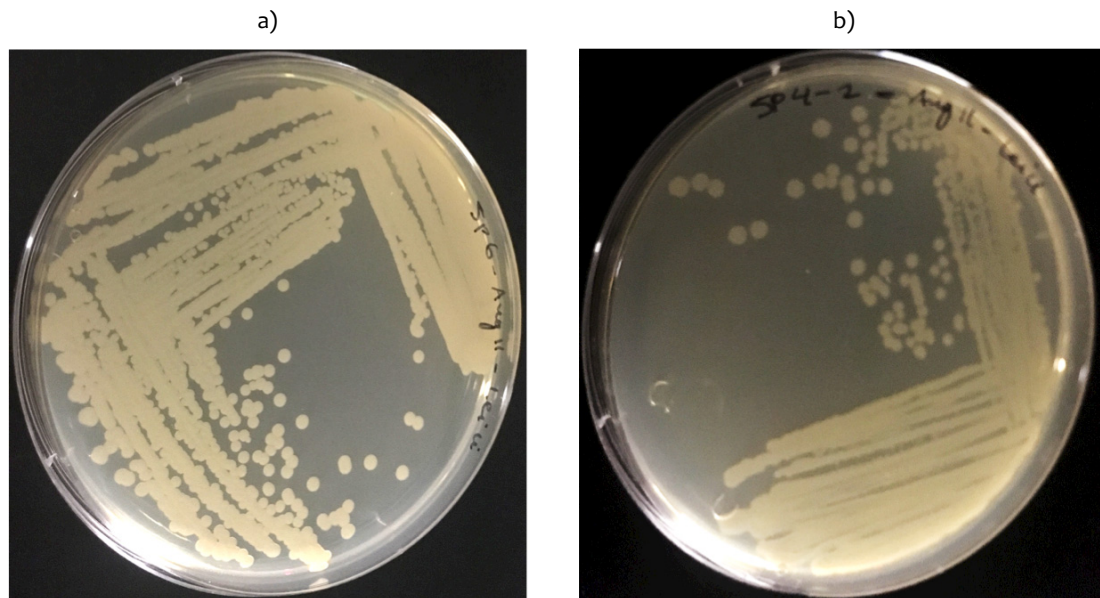
Figure 31   Two most biofilm producing bacteria on TSA plates identified as a) *Bacillus mycoides* and b) *Paenibacillus tundrae*

The genus *Paenibacillus* are rod-shaped, endospore-forming, Gram-positive or Gram variable bacteria. Based on the 16S rRNA gene sequence comparative study, this genus is derived from a Bacillus, group 3 [231]. Some of the sub species of this bacteria have been found to have an enzyme that can degrade plant derived organic matter in soils [232,233]. *Paenibacillus tundrae*, (from a biome in northern North America and Eurasia) were reported to be isolated from the Arctic foothills of Alaska [234]. They were characterized as motile rods that grow aerobically or anaerobically, with capability of nitrate reduction to nitrite. The optimum temperature for growth was determined to be 27°C with range of 13–37°C. The pH growth range was reported to be 5.2–8.8 with optimum at 6.4 [234]. The phylogenetic tree analysis depicted in Figure 32 confirms the correct identification of the species as *Paenibacillus tundrae*.
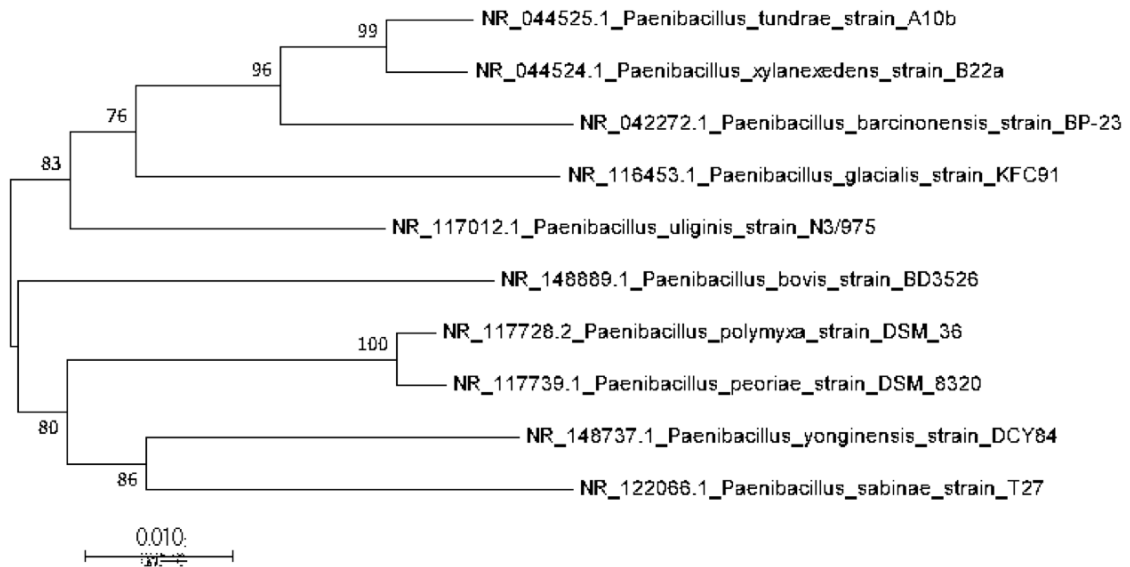
Figure 32   Phylogenetic analysis of the *Paenibacillus tundrae* based on the full length 16S rRNA, numbers at nodes are bootstrap values (%) based on neighbor joining analysis by repeating the analysis 500 times. The scale bar indicates 0.01 nucleotide divergence, in other words the number of nucleotides substitutions per site.

Bacillus mycoides, a Gram-positive and spore-forming species, is ubiquitous in soils and belongs to the family of Bacillaceae. *B. mycoides* was classified as a species in 1886, reclassified as *Bacillus cereus* in 1946 and then again reclassified as *B. mycoides* in 1986 [235]. It is reported that the taxonomic relatedness of *Bacillus cereus, Bacillus mycoides, Bacillus anthracis, and Bacillus thuringiensis* proposed difficulties in distinguishing and differentiating between these closely related species [236,237]. Afterward, *Bacillus weihenstephanensis* was isolated and added as the fifth species to the *Bacillus cereus* group due to the taxonomic similarity [238].

Currently, the *Bacillus Cereus* group has 21 closely connected species. Liu et al., 2018, investigated the reclassification of *B. weihenstephanensis* and suggested that *B. weihenstephanensis* as a later heterotypic synonym of *Bacillus mycoides* [239]. This high similarity can be observed in phylogenetic analysis shown in Figure 33.

B. mycoides is characterized as a non-motile, rod-shaped, aerobe, and a psychrotolerant (capable of growing at 7°C or below) bacteria [240].
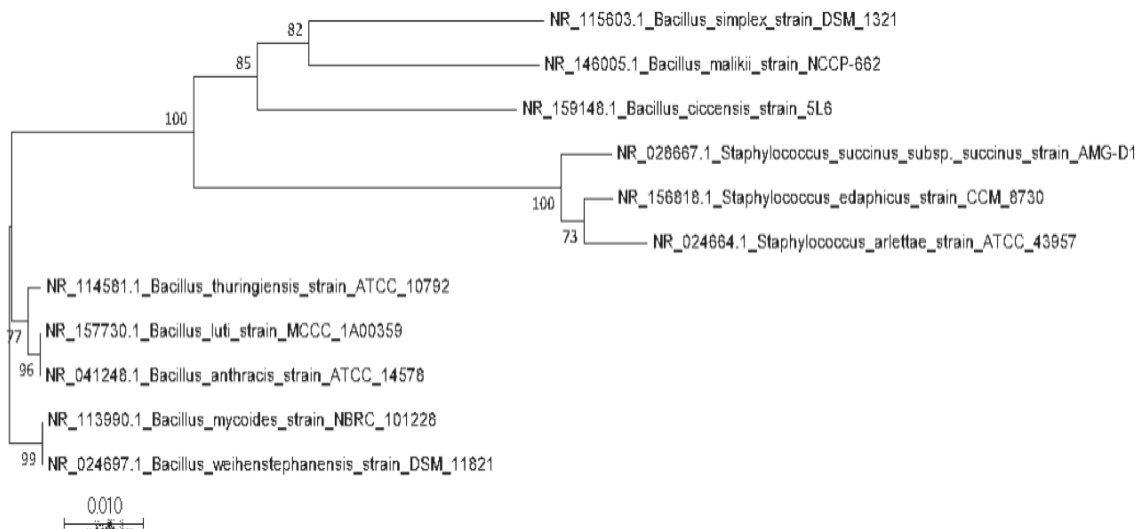
Figure 33   Phylogenetic analysis of the Bacillus mycoides based on the full-length 16S rRNA. Numbers at nodes are bootstrap values (%) based on neighbor joining analysis by repeating the analysis 500 times. The scale bar indicates 0.01 nucleotide divergence, in other words the number of nucleotides substitutions per site.

To further characterize the newly isolated bacteria, their growth curve and rate were determined using a rapid, high-throughput protocol which was adapted by the author (Chapter 4). The maximum growth rates (h⁻¹) of *B. mycoides* and *P. tundrae* were (mean± SD) 0.99 ± 0.03 and 0.85 ± 0.025, respectively.

C.VI - 7.2 Gene Mapping

To the knowledge of the authors, there are no published studies on the molecular mechanism of biofilm formation of *Bacillus mycoides or Paenibacillus tundrae,* despite the extensive literature search. *B. mycoides,* however, as mentioned is closely related to *Bacillus cereus* and is a subgroup of *Bacillus subtilis. B. cereus* shares many regulatory mechanisms and metabolic pathways with *B. subtilis* [241]; that is why *B. subtilis* was chosen to be studied in the literature for the regulatory mechanism on biofilm formation.

B. subtilis is a model organism for studying the molecular mechanism of biofilm formation as Gram-positive bacteria since the 1870s [242].

In general, regulatory genes that act at the transcriptional level contain DegU/DegS, Spo0A, SinI/SinR, SlrR/SlrA and AbrB control the biofilm formation in *B. subtilis* group [241]. Genes, such as *spo0A, spo0H* and *abrB*, are regulatory genes involved in the early stages of sporulation [243]. *B. subtilis* biofilm formation involves EPS (polysaccharides and proteins) production. The major components of EPS in *B. subtilis* is from an expression of *esp* operon (*epsABC…NO*) [244].

Chu, 2007 studied the molecular mechanism of *B. subtilis* comprehensively and reported that genes *yhxB* and the 15-gene-long *yveK- yvfF* operon, alternatively called *epsA-O*, are responsible for EPS formation. The *tasA* operon is involved in extracellular protein production called TasA, a major protein component in *B. subtilis* EPS [245]. Chu 2007 stated that without the exopolysaccharides and TasA (major protein component) *B. subtilis* cannot form biofilms. TasA turns into a long amyloid fiber that attached to the cells and provides the structural stability to the biofilm [246]. The fiber-like structure of EPS and biofilm was observed in the biofilm architecture of *B. mycoides* and *P. tundrae* (Figure 49 and Figure 50). TapA is a minor protein that anchors the TasA to the cells. The *tapA-sipW-tasA* operon encodes the type I signal peptidase W which produce TapA and TasA protein [244]. The s*ipW* and *tasA* genes and *eps operon* were found in the genome map of *B. mycoides* further demonstrating the potential ability of EPS production of this species.

There are different metabolic pathways for biofilm formation and all the regulatory genes are not needed to be involved to trigger and form EPS. There is a possibility of biofilm formation only with transcription of a small subset of matrix genes depending on environmental condition. However, the activation of *spo0A* is central for induction of biofilm formation in a multitude of environmental signals [244]. The *spo0A* gene was present in both *B. mycoides* and *P. tundrae* showing their ability for EPS and biofilm formation.

Table 17   Some of the genes involved in extracellular matrix production [244]

Gene or operon	Role of encoded proteins in matrix production	B. mycoides	P. tundrae
Eps operon	Exopolysaccharide synthesize	epsD, epsJ, epsG, epsL, epsN, epsF	epsO, epsE, epsD
tapA	Minor component of TasA fibres which anchors TasA fibres to the cell	NA	NA
sipW	Type I signal peptidase which process TapA and TasA,	sipW	NA
tasA	Major protein component of TasA fibres	tasA operon	NA
pgsB	Produces γ-poly-DL-glutamic acid, an extracellular protein; capsular polysaccharide biosynthesis	pgsA	NA
bslA1	Provides surface hydrophobicity	NA	NA
spo0A	Sporulation	spo0A	spo0A

It has been reported that in *B. subtilis, eps operon* is responsible for producing exopolysaccharides which binds the chain of bacteria together and form biofilm [243]. Kearn et al., (2005) found that the *sinR* is a master regulator, responsible for the transition from planktonic state to the sessile state. The *sinR* and *eps operon* genes are found in the genome map of *B. mycoides* and *P. tundrae* which shows their molecular capability of producing biofilm through the *SinR* pathway[243].

The *tapA-sipW-tasA* operon was not found in the genome map of *P. tundrae and* could be due to some of the genes were not completely identified in whole genome sequencing. There were some gene classified as unknown in the whole genome table provided by the IMR Lab. Also, two isolated species could use different metabolic pathways to form biofilm.

C.VI - 7.3 SEM Images

SEM images of biofilm of *B. mycoides* and *P. tundrae* in minimal media (M63) are shown in Figure 34 and Figure 35 with 5K resolution. Both species have a fiber-like strand that entraps the cells within them. The captured images were similar to the SEM images of *Bacillus*, *E. coli, Streptococcus and Clostridium perfringens* biofilms reported by other researchers [247–250]. They all have rod-shape cells entangled and interconnected in a series of fiber networks. The fiber-like strands shown in the SEM images contain EPS [247] which helps protect cells against the stressors such as dinfectants, oxidants, extereme temperatures, and nutrient deficiencies. More studies are needed to better comprehend the response of the cells to the environmental stressors.
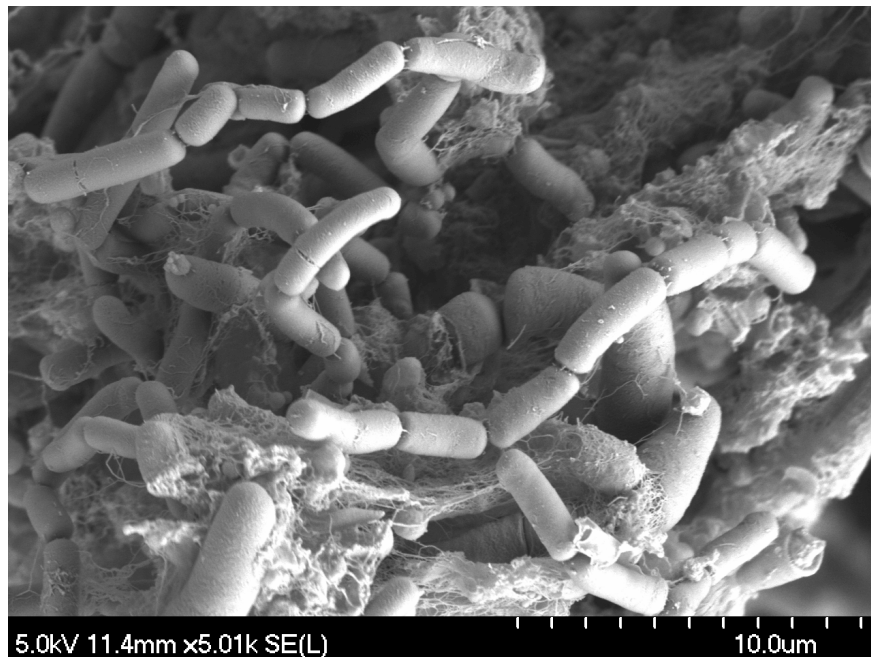
Figure 34   Biofilm architecture of Bacillus mycoides in minimal media are studied using scanning electron microscopy. The images are shown at 5K magnification.
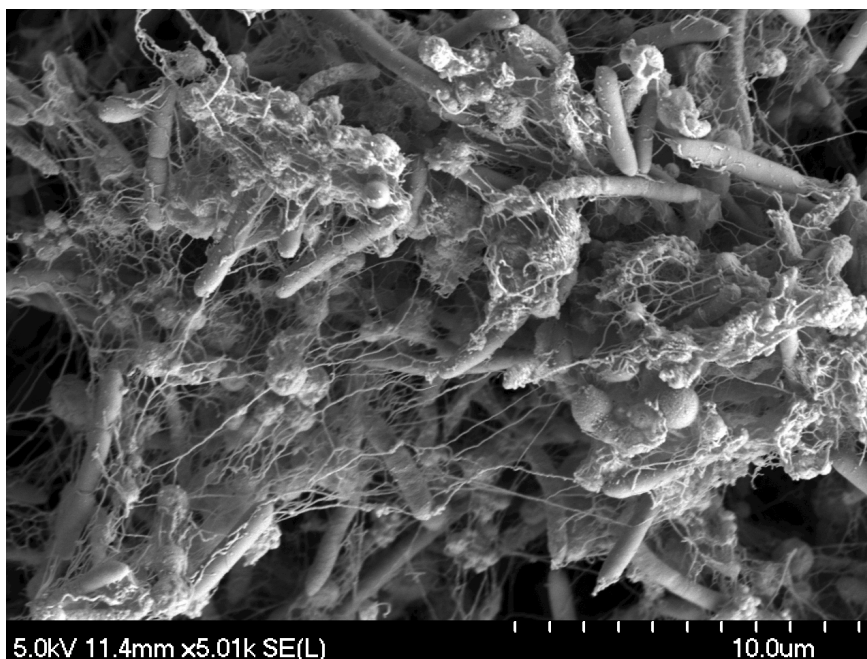
Figure 35   Biofilm architecture of *Paenibacillus tundrae* in minimal media are studied using scanning electron microscopy. The images are shown at 5K magnification.

C.VI - 7.4 Phosphorus Limitation

Since the phosphorus concentration of Pockwock Lake is very low the further removal with alum can negatively impact the phosphorus availability for the microbes in the biofilter. Without using the sedimentation process between the coagulation-flocculation and biofilters, some of the formed flocs transfer to the biofilter. It was hypothesized that the physical buildup of the flocs can inhibit the nutrient diffusion to the biofilm bacteria.

This set of experiments investigated the different levels of P limitation in a minimal media to simulate the drinking water low nutrient environment. It specifically aimed to study the biological responses of the isolated bacteria in pure culture. The biological responses were investigated by ATP of the biofilm, and EPS levels including protein, carbohydrate, and e-DNA.
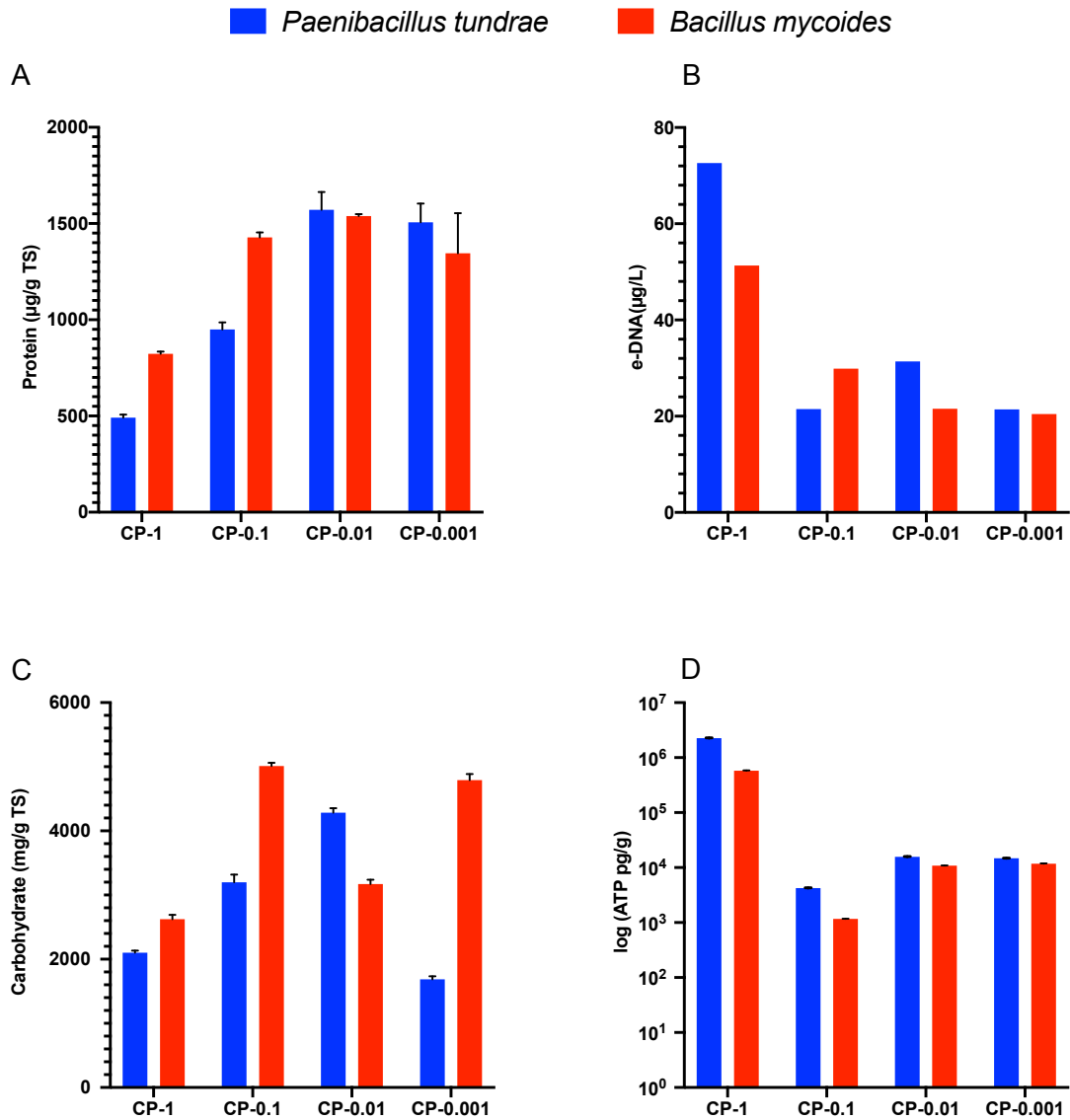
Figure 36   B. mycoides in red and *P. tundrae* in blue were cultured for 72 hours in extreme phosphorus limited conditions. Each value is an average of three measurements and error bars are standard deviation. The ratios are as CP-1 for regular phosphorus and CP-0.1, CP-0.01, and CP-0.001 represent different P limitation levels. The biological responses in EPS were measured as A) protein, B) e-DNA, C) carbohydrates and D) ATP.

The ATP levels in both species decreased noticeably by decreasing the phosphorus 10 times from C:P 1 to 0.1 (Figure 36). As shown the ATP levels reached a plateau by further P reduction. EPS-Protein and -carbohydrate concentrations generally increased by the P reduction and limitation in the media. The low carbohydrate level for C:P of 0.001 in *P. tundrae*

could be due to experimental errors. The e-DNA levels had a sharp decrease by changing the C:P ratio from 1 to 0.1; however, further reductions did not change e-DNA largely (Figure 36).

The results demonstrated while the ATP did not vary in the lower levels of phosphorus, the EPS concentration increased. It is reported that in a culture of *C. closterium* (diatom symbiotic strain) when growth stopped due to the P depletion, EPS accumulation rate was augmented [251]. The adherence (biofilm formation) of *Agrobacterium tumefaciens* (α-Proteobacteria) amplified significantly under P limitation in comparison to well supplied P medium, while the overall growth under P limitation was lower [252]. Nutrient depletion has been shown to trigger the EPS production in the biofilm of *B. subtilis* at the single cell level [253], which aligns with the higher production of protein and carbohydrate-EPS in different phosphorus limitation levels in this study. Biofilm formation and EPS production of *Escherichia coli O157:H7* strains ATCC 43895 (wild type) and 43895-EPS (extensive EPS-producing mutant) were investigated in high and low nutrient medium. No EPS or biofilm formation were observed in high nutrient, while in low nutrient medium (minimal salt broth) biofilm formation was reported [247], further confirming that low nutrient level can trigger the [204]EPS production in bacteria.

EPS production is a response to the nutrient composition of the growth medium. The EPS production by *A. salmonicida* (gram negative, gammaproteobacteria) was influenced by the growth conditions [254]. It is reported that the initial concentration of available carbon and nitrogen are crucial for EPS production, rather than the absolute ratio [254]. Similar effects have been reported for *Zoogloea strain MP6* (gram negative, betaproteobacteria) [255] and *Butyrivibrio fibriosolvens* (gram positive, clostridia) [256] for exopolysaccharides production.

A. salmonicida A450 produces EPS at the end of the logarithmic phase of growth (non-growing phase). Bacterial communities in natural ecosystems experience several periods of growth and non-growth in response to the environmental changes, with non-growing bacteria using their resources for the production and release of exopolysaccharides [254].

C.VI - 8 CONCLUSION

Two species were isolated for their phenotypic ability of biofilm production from full-scale drinking water biofilters. They were identified using 16s rRNA genome sequencing and comparing the sequences using the BLASTn software to the NCBI GenBank as *B. mycoides* and *P. tundrae*. The phylogenetic tree analysis confirmed the gene comparative results and bacterial identification. Genes related to the EPS and biofilm formation were identified in the whole genome maps of both species. The SEM images clearly presented the biofilm architecture.

The isolated bacteria were responsive to the P limitation in the media. The biological responses were measured as EPS and ATP on the formed biofilm. Decreasing the P level triggered the higher EPS production in both species. Therefore, our results suggest that the possible nutrient inhibition by flocs can cause higher EPS production.

Based on the results of this study, it is recommended to adjust the concentration of Phosphorus in drinking water biofilters to lower the EPS production. Future research must be done to simulate the source water characteristic and its impact on the EPS production. Also, understanding the regulatory and metabolic pathway triggered by nutrient, and specifically P reduction in the isolated bacteria, can further our knowledge on how to control the excess EPS production in the biofilter.

Chapter VII CONCLUSION

This chapter provides conclusions of the findings, as well as a selection of my journal articles and presentations relevant to this thesis.

C.VII - 1 THESIS CONCLUSION

The main objective of this thesis was to comprehend the biological root cause of challenging filter events. Accordingly, the two primary research questions were investigated:

1. How is the microbial community in biofilter through variation in water quality and challenging filter events changing?
2. Can the hydraulic performance challenges be explained using biological approaches?

These questions were investigated by a thorough study in full, pilot and lab -scale. In full- and pilot-scale studies, the hydraulic performance challenges were observed and addressed through the following hypotheses.

C.VII - 1.1 Hypothesis 1

The hypothesis 1 was evaluated in full-scale biofilters. This study includes two years of core biofilter sampling to establish a baseline and challenging filter events. The challenging events include two significant issues a) the filter media replacement and b) diatom algae bloom.

Hydraulic performance indicators along with biological activity parameters were monitored. Microbiome studies were used to establish the baseline microbiome (regular operation), and the temporal changes were studied. Filter media replacement was the most influential on the variation of the microbiome and microbial community structure, while the hydraulic performance indicators did not differ tremendously. Diatom bloom, which occurred in summer 2018, caused the lowest filter runtime and was studied as one of the most challenging filter events. The primary root cause was identified to be a diatom, which slightly shifted the microbial community structure as well but not as much as expected. Chlorination applied to revive the hydraulic performance shifted the microbiome to the lower layers of the

filter, while the beta diversity analysis did not show massive differences in microbial community structure. This study suggests that microbiome analysis is a sensitive monitoring strategy which provides insights into the dynamics and root causes of challenging filter events. Also, it furthers our knowledge about the biofilter performance and benefits operators with devising a more informed solution to resolve challenging situations.

C.VII - 1.2 Hypothesis 2

The possibility of reducing the floc carryovers to the biofilter using a sedimentation process was the focus of the pilot-scale studies. It was hypothesized that the fewer flocs could improve the hydraulic performance of the biofilter using implementation of a clarification step, sedimentation tank. The impact of deployment of a sedimentation tank on the three biofilters' hydraulic performance was studied using two parallel trains. This study showed that the head-loss accumulation rate decreased, and filter runtime was higher on average using the sedimentation tank. The biological activity of both trains was similar, and EPS appeared to be higher in direct biofiltration (non- sedimentation). It is established that excess EPS produced by the bacteria in biofilters contributes to the head-loss accumulation. In conclusion, sedimentation improved the biofilter performance.

C.VII - 1.3 Hypothesis 3

This study was done through an extensive literature search. There is a consensus in the literature that alum toxicity can trigger EPS production. Therefore, one of the contributors to increased EPS in the biofilters without sedimentation is likely to be found in the floc containing alum and the toxicity thereof.

C.VII - 1.4 Hypothesis 4

Floc carryover reduces the diffusion of nutrients to bacteria. Low nutrient conditions cause stress leading to an increased formation of EPS.

Two of the most biofilm-producing bacteria were isolated from full-scale drinking water biofilter. They were identified using 16S rRNA gene sequencing and characterized.

The first step of the characterization was collecting their growth curve and measuring their growth rate. A high-throughput method was successfully established to measure the bacteria's growth rate and verified by the isolated bacteria. The method development is captured in chapter V.

The phylogenetic tree analysis verified the identification of the isolated bacteria. SEM imaged their biofilm architecture. Finally, the impact of nutrient limitation, mainly the P limitation, was studied in the minimal media. The various ratios of limited P levels were considered C:P of 1, 0.1, 0.01, and 0. 001. The P reduction increased the EPS (protein and carbohydrate) production while the ATP decreased and reached a plateau.

This study suggests that the nutrient limitation, precisely P limitation caused by the flocs, can contribute to EPS production in direct biofiltration.

C.VII – 2 FUTURE OUTLOOK AND RECOMMENDATIONS

Some of the outcomes of this study have implication for optimizing and improving the operation and monitoring of drinking water biofiltration system.

- Employing sedimentation process increases filter runtime; no changes is necessary to the existing biofilters.
- Regular monitoring microbial community can help establishing the core microbiome and consequently having the ability to diagnose the changes.
- Understanding the microbiome of the filter can help creating informed solution for the challenging issues in drinking water biofilters.
- By understanding the impact of nutrient limitation, adjusting the phosphorus level can decrease the EPS production and thus the head-loss accumulation in the biofilter.

Based on the results of this study, further investigations are suggested as follows:

1. Study if the carried over flocs to the biofilter contributes to the EPS levels measured as alum flocculates the viruses and bacteria and other particulate matters.
2. Study how alum toxicity impacts the microbiome diversity and structure in drinking water biofilter.
3. Examine how phosphorus limitation in combination with alum toxicity triggers bacterial behavior.
4. Investigate the microbial activity, microbial composition of flocs formed by different coagulants.
5. Study the bacterial release mechanism and die-off kinetics in flocs settled in a biofilter.
6. Explore which coagulant produce more EPS production and changes in drinking water biofilter.
7. Compare the presence of floc with bacteria versus no floc in biofilm production.
8. Study if the flocs carried into the filter directly causes clogging and increased head-loss.
9. How alum residual in the water contributes to clogging in combination of bacterial activity

C.VII – 3 RELEVANT JOURNAL ARTICLES

L. Abkar, A. Taylor, A. Stoddart, G. Gagnon, "**Holistic monitoring strategies to study and predict the biological root causes of drinking water biofilter challenges**", *unpublished manuscript*

L.Abkar, G. Gagnon, "**Isolation, characterization of biofilm producing bacteria from drinking water biofiltration- P limitation impact on biological response**", *unpublished manuscript*

L. Abkar, M. Piercey, F. Wilfart, G. Gagnon, "**Development of a high-throughput method with a simplified inoculation and pathlength correction to determine microbial growth rates**", submitted to *Letters in Applied Microbiology*

L. Abkar, A. Stoddart, G. Gagnon, "**Sedimentation: Hydraulic improvement of drinking water biofiltration**", AWWAWater Science, 1(5), 2019, awarded the author highlight

C.VII - 4 RELEVANT POSTERS AND PODIUM PRESENTATIONS

Leili Abkar, Amina Stoddart, Graham Gagnon, "**Applying Sedimentation Integrated with Drinking Water Biofiltration Improves Hydraulic Performance**", AWWA Annual Conference and Exposition, Orlando, FL, June 2020.

Leili Abkar, Anita Taylor, Jessica Campbell, Martin Earl, Amina Stoddart, Graham Gagnon, "**Understanding Drinking Water Biofiltration: Monitoring and optimization approach**", Atlantic Canada Water Work Association (ACWWA) – Halifax, Nova Scotia, Sep. 2019- (Oral Presentation)

Leili Abkar, Anita Taylor, Jessica Campbell, Martin Earl, Amina Stoddart, Graham Gagnon, "**Microbial Community Variation as Monitoring Indicator in Drinking Water Biofilters**", Water quality technology conference, Dallas, TX, Nov. 2019 (Oral Presentation)

Leili Abkar, Amina Stoddart, Graham Gagnon, "**Optimizing biological filtration: A pilot scale study at JD Kline water treatment plant – Halifax-Canada**", Atlantic Canada Water Work Association (ACWWA) – Moncton, New Brunswick, Sep.2016- (Oral Presentation)

BIBLIOGRAPHY

1. Adams, C. A. *The Sustainable Development Goals, integrated thinking and the integrated report. IIRC and ICAS* (2017).

2. World Health Organization. *WHO | A global overview of national regulations and standards for drinking-water quality. WHO* (World Health Organization, 2018).

3. Hu, Z., Morton, L. W. & Mahler, R. L. Bottled water: United States consumers and their perceptions of water quality. *Int. J. Environ. Res. Public Health* **8**, 565–578 (2011).

4. Juuti, P. S., Katko, T. S. & Vuorinen, H. S. *Environmental history of water.* (IWA Publishing, 2007).

5. Angelakis, A. N., Mays, L. W., Demetris, K. & Mamassis, N. *Evolution of Water Supply Through the Millennia. Water Intelligence Online* **11**, (IWA Publishing, 2012).

6. Baker, M. N. *The Quest For Pure Water: The History Of Water Purification From The Earliest Records To The Twentieth Century.* (American Water Works Association, 1981).

7. Crittenden, J. C., Trussell, R. R., Hand, D. W., Howe, K. J. & Tchobanoglous, G. *Water treatment principles and design.* (John Wiley & Sons, Inc, 2012).

8. Bassett, S. S. Evaluation of a Side-By-Side Full-Scale Biofiltration Conversion in a Nutrient-Limited Environment. (Utah State University, 2018).

9. Tulchinsky, T. H. John Snow, Cholera, the Broad Street Pump; Waterborne Diseases Then and Now. *Case Stud. Public Heal.* 77–99 (2018). doi:10.1016/b978-0-12-804571-8.00017-2

10. Lauderdale, C. V. Engineered Biofiltration For Enhanced Hydraulic And Water Treatment Performance. (University of Florida, 2011).

11. Piche, A., Campbell, A., Cleary, S., Douglas, I. & Basu, O. D. Investigation of backwash strategy on headloss development and particle release in drinking water biofiltration. *J. Water Process Eng.* **32**, 100895 (2019).

12. Brown, J. C., Upadhyaya, G., Carter, J., Brown, T. & Lauderdale, C. V. *North American Biofiltration Knowledge Base-Project 4459. Water Research Foundation* (2016).

13. Kirisits, M. J., Emelko, M. B. & Pinto, A. J. Applying biotechnology for drinking water biofiltration: advancing science and practice. *Curr. Opin. Biotechnol.* **57**, 197–204 (2019).

14. Lamsal, R., Walsh, M. E. & Gagnon, G. A. Comparison of advanced oxidation processes for the removal of natural organic matter. *Water Res.* **45**, 3263–3269 (2011).

15. Kleiser, G. & Frimmel, F. H. Removal of precursors for disinfection by-products (DBPs) - Differences between ozone- and OH-radical-induced oxidation. *Sci. Total Environ.* **256**, 1–9 (2000).

16. Von Gunten, U. Ozonation of drinking water: Part I. Oxidation kinetics and product formation. *Water Research* **37**, 1443–1467 (2003).

17. Lauderdale, C. V., Chadik, P., Kirisits, M. J. & Brown, A. J. Engineered biofiltration: Enhanced biofilter performance through nutrient and peroxide addition. *J. Am. Water*

Works Assoc. **104**, 298–309 (2012).

18. Pinto, A. J., Xi, C. & Raskin, L. Bacterial community structure in the drinking water microbiome is governed by filtration processes. *Environ. Sci. Technol.* **46**, 8851–8859 (2012).

19. Kostakioti, M., Hadjifrangiskou, M. & Hultgren, S. J. Bacterial biofilms: Development, dispersal, and therapeutic strategies in the dawn of the postantibiotic era. *Cold Spring Harb. Perspect. Med.* **3**, (2013).

20. Flemming, H. C. & Wingender, J. The biofilm matrix. *Nature Reviews Microbiology* **8**, 623–633 (2010).

21. Flemming, H.-C. EPS—Then and Now. *Microorganisms* **4**, 41 (2016).

22. Di Martino, P. Extracellular polymeric substances, a key element in understanding biofilm phenotype. *AIMS Microbiol.* **4**, 274–288 (2018).

23. Flemming, H.-C. *et al.* Biofilms: An emergent form of bacterial life. *Nat. Rev. Microbiol.* **14**, 563–575 (2016).

24. Decho, A. W. & Gutierrez, T. Microbial extracellular polymeric substances (EPSs) in ocean systems. *Front. Microbiol.* **8**, (2017).

25. Rothschild, L. J. & Mancinelli, R. L. Life in extreme environments. *Nature* **409**, 1092–1101 (2001).

26. Yin, W., Wang, Y., Liu, L. & He, J. Biofilms: The microbial "protective clothing" in extreme environments. *Int. J. Mol. Sci.* **20**, (2019).

27. Watnick, P. & Kolter, R. Biofilm, city of microbes. *Journal of Bacteriology* **182**, 2675–2679 (2000).

28. Brown, J. C. & Jang, H. *Biofiltration Guidance Manual for Drinking Water Facilities- Project 4719.* (2020).

29. Fowler, S. J. & Smets, B. F. Microbial biotechnologies for potable water production. *Microb. Biotechnol.* **10**, 1094–1097 (2017).

30. Hallé, C., Huck, P. M. & Peldszus, S. Emerging contaminant removal by biofiltration: Temperature, concentration, and EBCT impacts. *Journal - American Water Works Association* **107**, E364–E379 (2015).

31. Liu, X., Huck, P. M. & Slawson, R. M. Factors Affecting Drinking Water Biofiltration. *J. / Am. Water Work. Assoc.* **93**, 90–101 (2001).

32. Urfer-Frund, D. Effect of Oxidant on Drinking Water Biofiltration. (University of Waterloo, 1998).

33. Urfer-Frund, D. & Huck, P. M. Effects of Hydrogen Peroxide Residuals on Biologically Active Filters. *Ozone Sci. Eng.* **19**, 371–386 (1997).

34. Lauderdale, C. V., Alito, C., Hooper, J., Dowdell, K. & Wert, E. C. *Optimizing Biofiltration for Various Source Water Quality Conditions.* (2017).

35. Keithley, S. E. & Kirisits, M. J. An improved protocol for extracting extracellular polymeric substances from granular filter media. *Water Res.* **129**, 419–427 (2018).

36. Lautenschlager, K. *et al.* Abundance and composition of indigenous bacterial communities in a multi-step biofiltration-based drinking water treatment plant. *Water Res.* **62**, 40–52 (2014).

37. Pharand, L., Dyke, M. Van, Anderson, W. & Huck, P. M. Assessment of biomass in drinking water biofilters by adenosine triphosphate. *J. Awwa* 433–444 (2014). doi:10.5942/jawwa.2014.106.0107

38. Stoddart, A. K. & Gagnon, G. A. Full-scale prechlorine removal: Impact on filter performance and water quality. *J. Am. Water Works Assoc.* **107**, E638–E647 (2015).

39. Tagra, S. K. Operational Challenges of a Direct Filtration Water Treatment Plant in Light of Lake Recovery. (Dalhousie University, 2020).

40. Abkar, L., Stoddart, A. K. & Gagnon, G. A. Sedimentation: Hydraulic improvement of drinking water biofiltration. *AWWA Water Sci.* **1**, (2019).

41. *Annual Report Twenty-Third.* (2019).

42. Comeau, A. M., Douglas, G. M. & Langille, M. G. I. Microbiome Helper: a Custom and Streamlined Workflow for Microbiome Research. *mSystems* **2**, (2017).

43. Douglas, G. M., Comeau, A. M. & Langille, M. G. I. Processing a 16S rRNA Sequencing Dataset with the Microbiome Helper Workflow. *Methods Mol. Biol.* **1849**, 131–141 (2018).

44. Martin, M. Cutadapt removes adapter sequences from high-throughput sequencing reads. *EMBnet.journal* **17**, 1–3 (2011).

45. Callahan, B. J. *et al.* DADA2: High-resolution sample inference from Illumina amplicon data. *Nat. Methods* **13**, 581–583 (2016).

46. Katoh, K. MAFFT: a novel method for rapid multiple sequence alignment based on fast Fourier transform. *Nucleic Acids Res.* **30**, 3059–3066 (2002).

47. Lozupone, C. A. & Knight, R. Species divergence and the measurement of microbial diversity. *FEMS Microbiol. Rev.* **32**, 557–578 (2008).

48. Lee, D. D. & Seung, H. S. Learning the parts of objects by non-negative matrix factorization. *Nature* **401**, 788–791 (1999).

49. Cai, Y., Gu, H. & Kenney, T. Learning Microbial Community Structures with Supervised and Unsupervised Non-negative Matrix Factorization. *Microbiome* **5**, 110 (2017).

50. Keithley, S. E. Impact of Phosphorus Limitation on the Hydraulic Performance of Drinking-Water Biologically Active Filters. (The University of Texas at Austin, 2017).

51. Lauderdale, C., Alito, C., Hooper, J., Dowdell, K. & Wert, E. *Optimizing Biofiltration for Various Source Water Quality Conditions.* (Water Research Foundation (WRF), 2018).

52. Stetson, S. B. Evaluation of a side-by-side full scale biofiltration conversion in a nutrient-limited environment. (2018).

53. Rahman, I. Direct Biofiltration and Nutrient (Phosphorous) Enhancement for Polymeric Ultrafiltration Membrane Fouling Control. (University of Waterloo, 2013).

54. Liu, X. Drinking water biofiltration: Assessing key factors and improving process

evaluation. *Civil Engineering* (University of Waterloo, 2001).

55. Evans, B. Filter Operation & Maintenance. in *Pacific Northwest section-AWWA* (2014).

56. Bryans, B. & De Groot, C. *Investigating High Wash Cost Savings through Floc Retention and Bed Expansion Testing.* (2014).

57. Moll, D. M., Summers, R. S., Fonseca, A. C. & Matheis, W. Impact of temperature on drinking water biofilter performance and microbial community structure. *Environ. Sci. Technol.* **33**, 2377–2382 (1999).

58. Azzeh, J., Taylor-Edmonds, L. & Andrews, R. C. Engineered Biofiltration for Ultrafiltration Fouling Control and DBP Precursor Removal. *Water Sci. Technol. Water Supply* **15**, (2014).

59. Dimas, N. Assessing Biofilm on Biofilter Media (Granular Activated Carbon and Anthracite) from a Pilot Scale Drinking Water Treatment Plant. (Ryerson University, 2016).

60. Mash, H., Dugan, T. S. & Lytle, D. Impact of Harmful Algal Blooms on Several Lake Erie Drinking Water Treatment Plants. in *58th IAGLR Conference on Great Lakes Research* (2015).

61. Stoddart, A. K., Schmidt, J. J. & Gagnon, G. A. Biomass evolution in full-scale anthracite-sand drinking water filters following conversion to biofiltration. *J. Am. Water Works Assoc.* **108**, E615–E623 (2016).

62. Booth, S., Carlson, P. & Kawamura, S. Minimizing Operational Interruption During Filter Bed Surveillance. in *American Water Works Association* (2006).

63. Jones, A., Murayama, M. & Knocke, W. R. Incorporating aluminum species in MnO x (s) coatings on water filtration media. *AWWA Water Sci.* **1**, e1114 (2019).

64. Jones, A. The Role of Aluminum within MnOx(s) - Coated Filtration Media in Drinking Water Treatment. (Virginia Polytechnic Institute, 2012).

65. Bringloe, T. T., Cottenie, K., Martin, G. K. & Adamowicz, S. J. The importance of taxonomic resolution for additive beta diversity as revealed through DNA barcoding. *Genome* **59**, 1130–1140 (2016).

66. Gardener, M. Chapter 10. Diversity: sample scale. in *Community Ecology: Analytical Methods Using R and Excel* (Pelagic Publishing Ltd, 2014).

67. Schrader, C., Schielke, A., Ellerbroek, L. & Johne, R. PCR inhibitors - occurrence, properties and removal. *Journal of Applied Microbiology* **113**, 1014–1026 (2012).

68. Parks, D. H. & Beiko, R. G. Measuring community similarity with phylogenetic networks. *Mol. Biol. Evol.* **29**, 3947–3958 (2012).

69. Ramanan, R., Kim, B. H., Cho, D. H., Oh, H. M. & Kim, H. S. Algae-bacteria interactions: Evolution, ecology and emerging applications. *Biotechnology Advances* **34**, 14–29 (2016).

70. Vignola, M., Werner, D., Wade, M. J., Meynet, P. & Davenport, R. J. Medium shapes the microbial community of water filters with implications for effluent quality. *Water Res.* **129**, 499–508 (2018).

71. Chan, S. *et al.* Monitoring biofilm function in new and matured full-scale slow sand filters using flow cytometric histogram image comparison (CHIC). *Water Res.* **138**, 27–36 (2018).

72. Bruno, A. *et al.* Changes in the Drinking Water Microbiome: Effects of Water Treatments Along the Flow of Two Drinking Water Treatment Plants in a Urbanized Area, Milan (Italy). *Front. Microbiol.* **9**, 2557 (2018).

73. Potgieter, S. *et al.* Long-term spatial and temporal microbial community dynamics in a large-scale drinking water distribution system with multiple disinfectant regimes. *Water Res.* **139**, 406–419 (2018).

74. Pinto, A. J., Schroeder, J., Lunn, M., Sloan, W. & Raskin, L. Spatial-temporal survey and occupancy-abundance modeling to predict bacterial community dynamics in the drinking water microbiomez. *MBio* **5**, (2014).

75. Douterelo, I., Jackson, M., Solomon, C. & Boxall, J. Spatial and temporal analogies in microbial communities in natural drinking water biofilms. *Sci. Total Environ.* **581–582**, 277–288 (2017).

76. Moll, D., Summers, R. S. & Breen, A. Microbial Characterization of Biological Filters Used for Drinking Water Treatment. *Appl. Environ. Microbiol.* **64**, 2755–2759 (1998).

77. Zhang, Y. & Liu, W. T. The application of molecular tools to study the drinking water microbiome–Current understanding and future needs. *Crit. Rev. Environ. Sci. Technol.* **49**, 1188–1235 (2019).

78. Lauderdale, C. V. *et al. Optimizing filter conditions for improved manganese control during conversion to biofiltration- Project 4448.* (Water Research Foundation, 2016).

79. Niemi, R. M., Heiskanen, I., Heine, R. & Rapala, J. Previously uncultured β-Proteobacteria dominate in biologically active granular activated carbon (BAC) filters. *Water Res.* **43**, 5075–5086 (2009).

80. Zeng, D. N. *et al.* Analysis of the bacterial communities associated with different drinking water treatment processes. *World J. Microbiol. Biotechnol.* **29**, 1573–1584 (2013).

81. Han, L. *et al.* Comparison of NOM removal and microbial properties in up-flow/down-flow BAC filter. *Water Res.* **47**, 4861–4868 (2013).

82. Gerrity, D. *et al.* Microbial community characterization of ozone-biofiltration systems in drinking water and potable reuse applications. *Water Res.* **135**, 207–219 (2018).

83. Oh, S., Hammes, F. & Liu, W. T. Metagenomic characterization of biofilter microbial communities in a full-scale drinking water treatment plant. *Water Res.* **128**, 278–285 (2018).

84. Zhang, Y., Oh, S. & Liu, W. T. Impact of drinking water treatment and distribution on the microbiome continuum: an ecological disturbance's perspective. *Environ. Microbiol.* **19**, 3163–3174 (2017).

85. Lautenschlager, K. *et al.* Abundance and composition of indigenous bacterial communities in a multi-step biofiltration-based drinking water treatment plant. *Water Res.* **62**, 40–52 (2014).

86. Balkwill, D. L., Fredrickson, J. K. & Romine, M. F. Sphingomonas and Related

Genera. in *The Prokaryotes* **7**, 605–629 (Springer New York, 2006).

87. Vaz-Moreira, I., Nunes, O. C. & Manaia, C. M. Diversity and antibiotic resistance patterns of Sphingomonadaceae isolates from drinking water. *Appl. Environ. Microbiol.* **77**, 5697–5706 (2011).

88. Henson, M., Lanclos, C., Faircloth, B. & Thrash, C. Cultivation and genomics of the first freshwater SAR11 (LD12) isolate. *Cultiv. genomics first Freshw. SAR11 Isol.* 093567 (2016). doi:10.1101/093567

89. Giovannoni, S. J. SAR11 Bacteria: The Most Abundant Plankton in the Oceans. *Ann. Rev. Mar. Sci.* **9**, 231–255 (2017).

90. Tamura, T. The family Sporichthyaceae. in *The Prokaryotes: Actinobacteria* 883–888 (Springer-Verlag Berlin Heidelberg, 2014). doi:10.1007/978-3-642-30138-4_182

91. Komagata, K., Iino, T. & Yamada, Y. The family Acetobacteraceae. in *The Prokaryotes: Alphaproteobacteria and Betaproteobacteria* **9783642301**, 3–78 (Springer-Verlag Berlin Heidelberg, 2014).

92. Liu, J. *et al.* Occurrence and fate of ultramicrobacteria in a full-scale drinking water treatment plant. *Front. Microbiol.* **9**, 2922 (2018).

93. Coenye, T. The family Burkholderiaceae. in *The Prokaryotes: Alphaproteobacteria and Betaproteobacteria* **9783642301**, 759–776 (Springer-Verlag Berlin Heidelberg, 2014).

94. McIlroy, S. J. & Nielsen, P. H. The family saprospiraceae. in *The Prokaryotes: Other Major Lineages of Bacteria and The Archaea* **9783642389**, 863–889 (Springer-Verlag Berlin Heidelberg, 2014).

95. Delafont, V., Brouke, A., Bouchon, D., Moulin, L. & Héchard, Y. Microbiome of free-living amoebae isolated from drinking water. *Water Res.* **47**, 6958–6965 (2013).

96. Proctor, C. R., Edwards, M. A. & Pruden, A. Microbial composition of purified waters and implications for regrowth control in municipal water systems. *Environ. Sci. Water Res. Technol.* **1**, 882–892 (2015).

97. Oh, S., Choi, D. & Cha, C. J. Ecological processes underpinning microbial community structure during exposure to subinhibitory level of triclosan. *Sci. Rep.* **9**, (2019).

98. Cania, B. *et al.* A long-term field experiment demonstrates the influence of tillage on the bacterial potential to produce soil structure-stabilizing agents such as exopolysaccharides and lipopolysaccharides. *Environ. Microbiomes* **14**, 1 (2019).

99. Reza, M. & Cuenca, M. A. Nitrification and denitrifying phosphorus removal in an upright continuous flow reactor. *Water Sci. Technol.* **73**, 2093–2100 (2016).

100. Hahn, M. W., Jezberová, J., Koll, U., Saueressig-Beck, T. & Schmidt, J. Complete ecological isolation and cryptic diversity in Polynucleobacter bacteria not resolved by 16S rRNA gene sequences. *ISME J.* **10**, 1642–1655 (2016).

101. Kaestli, M. *et al.* Opportunistic pathogens and large microbial diversity detected in source-to-distribution drinking water of three remote communities in Northern Australia. *PLoS Negl. Trop. Dis.* **13**, (2019).

102. Wakelin, S. *et al.* Microbial community structure of a slow sand filter schmutzdecke: A phylogenetic snapshot based on rRNA sequence analysis. *Water Sci. Technol. Water Supply* **11**, 426–436 (2011).

103. Webster, T. M. & Fierer, N. Microbial dynamics of biosand filters and contributions of the microbial food web to effective treatment of wastewater-impacted water sources. *Appl. Environ. Microbiol.* **85**, (2019).

104. Oren, A. The family Xanthobacteraceae. in *The Prokaryotes: Alphaproteobacteria and Betaproteobacteria* **9783642301**, 709–726 (Springer-Verlag Berlin Heidelberg, 2014).

105. van der Kooij, D., Veenendaal, H. R., Italiaander, R., van der Mark, E. J. & Dignum, M. Primary colonizing Betaproteobacteriales play a key role in the growth of Legionella pneumophila in biofilms on surfaces exposed to drinking water treated by slow sand filtration. *Appl. Environ. Microbiol.* **84**, (2018).

106. Oren, A. & Xu, X. W. The family hyphomicrobiaceae. in *The Prokaryotes: Alphaproteobacteria and Betaproteobacteria* **9783642301**, 247–281 (Springer-Verlag Berlin Heidelberg, 2014).

107. Amin, S. A., Parker, M. S. & Armbrust, E. V. Interactions between Diatoms and Bacteria. *Microbiol. Mol. Biol. Rev.* **76**, 667–684 (2012).

108. Zhou, J. *et al.* Microbial community structure and associations during a marine dinoflagellate bloom. *Front. Microbiol.* **9**, (2018).

109. Koedooder, C. *et al.* Diatom-bacteria interactions modulate the composition and productivity of benthic diatom biofilms. *Front. Microbiol.* **10**, (2019).

110. Ramanan, R. *et al.* Phycosphere bacterial diversity in green algae reveals an apparent similarity across habitats. *Algal Res.* **8**, 140–144 (2015).

111. Ward, N. L. *et al.* Three genomes from the phylum Acidobacteria provide insight into the lifestyles of these microorganisms in soils. *Appl. Environ. Microbiol.* **75**, 2046–2056 (2009).

112. Wakelin, S. A., Page, D. W., Pavelic, P., Gregg, A. L. & Dillon, P. J. Rich microbial communities inhabit water treatment biofilters and are differentially affected by filter type and sampling depth. *Water Sci. Technol. Water Supply* **10**, 145–156 (2010).

113. Acharya, S. M., Kurisu, F., Kasuga, I. & Furumai, H. Chlorine Dose Determines Bacterial Community Structure of Subsequent Regrowth in Reclaimed Water. *J. Water Environ. Technol.* **14**, 15–24 (2016).

114. Glaeser, S. P. & Kämpfer, P. The family Sphingomonadaceae. in *The Prokaryotes: Alphaproteobacteria and Betaproteobacteria* **9783642301**, 641–707 (Springer-Verlag Berlin Heidelberg, 2014).

115. Wang, F. *et al.* Molecular analysis of bacterial community in the tap water with different water ages of a drinking water distribution system. *Front. Environ. Sci. Eng.* **12**, (2018).

116. Le Bihan, Y. & Lessard, P. Monitoring biofilter clogging: Biochemical characteristics of the biomass. *Water Res.* **34**, 4284–4294 (2000).

117. Evans, A. N. The Effect of Nutrient Limitations on the Production of Extracellular

Polymeric Substances by Drinking-Water Bacteria. (University of Texas at Austin, 2013).

118. Keithley, S. E. & Kirisits, M. J. Enzyme-Identified Phosphorus Limitation Linked to More Rapid Headloss Accumulation in Drinking Water Biofilters. *Environ. Sci. Technol.* **53**, 2027–2035 (2019).

119. Lauderdale, C. V., Chadik, P., Kirisits, M. J. & Brown, A. J. Engineered biofiltration: Enhanced biofilter performance through nutrient and peroxide addition. *J. Am. Water Works Assoc.* **104**, 73–74 (2012).

120. Mauclaire, L., Schürmann, A., Thullner, M., Zeyer, J. & Gammeter, S. Sand filtration in a water treatment plant: Biological parameters responsible for clogging. *J. Water Supply Res. Technol. - AQUA* **53**, 93–108 (2004).

121. LeChevallier, M. W., Becker, W. C., Schorr, P. & Lee, R. G. Evaluating the performance of biologically active rapid filters. *J. / Am. Water Work. Assoc.* **84**, 136–140 (1992).

122. Heiderscheidt, E., Leiviskä, T. & Kløve, B. Coagulation of humic waters for diffused pollution control and the influence of coagulant type on DOC fractions removed. *J. Environ. Manage.* **181**, 883–893 (2016).

123. Jarvis, P., Jefferson, B. & Parsons, S. A. Floc structural characteristics using conventional coagulation for a high doc, low alkalinity surface water source. *Water Res.* **40**, 2727–2737 (2006).

124. Sillanpää, M., Ncibi, M. C., Matilainen, A. & Vepsäläinen, M. Removal of natural organic matter in drinking water treatment by coagulation: A comprehensive review. *Chemosphere* **190**, 54–71 (2018).

125. Nissinen, T. K., Miettinen, I. T., Martikainen, P. J. & Vartiainen, T. Molecular size distribution of natural organic matter in raw and drinking waters. *Chemosphere* **45**, 865–873 (2001).

126. Bell, K. *et al.* *Enhanced and Optimized Coagulation for Particulate and Microbial Removal.* (1998).

127. USEPA. *Effect of Treatment on Nutrient Availability. United States Environmental Protection Agency* (2007).

128. Geng, Y. Application of Flocs Analysis for Coagulation Optimization at the Split Lake Water Treatment Plant. (University of Manitoba, 2005).

129. Amador, J., Evans, P., Smith, J., Metz, D. & Kashinkunti, R. Chemically enhanced biological filtration to improve water quality and minimize cost. in *Biological Treatment Symposium 2013* 499–514 (2013).

130. Stoddart, A. K. & Gagnon, G. A. Water quality and filter performance of nutrient-, oxidant- and media-enhanced drinking water biofilters. *Environ. Sci. Water Res. Technol.* (2017). doi:10.1039/C6EW00293E

131. Knowles, A. D. Optimizing the removal of natural organic matter in drinking water while avoiding unintended consequences following coagulation. (Dalhousie University, 2011).

132. Knowles, A. D., Mackay, J. & Gagnon, G. A. Pairing a pilot plant to a direct filtration water treatment plant. *Can. J. Civ. Eng.* **39**, 689–700 (2012).

133. Markechova, D., Tomkova, M. & Sadecka, J. Fluorescence excitation-emission matrix spectroscopy and parallel factor analysis in drinking water treatment: a review. *Polish J. Environ. Stud.* **22**, 1289–1295 (2013).

134. Stoddart, A. K. & Gagnon, G. A. Application of photoelectrochemical chemical oxygen demand to drinking water. *J. Am. Water Works Assoc.* **106**, E383–E390 (2014).

135. Dubois, M., Gilles, K., Hamilton, J., Rebers, P. & Smith, F. Colorimetric Method for Determination of Sugars and Related Substances. *Anal. Chem* **28**, 350 (1956).

136. Summers, R. S., Hooper, S. M., Shukairy, H. M., Solarik, G. & Owen, D. Assessing DBP yield: Uniform formation conditions. *J. / Am. Water Work. Assoc.* **88**, 80–93 (1996).

137. Grace, M. A., Healy, M. G. & Clifford, E. Performance and surface clogging in intermittently loaded and slow sand filters containing novel media. *J. Environ. Manage.* **180**, 102–110 (2016).

138. Piña, R. G. & Cervantes, C. Microbial interactions with aluminium. *BioMetals* **9**, 311–316 (1996).

139. Michel, B. After 30 years of study, the bacterial SOS response still surprises us. *PLoS Biol.* **3**, 1174–1176 (2005).

140. Little, J. W. & Mount, D. W. The SOS regulatory system of Escherichia coli. *Cell* **29**, 11–22 (1982).

141. Van der Veen, S. & Abee, T. Bacterial SOS response: A food safety perspective. *Curr. Opin. Biotechnol.* **22**, 136–142 (2011).

142. Guzzo, A. & Diorio, C. Transcription of the Escherichia coli fliC Gene Is Regulated by Metal Ions. *Biochemistry* **57**, 2255–2259 (1991).

143. Ghadaksaz, A., Imani Fooladi, A. A., Hosseini, H. M. & Amin, M. The prevalence of some Pseudomonas virulence genes related to biofilm formation and alginate production among clinical isolates. *J. Appl. Biomed.* **13**, 61–68 (2015).

144. Tanner, C. C., Sukias, J. P. . & Upsdell, M. P. Organic matter accumulation during maturation of gravel-bed constructed wetlands treating farm dairy wastewaters. *Water Res.* **32**, 3046–3054 (1998).

145. Rich, L. G. A Critical Look at Rock Filters. *J. Environ. Eng.* **114**, 219–223 (1988).

146. Bratby, J. *Coagulation and flocculation in water and wastewater treatment*. *IWA* (2016). doi:10.2166/9781780407500

147. Duan, J. & Gregory, J. Coagulation by hydrolysing metal salts. *Adv. Colloid Interface Sci.* **100–102**, 475–502 (2003).

148. Sarpola, A. The Hydrolysis of Aluminium, A Mass Spectrometric Study. *Environmental Engineering* (UNIVERSITY OF OULU, 2007).

149. Klotz, K. *et al.* The health effects of aluminum exposure. *Dtsch. Arztebl. Int.* **114**, 653–659 (2017).

150. Krewski, D. *et al.* Human health risk assessment for aluminium, aluminium oxide, and aluminium hydroxide. *J. Toxicol. Environ. Heal. - Part B Crit. Rev.* **10**, 1–269 (2007).

151. Lewandowska-Szumiel, M., Komender, J., Glin, W. & Patologii, L. Aluminum in human pathology. *Pol Arch Med Wewn* **79**, 159–170 (1988).

152. Wills, M. R. & Savory, J. Aluminum and chronic renal failure: Sources, absorption, transport, and toxicity. *Crit. Rev. Clin. Lab. Sci.* **27**, 59–107 (1989).

153. Quarello, F. *et al.* Aluminum in chronic hemodialysis. Possible influence on osteomalacic bone disease. *Minerva Nefrol.* **27**, 635–644 (1980).

154. Ihle, B. *et al.* Aluminum Associated Bone Disease: Clinico-Pathologic Correlation. *Am. J. Kidney Dis.* **2**, 255–263 (1982).

155. Quarles, D. L., Gitelman, H. J. & Drezner, M. K. Aluminum: Culprit or accessory in the genesis of renal osteodystrophy. *Semin. Nephrol.* **6**, 90–101 (1986).

156. Health Canada. *Aluminum in drinking water: Guideline technical document for consultation.* (2019).

157. IPCS. *Environmental Health Criteria 194 For Aluminium. International Programme on Chemical Safety* (1997).

158. Panasenkov YuV. Determination of the effect of aluminium sulphate on natural microbial coenoses in experiment. *J. Hyg. Epidemiol. Microbiol. Immunol.* **31**, 279–286 (1987).

159. Zwarun, A. A., Bloomfield, B. J. & Thomas, G. W. Effect of Soluble and Exchangeable Aluminum on a Soil Bacillus. *Soil Sci. Soc. Am. J.* **35**, 460–463 (1971).

160. Thompson, G. W. & Medve, R. J. Effects of Aluminum and Manganese on the Growth of Ectomycorrhizal Fungi. *Appl. Environ. Microbiol.* **48**, 556–560 (1984).

161. Ali, Z. M. Synergistic antibacterial interaction between an alum and antibiotics on some microorganism. *Sci. J. Med. Res.* **02**, 47–51 (2018).

162. Jowkar, M. M., Khalighi, A., Kafi, M. & Hassanzadeh, N. Evaluation of aluminum sulfate as vase solution biocide on postharvest microbial and physiological properties of 'Cherry Brandy' rose. *Acta Hortic.* **1012**, 615–626 (2013).

163. Cook, K. L., Rothrock, M. J., Warren, J. G., Sistani, K. R. & Moore, P. A. Effect of Alum Treatment on the Concentration of Total and Ureolytic Microorganisms in Poultry Litter. *J. Environ. Qual.* **37**, 2360–2367 (2008).

164. Al Zubaidy, E. A. H., Mohammad, F. S. & Bassioni, G. Effect of pH, salinity and temperature on aluminum cookware leaching during food preparation. *Int. J. Electrochem. Sci.* **6**, 6424–6441 (2011).

165. Cardwell, A. S. *et al.* Chronic toxicity of aluminum, at a pH of 6, to freshwater organisms: Empirical data for the development of international regulatory standards/criteria. *Environ. Toxicol. Chem.* **37**, 36–48 (2018).

166. Gensemer, R. W. & Playle, R. C. The bioavailability and toxicity of aluminum in aquatic environments. *Crit. Rev. Environ. Sci. Technol.* **29**, 315–450 (1999).

167. Arul Prakash, F., Dushendra Babu, G. J., Lavanya, M., Vidhya, K. S. & Devasena, T.

Toxicity Studies of Aluminium Oxide Nanoparticles in Cell Lines. *Int. J. Nanotechnol. Appl.* **5**, 99–107 (2011).

168. Barra, P. J. *et al.* Understanding the strategies to overcome phosphorus-deficiency and aluminum-toxicity by ryegrass endophytic and rhizosphere phosphobacteria. *Front. Microbiol.* **9**, 1155 (2018).

169. Illmer, P. & Erlebach, C. Influence of A1 on growth, cell size and content of intracellular water of Arthrobacter sp. PI/1-95. *Antonie van Leeuwenhoek, Int. J. Gen. Mol. Microbiol.* **84**, 239–246 (2003).

170. Pifia, R. G. *et al.* MINI-REVIEW Microbial interactions with aluminium. *Biometals* 311–316 (1996).

171. Lemire, J., Kumar, P., Mailloux, R., Cossar, K. & Appanna, V. D. Metabolic adaptation and oxaloacetate homeostasis in P. fluorescens exposed to aluminum toxicity. *J. Basic Microbiol.* **48**, 252–259 (2008).

172. Mora, M. de la L. *et al.* Aluminum-tolerant bacteria improve the plant growth and phosphorus content in ryegrass grown in a volcanic soil amended with cattle dung manure. *Appl. Soil Ecol.* **115**, 19–26 (2017).

173. Beloin, C. *et al.* Global impact of mature biofilm lifestyle on Escherichia coli K-12 gene expression. *Mol. Microbiol.* **51**, 659–674 (2004).

174. Mattson, M. P. Hormesis defined. *Ageing Res. Rev.* **7**, 1–7 (2008).

175. Cui, X. *et al.* Science of the Total Environment Low concentrations of Al (III) accelerate the formation of bio fi lm : Multiple effects of hormesis and fl occulation. *Sci. Total Environ.* **634**, 516–524 (2018).

176. Cui, X. *et al.* Acceleration of saturated porous media clogging and silicon dissolution due to low concentrations of Al(III) in the recharge of reclaimed water. *Water Res.* **143**, 136–145 (2018).

177. Bulson, P. C., Johnstone, D. L., Gibbons, H. L. & Funk, W. H. Removal and inactivation of bacteria during alum treatment of a lake. *Appl. Environ. Microbiol.* **48**, 425–430 (1984).

178. Reuß, D. R. *et al.* Large-scale reduction of the Bacillus subtilis genome: Consequences for the transcriptional network, resource allocation, and metabolism. *Genome Res.* **27**, 289–299 (2017).

179. Sparkes, A. *et al.* Towards Robot Scientists for autonomous scientific discovery. *Automated Experimentation* **2**, (2010).

180. Zwietering, M. H., Jongenburger, I., Rombouts, F. M. & Van 't riet, K. Modeling of the Bacterial Growth Curve. *Appl. Environ. Microbiol.* **56**, 1875–1881 (1990).

181. Pla, M., Oltra, S., Esteban, M., Andreu, S. & Palop, A. Comparison of Primary Models to Predict Microbial Growth by the Plate Count and Absorbance Methods. *Biomed Res. Int.* **2015**, 1–14 (2015).

182. Choe, D. *et al.* Adaptive laboratory evolution of a genome-reduced Escherichia coli. *Nat. Commun.* **10**, (2019).

183. Lum, P. Y. *et al.* Discovering Modes of Action for Therapeutic Compounds Using a Genome-Wide Screen of Yeast Heterozygotes. *Cell* **116**, 121–137 (2004).

184. Cagnon, C. *et al.* Development of a forward genetic screen to isolate oil mutants in the green microalga Chlamydomonas reinhardtii. *Biotechnol. Biofuels* **6**, 178 (2013).

185. Stevenson, K., McVey, A. F., Clark, I. B. N., Swain, P. S. & Pilizota, T. General calibration of microbial growth in microplate readers. *Sci. Rep.* **6**, 4–10 (2016).

186. Matlock, B. C., Beringer, R. W., Ash, D. L., Page, A. F. & Allen, M. W. *Differences in Bacterial Optical Density Measurements between Spectrophotometers. Technical Note from ThermoScientific* (2011).

187. Hall, B. G., Acar, H., Nandipati, A. & Barlow, M. Growth rates made easy. *Mol. Biol. Evol.* **31**, 232–238 (2014).

188. Rolfe, M. D. *et al.* Lag phase is a distinct growth phase that prepares bacteria for exponential growth and involves transient metal accumulation. *J. Bacteriol.* **194**, 686–701 (2012).

189. Djordjevic, D., Wiedmann, M. & Mclandsborough, L. A. Microtiter Plate Assay for Assessment of Listeria monocytogenes Biofilm Formation. *Appl. Environ. Microbiol.* **68**, 2950–2958 (2002).

190. O'Toole, G. A. Microtiter Dish Biofilm Formation Assay. *J. Vis. Exp.* **47**, (2011).

191. Campbell, J. High-throughput assessment of bacterial growth inhibition byOptical Density Measurements. *Curr Protoc Chem Biol.* **3**, 1–20 (2012).

192. Toussaint, M. & Conconi, A. High-throughput and sensitive assay to measure yeast cell growth: A bench protocol for testing genotoxic agents. *Nat. Protoc.* **1**, 1922–1928 (2006).

193. Goughenour, K. D., Balada-Llasat, J.-M. & Rappleye, C. A. Quantitative Microplate-Based Growth Assay for Determination of Antifungal Susceptibility of Histoplasma capsulatum Yeasts. *J. Clin. Microbiol.* **53**, 3286–3295 (2015).

194. Qiu, T. A. *et al.* Growth-Based Bacterial Viability Assay for Interference-Free and High-Throughput Toxicity Screening of Nanomaterials. *Anal. Chem.* **89**, 2057–2064 (2017).

195. Kurokawa, M. & Ying, B.-W. Precise, High-throughput Analysis of Bacterial Growth. *J. Vis. Exp.* e56197–e56197 (2017). doi:10.3791/56197

196. Bredit, F., Romick, T. . & H.P., F. A Rapid Methof for Determination of Bacterial Growth Kinetics. *Rapid Methods Autom. Microbiol.* **59**, 59–68 (1994).

197. Sieben, M., Giese, H., Grosch, J. H., Kauffmann, K. & Büchs, J. Permeability of currently available microtiter plate sealing tapes fail to fulfil the requirements for aerobic microbial cultivation. *Biotechnol. J.* **11**, 1525–1538 (2016).

198. Zimmermann, H. F., John, G. T., Trauthwein, H., Dingerdissen, U. & Huthmacher, K. Rapid evaluation of oxygen and water permeation through microplate sealing tapes. *Biotechnol. Prog.* **19**, 1061–1063 (2003).

199. Delaney, N. F. *et al.* Development of an Optimized Medium, Strain and High-

Throughput Culturing Methods for Methylobacterium extorquens. *PLoS One* **8**, (2013).

200.	Haire, T. C. *et al.* Robust microplate-based methods for culturing and in vivo phenotypic screening of Chlamydomonas reinhardtii. *Front. Plant Sci.* **9**, (2018).

201.	McBirney, S. E., Trinh, K., Wong-Beringer, A. & Armani, A. M. Wavelength-normalized spectroscopic analysis of Staphylococcus aureus and Pseudomonas aeruginosa growth rates. *Biomed. Opt. Express* **7**, 4034 (2016).

202.	Bartlett, J. W. & Frost, C. Reliability, repeatability and reproducibility: Analysis of measurement errors in continuous variables. *Ultrasound Obstet. Gynecol.* **31**, 466–475 (2008).

203.	Chavez, M., Ho, J. & Tan, C. Reproducibility of High-Throughput Plate-Reader Experiments in Synthetic Biology. *ACS Synth. Biol.* **6**, 375–380 (2017).

204.	Hart, S. F. M., Skelding, D., Waite, A. J., Burton, J. C. & Shou, W. High-throughput quantification of microbial birth and death dynamics using fluorescence microscopy. *Quant. Biol.* **7**, 69–81 (2019).

205.	Periago, P. M., Abee, T. & Wouters, J. A. Analysis of the heat-adaptive response of psychrotrophic Bacillus weihenstephanensis. *Int. J. Food Microbiol.* **79**, 17–26 (2002).

206.	Wong, A. W. T. Investigating the Enhancement of Biological Filtration with Capping Material Designs and Nutrient Amendments. (University of Waterloo, 2015).

207.	Fang, W., Hu, J. Y. & Ong, S. L. Influence of phosphorus on biofilm formation in model drinking water distribution systems. *J. Appl. Microbiol.* **106**, 1328–1335 (2009).

208.	Liu, J. R., Liu, C. T., Edwards, E. A. & Liss, S. N. Effect of phosphorus limitation on microbial floc structure and gene expression in activated sludge. *Water Sci. Technol.* **54**, 247–255 (2006).

209.	Environmental Protection Agency. *Water Treatment Manuals: Coagulation, flocculation & Clarification.* (An Ghníomhaireacht um Chaomhnú Comhshaoil, 2002).

210.	Matilainen, A., Vepsäläinen, M. & Sillanpää, M. Natural organic matter removal by coagulation during drinking water treatment : A review. *Adv. Colloid Interface Sci.* **159**, 189–197 (2010).

211.	Sproul, O. J. *Critical Review of Virus Removal by Coagulation Processes and pH Modifications.* (.S. Environmental Protection Agency, Washington, D.C., EPA/600/2-80/004., 1980).

212.	Ebeling, J., Ogden, S., Sibrell, P. & Rishel, K. Application of Chemical Coagulation Aids for the Removal of Suspended Solids (TSS) and Phosphorus from the Microscreen Effluent Discharge of an Intensive Recirculating Aquaculture System. *N. Am. J. Aquac.* **66**, 198–207 (2004).

213.	Graziani, M. & McLean, D. *Phosphorus Treatment and Removal Technologies.* (2006).

214.	Pilgrim, K. M. & Brezonik, P. L. Treatment of lake inflows with alum for phosphorus removal. *Lake Reserv. Manag.* **21**, 1–9 (2005).

215.	Lazazzera, B. A. Quorum sensing and starvation: Signals for entry into stationary

phase. *Curr. Opin. Microbiol.* **3**, 177–182 (2000).

216. Thompson, L. J., Gray, V., Lindsay, D. & Von Holy, A. Carbon:nitrogen:phosphorus ratios influence biofilm formation by Enterobacter cloacae and Citrobacter freundii. *J. Appl. Microbiol.* **101**, 1105–1113 (2006).

217. Rittmann, B. E. & McCarty, P. L. Environmental Biotechnology: Principles and Applications. *Biotechnology* 463 (2001). Available at: http://books.google.com/books?id=S6CiK7Nh9oIC&printsec=frontcover.

218. Redfield, A. C. On the Proportions of Organic Derivatives in Sea Water and Their Relation to the Composition of Plankton. *University Press of Liverpool, James Johnstone Memorial Volume* 1767–192 (1934). doi:citeulike-article-id:11236440

219. Redfield, A. C. The chemical factors in the environment. *Am. Sci.* **46**, 205–221 (1958).

220. Mckie, M. J., Taylor-edmonds, L., Andrews, S. A. & Andrews, R. C. Engineered bio fi ltration for the removal of disinfection by-product precursors and genotoxicity. *Water Res.* **81**, 196–207 (2015).

221. Pharand, L. Carbon and Nitrogen Removal at a Full-Scale Municipal Drinking Water Treatment Plant employing Sand-ballasted Clarification , Ozone and Biofiltration. (2014).

222. Vahala, R., Moramarco, V., Niemi, R. M., Rintala, J. & Laukkanen, R. The Effects of Nutrients on Natural Organic Matter (NOM) Removal in Biological Activated Carbon (BAC) Filtration. *Acta Hydrochim. Hydrobiol.* **26**, 196–199 (1998).

223. Miettinen, I. T., Vartiainen, T. & Martikainen, P. J. Phosphorus and bacterial growth in drinking water. *Appl. Environ. Microbiol.* **63**, 3242–3245 (1997).

224. Sang, J., Zhang, X., Yu, G. & Wang, Z. Phosphorus limitation on bacterial regrowth in drinking water. *J. Environ. Sci. (China)* **15**, 773–8 (2003).

225. Kirisits, M. J., Evans, A. & Lauderdale, C. Effect of phosphorus limitation on the production of extracellular polymeric substances (EPS) by drinking-water bacteria | Request PDF. in *Biological Treatment Symposium 2013* 59–63 (2013).

226. Granger, H. C., Stoddart, A. K. & Gagnon, G. A. Direct Biofiltration for Manganese Removal from Surface Water. *Environ. Eng.* **140**, (2014).

227. Saitou, N. & Nei, M. The neighbor-joining method: a new method for reconstructing phylogenetic trees. *Mol. Biol. Evol.* **4**, 406–25 (1987).

228. Kumar, S., Stecher, G. & Tamura, K. MEGA7: Molecular Evolutionary Genetics Analysis Version 7.0 for Bigger Datasets. *Mol. Biol. Evol.* **33**, 1870–1874 (2016).

229. Felsenstein, J. Confidence Limits on Phylogenies: an Approach Using the Bootstrap. *Evolution (N. Y).* **39**, 783–791 (1985).

230. Kimura, M. A simple method for estimating evolutionary rates of base substitutions through comparative studies of nucleotide sequences. *J. Mol. Evol.* **16**, 111–120 (1980).

231. Sáez-Nieto, J. A. *et al.* Paenibacillus spp. isolated from human and environmental samples in Spain: detection of 11 new species. *New Microbes New Infect.* **19**, 19–27 (2017).

232. Rivas, R., Garciá-Fraile, P., Mateos, P. F., Martínez-Molina, E. & Velázquez, E. Paenibacillus cellulosilyticus sp. nov., a cellulolytic and xylanolytic bacterium isolated from the bract phyllosphere of Phoenix dactylifera. *Int. J. Syst. Evol. Microbiol.* **56**, 2777–2781 (2006).

233. Park, M. J. *et al.* Paenibacillus soli sp. nov., a xylanolytic bacterium isolated from soil. *Int. J. Syst. Evol. Microbiol.* **57**, 146–150 (2007).

234. Nelson, D., Glawe, A., Labeda, D., Cann, I. & Mackie, R. Paenibacillus tundrae sp. nov. and Paenibacillus xylanexedens sp. nov., Psychrotolerant, Xylan-Degrading, Bacteria from Alaskan Tundra. *Int. J. Syst. Evol. Microbiol.* **59**, 1708–1714 (2009).

235. Goodwin, A. E., Roy Jnr, J. S., Grizzle, J. M. & Goldsby Jnr, M. T. Bacillus mycoides: A bacterial pathogen of channel catfish. *Dis. Aquat. Organ.* **18**, 173–179 (1994).

236. Nakamura, L. K. & Jackson, M. A. Clarification of the taxonomy of Bacillus mycoides. *Int. J. Syst. Bacteriol.* **45**, 46–49 (1995).

237. Wintzingerode, F., Rainey, F. A., Kroppenstedt, R. M. & Stackebrandt, E. Identification of environmental strains of Bacillus mycoides by fatty acid analysis and species-specific 16S rDNA oligonucleotide probe. *FEMS Microbiol. Ecol.* **24**, 201–209 (2006).

238. Lechner, S. *et al.* Bacillus weihenstephanensis sp. nov. is a new psychrotolerant species of the Bacillus cereus group. *Int. J. Syst. Bacteriol.* **48**, 1373–1382 (1998).

239. Liu, Y., Lai, Q. & Shao, Z. Genome analysis-based reclassification of bacillus weihenstephanensis as a later heterotypic synonym of bacillus mycoides. *Int. J. Syst. Evol. Microbiol.* **68**, 106–112 (2018).

240. Soufiane, B. & Côté, J. C. Bacillus weihenstephanensis characteristics are present in Bacillus cereus and Bacillus mycoides strains. *FEMS Microbiol. Lett.* **341**, 127–137 (2013).

241. Houry, A., Briandet, R., Aymerlch, S. & Gohar, M. Involvement of motility and flagella in Bacillus cereus biofilm formation. *Microbiology* **156**, 1009–1018 (2010).

242. Cohn, F. Untersuchungen über bacterien. IV. Beiträge zur biologie der Bacillen. *Beiträge zur Biol. der Pflanz.* **7**, 249–276 (1877).

243. Kearns, D. B., Chu, F., Branda, S. S., Kolter, R. & Losick, R. A master regulator for biofilm formation by Bacillus subtilis. *Mol. Microbiol.* **55**, 739–749 (2005).

244. Vlamakis, H., Chai, Y., Beauregard, P., Losick, R. & Kolter, R. Sticking together: Building a biofilm the Bacillus subtilis way. *Nat. Rev. Microbiol.* **11**, 157–168 (2013).

245. Chu, F. Regulatory pathways governing biofilm formation in Bacillus subtilis. (Harvard University, 2007).

246. Romero, D., Aguilar, C., Losick, R. & Kolter, R. Amyloid fibers provide structural integrity to Bacillus subtilis biofilms. *Proc. Natl. Acad. Sci. U. S. A.* **107**, 2230–2234 (2010).

247. Ryu, J. H., Kim, H. & Beuchat, L. R. Attachment and biofilm formation by Escherichia coli O157:H7 on stainless steel as influenced by exopolysaccharide production, nutrient availability, and temperature. *J. Food Prot.* **67**, 2123–2131 (2004).

248. Morikawa, M. Beneficial biofilm formation by industrial bacteria Bacillus subtilis and related species. *J. Biosci. Bioeng.* **101**, 1–8 (2006).

249. Wen, Z. T., Baker, H. V. & Burne, R. A. Influence of BrpA on critical virulence attributes of Streptococcus mutans. *J. Bacteriol.* **188**, 2983–2992 (2006).

250. Toyofuku, M. *et al.* Environmental factors that shape biofilm formation. *Biosci. Biotechnol. Biochem.* **80**, 7–12 (2016).

251. Staats, N., Stal, L. J. & Mur, L. R. Exopolysaccharide production by the epipelic diatom Cylindrotheca closterium: Effects of nutrient conditions. *J. Exp. Mar. Bio. Ecol.* **249**, 13–27 (2000).

252. Danhorn, T., Hentzer, M., Givskov, M., Parsek, M. R. & Fuqua, C. Phosphorus limitation enhances biofilm formation of the plant pathogen Agrobacterium tumefaciens through the PhoR-PhoB regulatory system. *J. Bacteriol.* **186**, 4492–4501 (2004).

253. Zhang, W. *et al.* Nutrient depletion in Bacillus subtilis biofilms triggers matrix production. *New J. Phys.* **16**, 015028 (2014).

254. Bonet, R., Simon-Pujol, M. D. & Congregado, F. Effects of nutrients on exopolysaccharide production and surface properties of Aeromonas salmonicida. *Appl. Environ. Microbiol.* **59**, 2437–2441 (1993).

255. Unz, R. F. & Farrah, S. R. Exopolymer production and flocculation by zoogloea mp6. *Appl. Environ. Microbiol.* **31**, 623–626 (1976).

256. Wachenheim, D. E. & Patterson, J. A. Anaerobic production of extracellular polysaccharide by Butyrivibrio fibrisolvens nyx. *Appl. Environ. Microbiol.* **58**, 385–391 (1992).
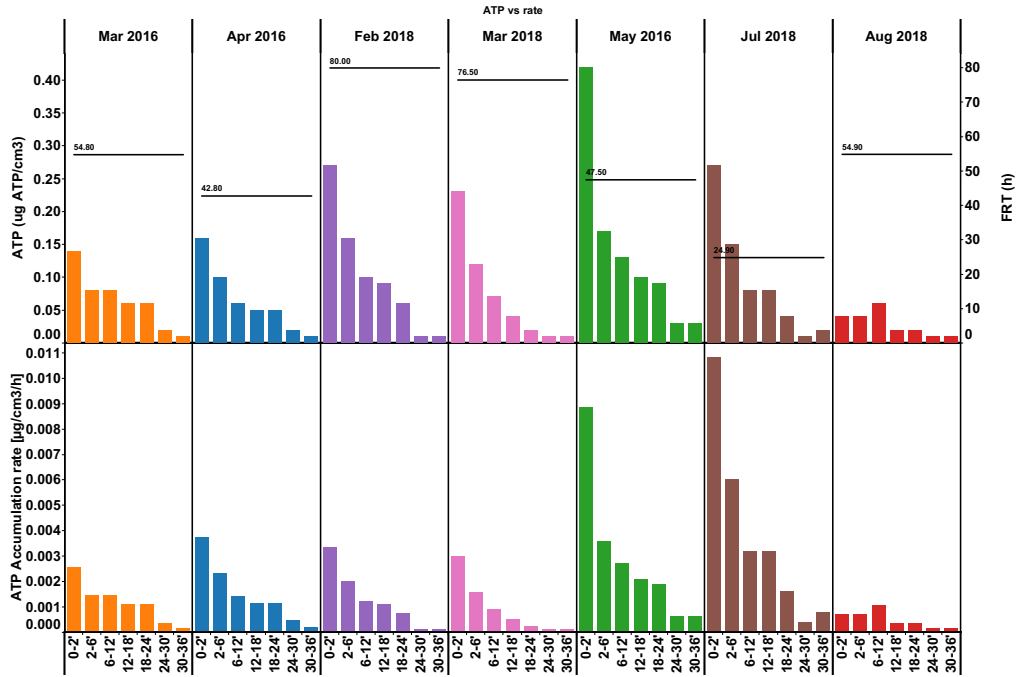
Figure 37   Comparing the ATP versus the normalized ATP. Using the normalized ATP, the differences between the different filter event is more distinguishable while using the ATP in July 2018, diatom bloom on top of the filter media is similar to the Feb 2018; however, the similar ATP was reached in one fourth of Feb2018 FRT.
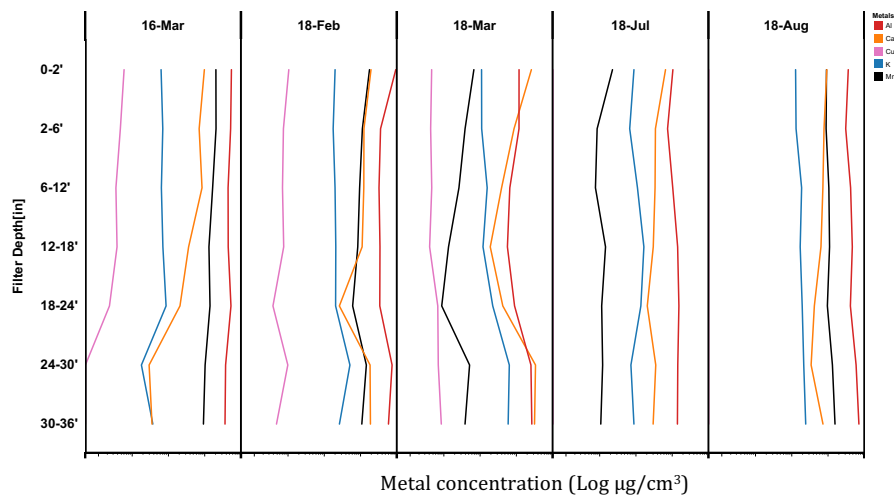

Figure 38   Deposited metals in different sampling events through the filter depth. The metal concentration is represented in log scale.
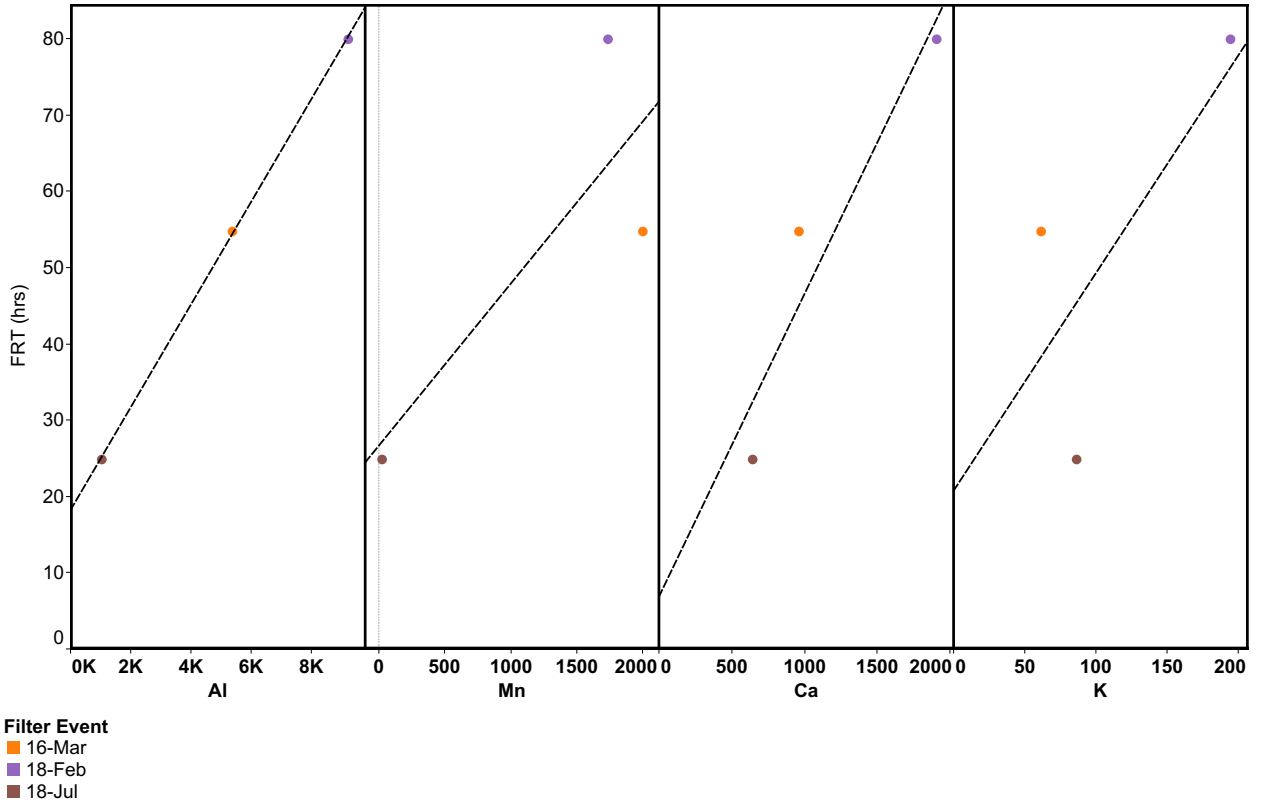
Figure 39   Correlation between aluminum concentration on top of the biofilter media (old media) and FRT. Shows that the filter runtime has a strong impact on the concentration deposited on the media. The higher the filter runtime the higher the metal concentration.
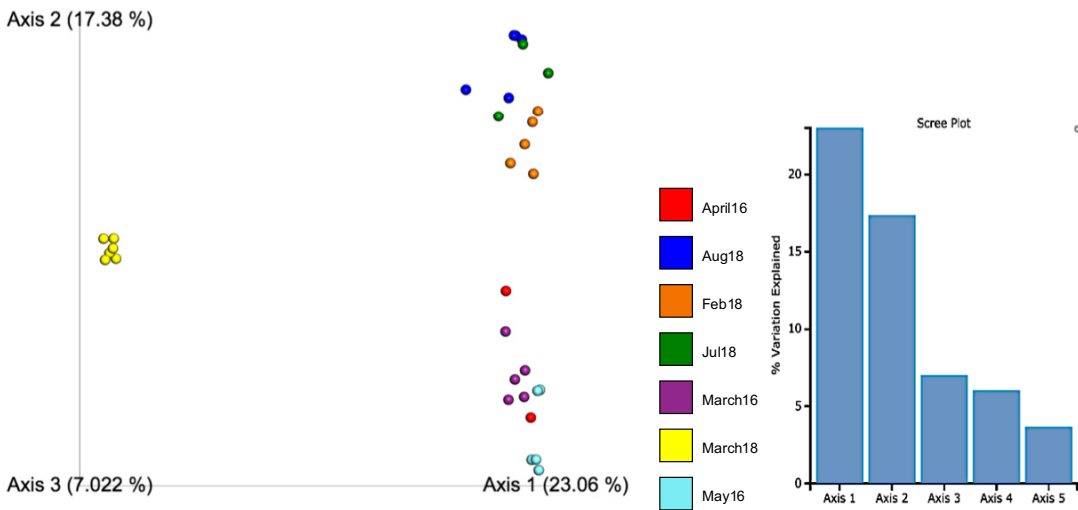

Figure 40   Jaccard distance beta diversity analysis with the scree plot
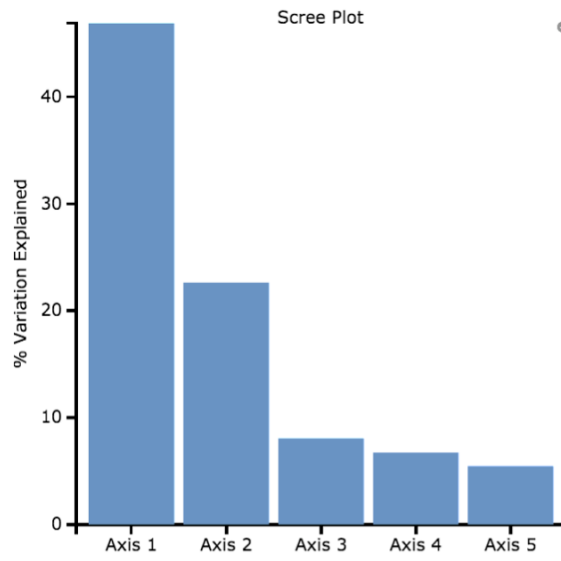
Figure 41   Scree plot for Weighted Uni-Frac beta diversity analysis
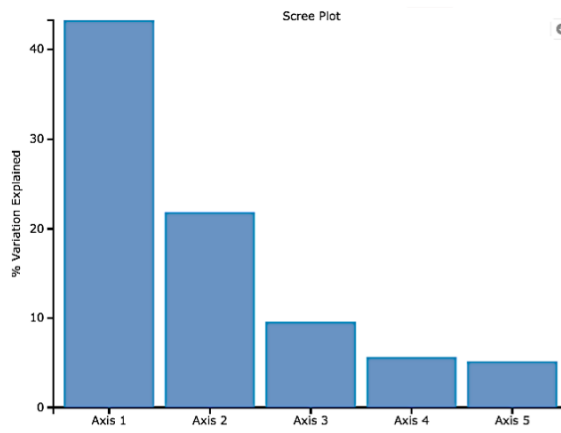

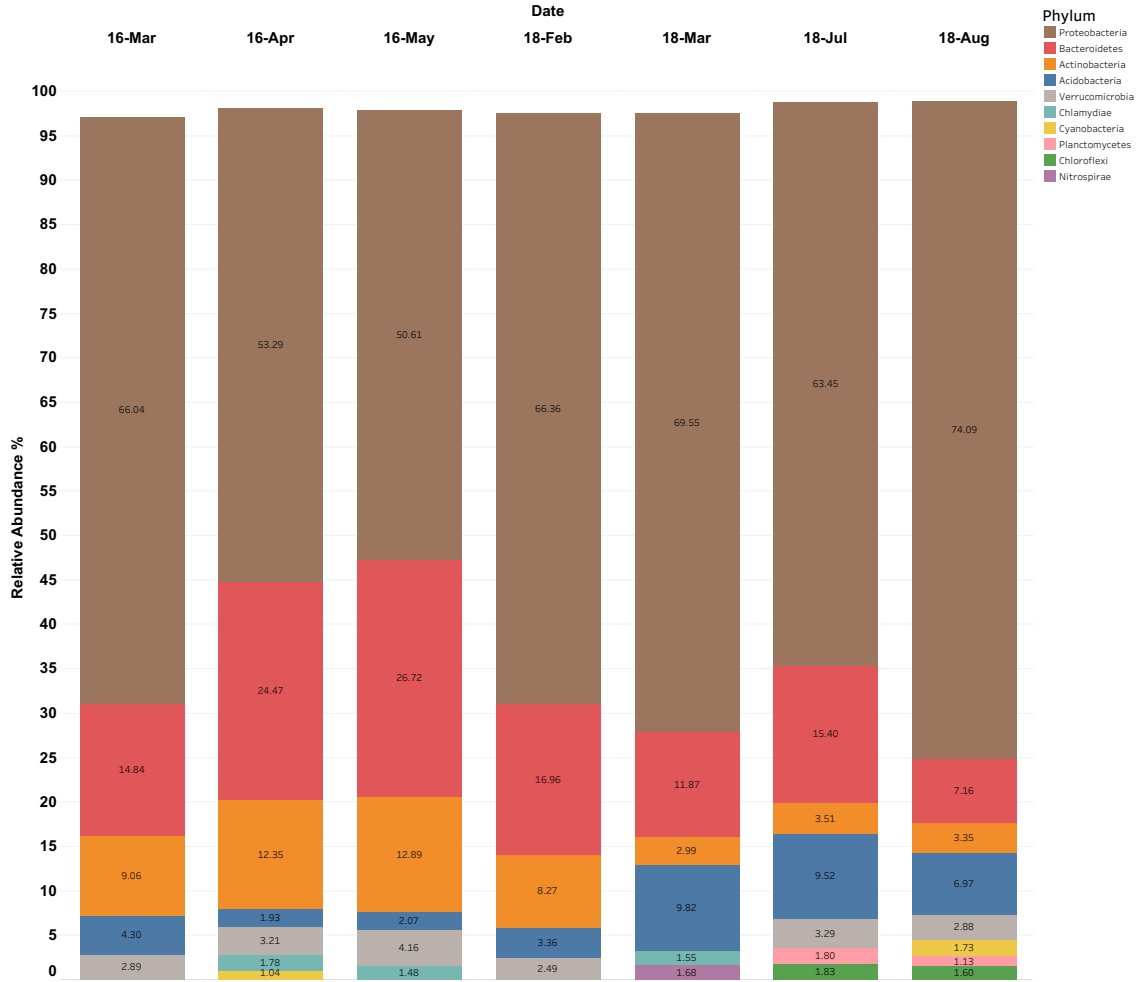Figure 42   Scree plot for Bray-Curtis beta diversity analysis

Figure 43   Relative abundance of all the filter events at phylum level. As shown the protobacteria followed by Bacteroidetes are the most abundant phyla in all the biofilters

APPENDIX B – MICROPLATE READER ABSORBANCE TEST

INTRODUCTION

To make sure of the repeatability and accuracy of data collected from the microplate reader in the absorbance range (400-800 nm); the manufacturer, BioTek, provided three different tests.

- Absorbance Liquid Test 1 and Absorbance Plate Test or
- Absorbance Liquid Test 2
- Absorbance Liquid Test 3 or Absorbance Plate Test at 340 nm (using BTI#7260551)

The cost of the Plate Test is high, and it must be ordered separately from BioTek. Absorbance Liquid Test 3 is focused on the UV range. Therefore, after consulting with BioTek technicians, Wendy Cannan, Absorbance Liquid Test 2 was suggested to check the absorbance range accuracy and repeatability of the Synergy H1.

The objective of this test is to examine the **repeatability** and **accuracy** and **alignment** of the microplate reader. Definition of these terms is as follows based on the Synergy H1 operating Manual.

MATERIALS

- New 96-well clear flat-bottom microplate (Use the plate that you are intended to use in your experiment)
- Ten test tubes, numbered consecutively, set in a rack
- Calibrated hand pipette (Class A volumetric pipette recommended)
- Stock Solution A or B (see instructions for Liquid Test 1)
- 0.05% solution of Tween 20 (with deionized water)
- Use the Gen5 protocol **"Abs Test 2"**

PREPARATION STEPS

Preparing the Solutions

- Deionized water
- FD&C Yellow No. 5 dye powder
- Tween 20 (polyoxyethylene (20) sorbitan monolaurate) As wetting agent
- Precision balance with capacity of 100 g minimum and readability of 0.001 g
- Weigh dish
- 1-liter volumetric flask (*2)

Stock Solution FD&C Yellow No. 5 dye powder

- Weigh out 0.092 g of FD&C Yellow No. 5 dye powder into a weigh boat.
- Rinse the contents into a 1-liter volumetric flask.
- Add 0.5 mL of Tween 20.
- Fill to 1 liter with DI water; cap and shake well.

Stock Solution of 0.05% Tween 20

- Add 0.5 ml of Tween20 in 1-liter volumetric flask
- Fill to 1 liter with DI water; cap and shake well.

Serial dilution

Create a percentage dilution series, beginning with 100% of the original concentrated stock solution in the first tube, 90% of the original solution in the second tube, 80% in the third tube, all the way to 10% in the tenth tube. Dilute using the 0.05% solution of deionized water and Tween 20 (see Table 18)

Table 18   Dilution series by volume

Tube number	1	2	3	4	5	6	7	8	9	10
Volume of FD&C Yellow Stock solution	20	18	16	14	12	10	8	6	4	2
Volume of 0.05% Tween 20	0	2	4	6	8	10	12	14	16	18

Preparing the 96 well microplate

- Pipette 200 µL of the concentrated solution from Tube 1 into each well of the first
- column, A1 to H1, of a new flat-bottom microplate.
- Pipette 200 µL from each of the remaining tubes into the wells of the corresponding column of the microplate (Tube 2 into wells A2 to H2, Tube 3 into wells A3 to H3, and so on).
- Use protocol **"Abs Test 2"** and read.

Record the data and use the run linearity test, repeatability and alignment test

Processing data

Linearity and Accuracy

The plate is read five times at 450/630 nm ("Normal" position), resulting in five sets of Delta OD data. Calculate results for Linearity:

Calculate the mean absorbance for each well and average the means for each concentration.

Perform a regression analysis on the data to determine if there is adequate linearity. Since it is somewhat difficult to achieve high pipetting accuracy when conducting linear dilutions, an R2 value of at least 0.9900 is considered adequate.

Repeatability

To calculate the results for repeatability, please follow the following three (3) steps

- Calculate the Mean and Standard Deviation for the five readings taken at each concentration. Only one row of data needs to be analyzed.
- For each Mean below 2.000 OD, calculate the Allowed Deviation using the Repeatability specification for a 96-well plate of ±1.0% ±0.005 OD. (If above 2.000 OD, apply the ±3.0% ±0.005 specification.)
- The Standard Deviation for each set of readings should be less than the Allowed Deviation

Example: Readings of 1.950, 1.948, 1.955, 1.952, and 1.950 will result in a Mean of 1.951, and a Standard Deviation of 0.0026. The Mean (1.951) multiplied by 1.0% (1.951 x 0.010) = 0.0195, which, when added to the 0.005 (0.0195 + 0.005) = 0.0245 OD, which is the Allowed Deviation. Since the Standard Deviation is less than this value, the reader meets the test criteria.

Alignment

After gathering data for the Linearity Test, the plate is read five more times with the A1 well in the H12 position ("Turnaround" position). This results in values for the four corner wells that can be used to assess alignment. Calculate results for the Alignment Test:

- Calculate the means of the wells A1 and H1 in the Normal plate position (data from Linearity Test) and in the Turnaround position.
- Compare the mean reading for well A1 to its mean reading when in the H12 position. Next, compare the mean values for the H1 well to the same well in the A12 position. The difference in the values for any two corresponding wells should be within the Accuracy specification for 96-well plates. If the four corner wells are within the accuracy range, the reader is in alignment.

Example: If the mean of well A1 in the normal position is 1.902, where the specified accuracy is ±1.0% ±0.010 OD, then the expected range for the mean of the same well in the H12 position is 1.873 to 1.931 OD. (1.902 x 1.0% = 0.019 + 0.010 = 0.029, which is added to and subtracted from 1.902 for the range.)

Interpretation of Sample Results

Linearity

The calculated R-squared is 0.9998 which is considered adequate. The result prove that data has linearity and consequently the **accuracy**.
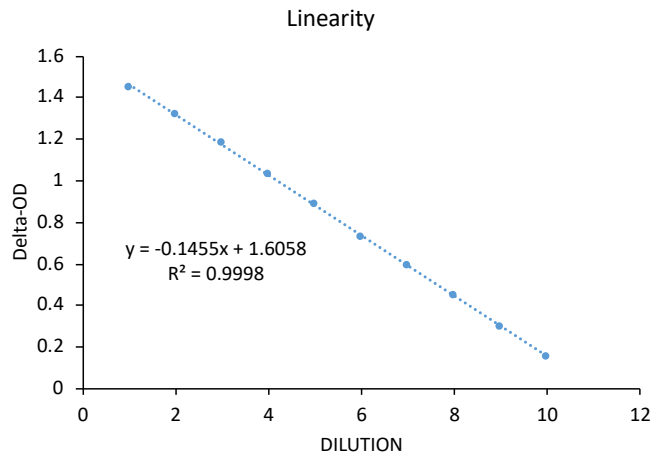
Figure 44   The adequate linearity (r2> 0.9900) shows the accuracy of the microplate reader. The Y axis shows the average of (OD450-OD630) and Y axis is different concentration of Yellow color

Repeatability

All the standard deviations calculated for each well are within the acceptable deviation.

The results prove that the collected data from Microplate reader is **repeatable**.

Alignment

This data set is shared with Biotek Technicians to be sure of the conclusion.

Table 19   Alignment Data

Normal Position		Turn Around Position	
A1	1.407	**A1**	0.005
H12	0.005	**H12**	1.397

H12 = 0.005 and A1 = 0.005, A1=1.0407 and H12= 1.397 are within the accuracy range.

These results prove that the microplate reader is **aligned.**

APPENDIX C – GROWTH RATE IN MICROPLATE READER-
EXPERIMENTAL PROTOCOL

Step 1 - Preparing Bacterial Stock in Glycerol

This procedure starts with bacteria that have already been transferred to agar plates.

All of the steps below must be followed in a sterile condition (i.e., between two flames or in a safety cabinet). All the material and tools are autoclaved for 20 minutes. Gloved hands are disinfected and kept wet with hand disinfectant or 70% Alcohol solution for at least 1 minute and not removed from the safety cabinet after, or the disinfecting procedure has to be repeated before introducing the hand back into the safety cabinet.

Caution: Ensure the disinfectant is completely evaporated before working with an open flame.

TSB powder is a commercially available product and can be prepared based on the instruction on the package (Weigh 3 gr of Tryptic soy broth (TSB) powder and dissolve in 100 ml distilled water).

10. Prepare a flask with 10 ml of Tryptic Soy Broth (TSB)
11. Using a loop, scoop one loop-full of bacteria from the agar plate
12. Add the content of the loop into the flask with TSB
13. Incubate the flask over night at $30\pm1°C$ and orbital shaking at 150 rpm)

Note: depending on the type of strain, temperature and shaking may need to be adjusted.

14. Prepare a flask with 10 ml of TSB
15. Transfer 500µL of the overnight culture to the flask with fresh TSB
16. Incubate it for 6-8 hours (to get to the exponential phase)
17. Transfer the culture to a 15 ml falcon tube
18. Centrifuge the culture at 3500 rpm for 10 minutes.

19. Decant the broth and gently wash the cells three times with Phosphate Buffer Saline (PBS).
20. Adjust the optical density of the cells to 0.6±0.05 by titrating PBS solution using a pipette.
21. Accurately record the added amount of PBS
22. Titrate glycerol to the solution to reach 20% v/v
23. Cap the falcon tube and vortex for 15 seconds
24. Transfer 1.5 ml of the solution to 2 ml microtubes
25. Put the microtubes in an appropriate box and store it in the freezer at -80°C.

Step 2 - Inoculum Preparation

TSB powder is a commercially available product and can be prepared based on the instruction on the package (Weigh 3 gr of Tryptic soy broth (TSB) powder and dissolve in 100 ml distilled water).

1. Let the microtubes with bacterial stock thaw at room temperature for 30 minutes or until the content is visually liquid. It is recommended to not accelerate thawing
2. Prepare a flask with 10 ml of TSB
3. Transfer 50μL of stock solution to 10 ml fresh TSB
4. Incubate the flask it over night at 30±1°C and orbital shaking at 150 rpm

Note: depending on the type of strain, temperature and shaking may need to be adjusted.

5. Prepare a flask with 10 ml of TSB
6. Transfer 500μL of the overnight culture to the flask with fresh TSB
7. Incubate it for 6-8 hours (to get to the exponential phase)
8. Transfer the culture to a 15 ml falcon tube
9. Centrifuge the culture at 3500 rpm for 10 minutes.
10. Decant the broth and gently wash the cells three times with Phosphate Buffer Saline (PBS).
11. Adjust the optical density of the cells to 0.6±0.05 by titrating PBS solution using a pipette.
12. Accurately record the added amount of PBS

Step 3 - Preparing the Growth Medium

In this protocol the nutrient rich medium used is TSB and minimal medium is M63.

TSB powder is a commercially available product and can be prepared based on the instruction on the package (Weigh 3 gr of Tryptic soy broth (TSB) powder and dissolve in 100 ml distilled water).

M63 preparation:

Prepare a 5-times concentrated mixed salt stock solution:

- Weigh 15g KH_2PO_4
- Weigh 35g K_2HPO_4
- Weigh 10g $(NH_4)_2SO_4$
- Add all three amounts to 1 L of distilled water

Prepare stock solution of $MgSO_4.7H_2O$:

- Weigh 24.6 g $MgSO_4$
- Add the $MgSO_4$ to 100ml of distilled water (concentration :1 M)

Prepare stock solution of glucose:

- Weigh 20g of glucose
- Add the glucose to 100 ml of distilled water (concentration: 20.0% w/v).

Prepare stock solution of $FeSO_4.7H_2O$. dissolve iron sulfate in the sulfuric acid and then add distilled water to reach to the concentration of 50 mg/L.

Prepare stock solution of arginine. Dissolve 20gr of arginine in 100 ml of distilled water (concentration: 20% w/v). Sterilize arginine with 0.25μm syringe filter.

To prepare 100ml of M63, add below mentioned volume of each stock solution to a 200 ml sterilized bottle with cap.

- 20 ml of the mixed salt stock solution
- 1 ml of glucose stock
- 100μL of $MgSO_4.7H_2O$ stock solution
- 2 ml of arginine stock solution
- 1 ml of $FeSO_4.7H_2O$ stock solution.
- Tighten the cap and swirl gently, it can be stored in the room temperature.

Step 4 - Transferring the Growth Medium to Microplate reader

1. Choose a transparent sterile flat bottom well plate with lid (i.e. 96 well plate, 6 well plate, 12 well plate)
2. Make sure that you have the pathlength correction for your plate. You can measure that with DI water and the path length correction procedure in the microplate reader.
3. Draw a table according the selected well plate (for example 8*12 for 96 well plate) to indicate the positions of the inoculated culture samples on the plate.
4. Print out the table and use it as a reference table for the experiment. Note: The wells located on the edges of the microplate should only contain distilled water due to the fact that evaporation on the edge wells are higher.
5. Place a sterilized microplate with lid, P-1000, 1000-µL pipette tips, P-200, 200-µL pipette tips, several 1.5-mL microtubes, an 8-multichannel pipette, a sterilized 150 ml beaker, room temperature growth medium, and the inoculum stocks in the safety cabinet.
6. Transfer the calculated amount of inoculum to the growth medium in a beaker. Note: the ratio of inoculum to the growth medium is 5%.
7. Gently shake the beaker after adding the inoculum prior to loading to microplate.
8. Fill the wells at the edge of the microplate with 200 µL sterile growth medium pipette (P-200).
9. Load 200 µL of each sample prepared to the microplate wells according to the reference table.
10. Place the 96-well microplate on the plate reader.

Step 5 - Setting up Microplate Reader

1. Open the software.
2. Open "Protocols" in "Task Manager" and choose "Create New".
3. Choose "Standard Protocol".
4. Open "Procedure" and adjust the settings.
5. Open "Set Temperature" and select "Incubator On". Set "Temperature" to the desired temperature and "Gradient" to 1 °C. It is very important to have the Gradient option "on" to avoid any condensation on the lid that otherwise causes unreliable data.
6. Check "Preheat" before continuing with the next step.
7. Open "Start Kinetic", set "Run time" for 24:00:00 or 48:00:00, and "Interval" for 00:30:00 or 01:00:00. Note: It takes approximately 1 min to read an entire 96 well plate.
8. Open "Shake" and set "Shake Mode" as "Linear". Check "Constitution Shake" and set "Frequency" at 567 cpm.

9. Open "Read", check "Absorbance", "Endpoint/Kinetic", and "Monochromators." Set "Wavelength" to 600.
10. Click "Validate" to confirm that the procedure is correct. Click "Save" to save it as a new program for future use.

Step 6 - Recording Growth Curve

1. Open "Read Now" in "Task Manager" and choose the program (next section).
2. Click "OK" to start measuring.
3. Save the recording as a new experimental file for data analysis

Step 7 - Data Analysis

Export the results of the real-time growth-rate data in to excel format and transfer the data with a USB memory stick.

Note: You can see the overall curve in the image option of the results section as well.

1. Open the excel file with and rearrange the hourly recorded data based on the reference table.
2. Subtract the mean value of the blank reads at time zero from the hourly reads of each well.
3. Divide all the data point with the initial OD_{600}.
4. Transfer all data point to natural logarithm.

APPENDIX D– BACTERIAL GROWTH AND OPTICAL DENSITY (OD)

INTRODUCTION

OD measurements of bacterial culture are a common method in microbiology to monitor bacterial growth. This measurement normally happens at a wavelength of 600 nm relying on light scattering rather than light absorption related to the cell density (cell number or concentration) based on the Beer-Lambert law [185,186]. OD is a measurement of turbidity [186] that can be applied in a specific range of cell density. While Beer-Lambert law explains the dependency of the absorbance to the concentration (i.e., cell density, cell number), path length and absorptivity coefficient; Stevenson et al., 2016 discussed how the shape and cell size of the bacteria impacts overestimating or underestimating the measurement. They conclude that one must be aware of changing cell sizes during growth. If changing in the bacterial cell size is considerable, OD is not a suitable method and direct cell count should be considered to monitor growth and evaluating growth rate [185]. In addition, the geometry and optical system of a spectrophotometer influences the OD readings [186].

WHAT IS GROWTH RATE AND HOW TO CALCULATE IT?

The specific growth rate is of interest in nutrient rich and minimal media, studying for example the impact of different antibiotic regimes, and measuring the toxicity level of chemicals in bacterial species simultaneously. The specific growth rate is determined in the exponential growth phase, where the increase in the number of cells is proportional to increase in the mass of cells.

To mathematically describe the specific growth rate

$$\frac{dx}{dt} = \mu x \tag{2.}$$

In which x represent the cell density or cell number and t is time [187,195]. Integrating the above equation will result in

$$\mu = \frac{ln\left(\frac{x_{t+1}}{x_t}\right)}{t_{i+1} - t_i} \qquad (3.)$$

As explained, the number of cells (cell density) in a specific range is proportional to the absorbance of the light at a particular wavelength (for bacteria is 600nm). So specific growth rate can be calculated in any given time picked during the exponential growth phase by measuring the OD_{600}. The maximum growth rate can be calculated by determining the inflection point of the OD curve and the associated growth rate.
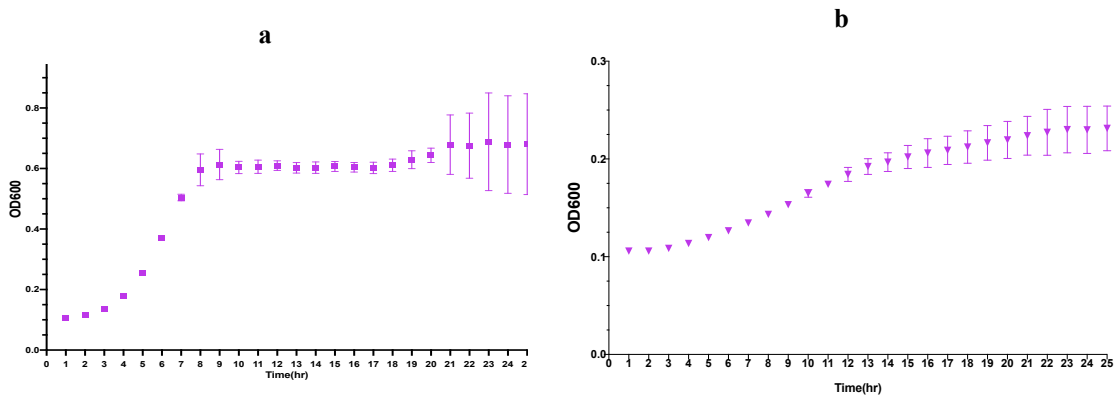
Figure 45   Growth curve for two species in (a) *P. tundrae* and (b) *B. mycoides* in minimal medium by microplate reader. The x-axis shows growth time in hours and the y-axis represents OD600. Each point is an average of 4 measurements. Error bars represent standard deviation.

SPATIAL / GLOBAL BIAS

The cell-to-cell variability of a microplate reader is typically very low, as can be observed in the blank-reads in Figure 46. The readings are OD600 for 200 μL of DI water and the range in the columns changes from 0.09 ± 0.0 to 0.092 ± 0.004. Mean of each column compared statistically using ANOVA and showed no significant differences (Kruskal-Walls, P-Value=0.75, alpha=0.05)

However, temperature and shaking inconsistencies can lead to locational growth biases. In some cases, the airflow in plate reader leads to a variability of evaporation across the plate. It is therefore important, to determine the locational bias for the specific bacteria across the complete plate, using the inoculant size, temperature settings, plate and cover model and time span set out for the experiments ahead.
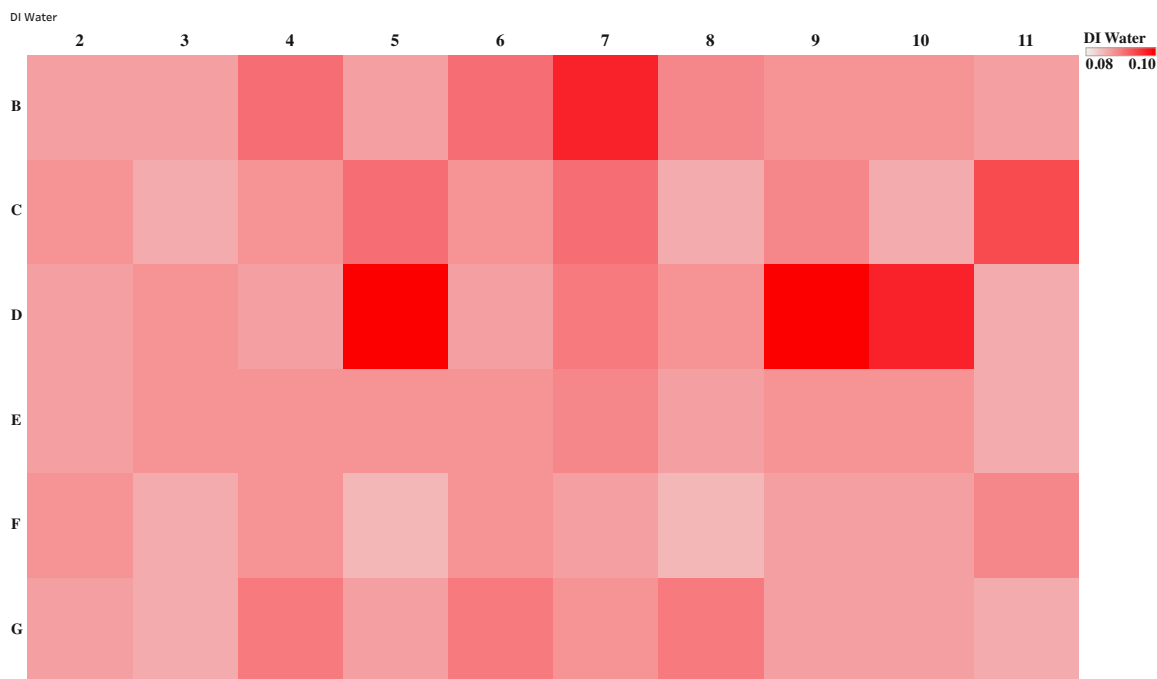

Figure 46   Spatial bias using DI water in a 96-well plate using microplate reader. OD values are absorbacnce at 600nm.

P. tundrea in nutrient rich media was pipetted to the non-edge wells with 1% inoculant size and one hour reading interval. The method is explained in detail in Chapter V, section CV- 6.2 and CV-7.3. In this experiment, the bias is determined for maximum growth rate for each well.

A culture of *P. tundrae* in nutrient rich media was used to explore bias between the microwells. Figure 47 demonstrate the heat map of the growth rate distribution of the *P. tundrae* culture in a 96-well plate. The edge wells were used as blanks since the evaporation rate is considered to be higher compared to the non-edge wells [195]. Changing color intensity

represents varying growth rate values. At first glance, location of the well seems to have a great influence on the obtained growth rate results. However, when comparing the mean of each column including 6 non-edge wells, there was no significant difference (Kruskal-Wallis P-Value=0.85, alpha=0.05). columns are marked by numbers 1-11. The descriptive statistical analysis for each column is represented in Table 20. This ensures uniformity of the protocol as long as each 6 replicate (wells) are in one column there is no difference between the necessary precision and accuracy of this method to reliably measure the differences between these two strains.
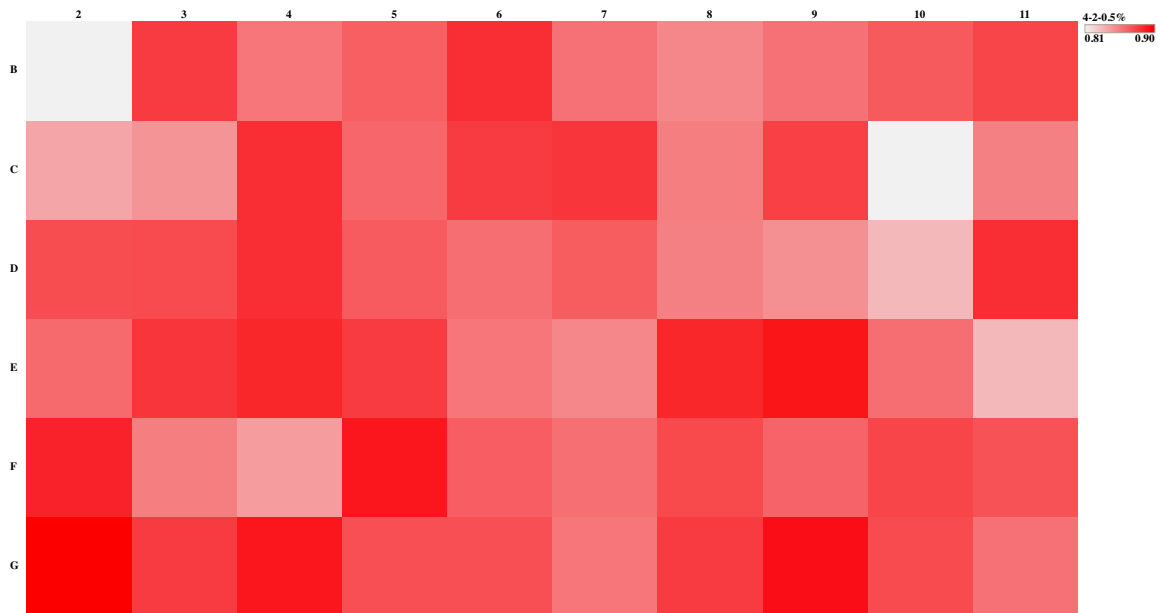

Figure 47   *Spatial* bias of maximum growth rate in a 96-well plate. *P. tundrae* in nutrient rich media with 1% inoculum and 30-minutes time interval sampling is distributed in all the non-edge wells (200µL). The graduation from white to red is shown on the scale. The higher color intensity the higher the value.

Table 20   Descriptive statistical analysis of maximum growth rates of *P. tundrae* in different columns of a 96-well plate.

| Columns	2	3	4	5	6	7	8	9	10	11
Number of values	6	6	6	6	6	6	6	6	6	6
Minimum	0.81	0.85	0.84	0.86	0.86	0.85	0.85	0.85	0.81	0.83
25% Percentile	0.83	0.85	0.85	0.86	0.86	0.85	0.85	0.85	0.82	0.84
Median	0.86	0.87	0.88	0.87	0.87	0.86	0.86	0.87	0.86	0.86
75% Percentile	0.89	0.88	0.89	0.88	0.88	0.87	0.88	0.89	0.87	0.88
Maximum	0.91	0.88	0.89	0.89	0.88	0.88	0.89	0.89	0.88	0.88
Mean	0.86	0.86	0.8733	0.87	0.87	0.86	0.86	0.87	0.85	0.86
Std. Deviation	0.035	0.014	0.019	0.010	0.009	0.01	0.01	0.02	0.02	0.02
Std. Error of Mean	0.014	0.006	0.008	0.004	0.003	0.004	0.007	0.007	0.01	0.008
Lower 95% CI	0.82	0.85	0.85	0.862	0.86	0.85	0.84	0.85	0.82	0.84
Upper 95% CI	0.90	0.88	0.89	0.884	0.87	0.87	0.88	0.89	0.88	0.88
Mean ranks	29.33	31.67	38.17	36.58	32.83	25.00	27.58	34.83	22.67	26.33

APPENDIX E – SUPPLEMENTAL MATERIAL FOR CHAPTER VI

Table 21   Bacterial growth measures as optical density at 600 nm for each species at the end of
incubation for 72 hours at 30° C -each value is an average of five replicates

Species Number	OD$_{600}$	STD
4	0.25	0.05
5	1.36	0.12
6	0.98	0.13
7	0.43	0.02
8	0.32	0.05
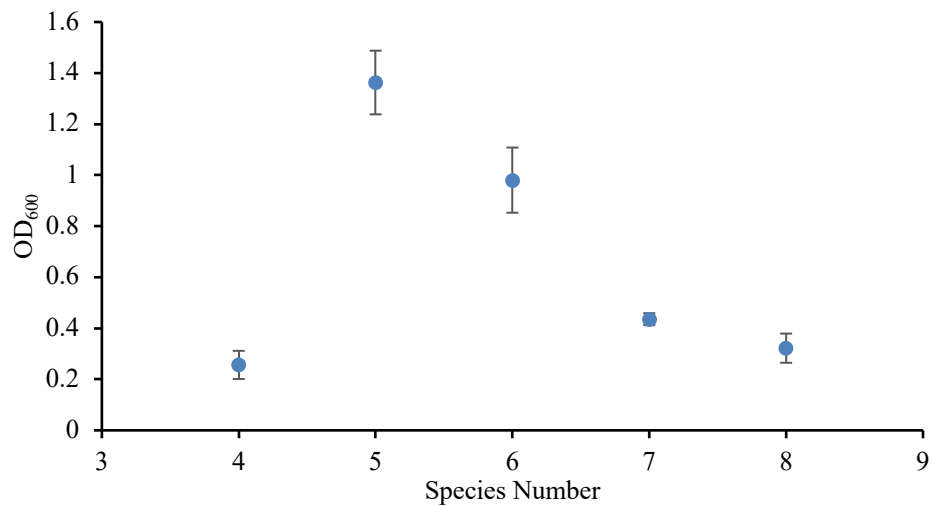
Figure 48   Bacterial growth measures as Optical density at 600 nm for each species at the end of incubation for
72 hours at 30 °C – Error bars are standard deviation of 5 replicates

Table 22   Biofilm development in each well at 550 nm – each value is an average of five replicates.

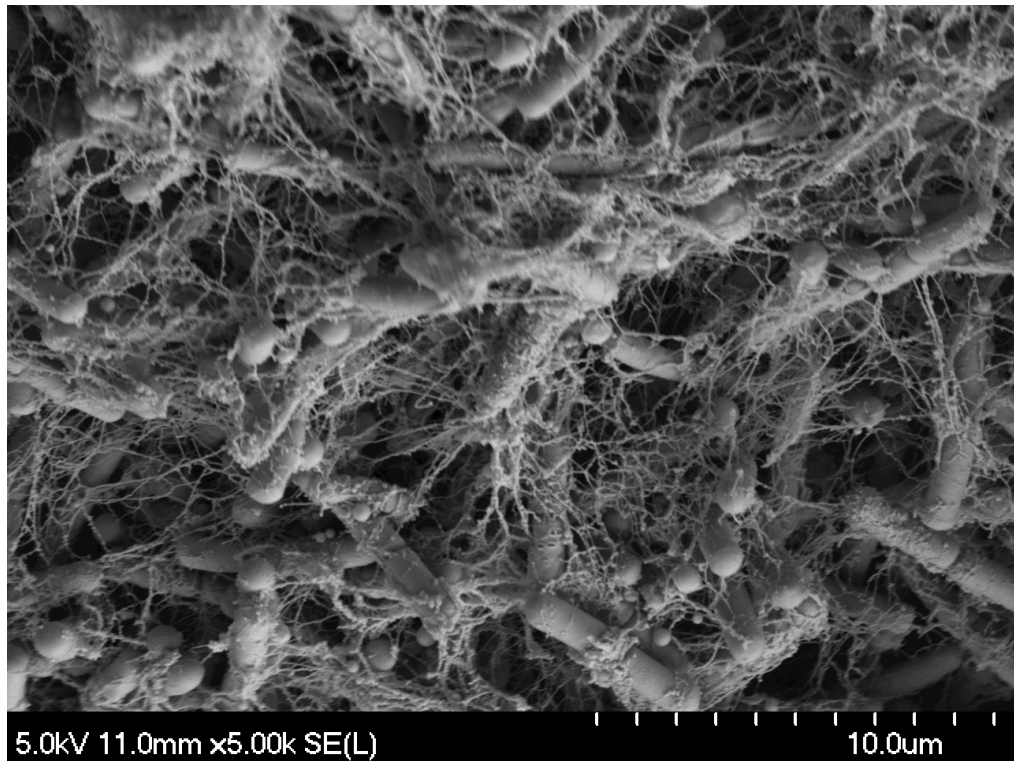| Species Number	Biofilm OD$_{550}$	STD
4	1.18	0.16
5	0.49	0.27
6	2.45	0.54
7	0.12	0.08
8	0.61	0.11

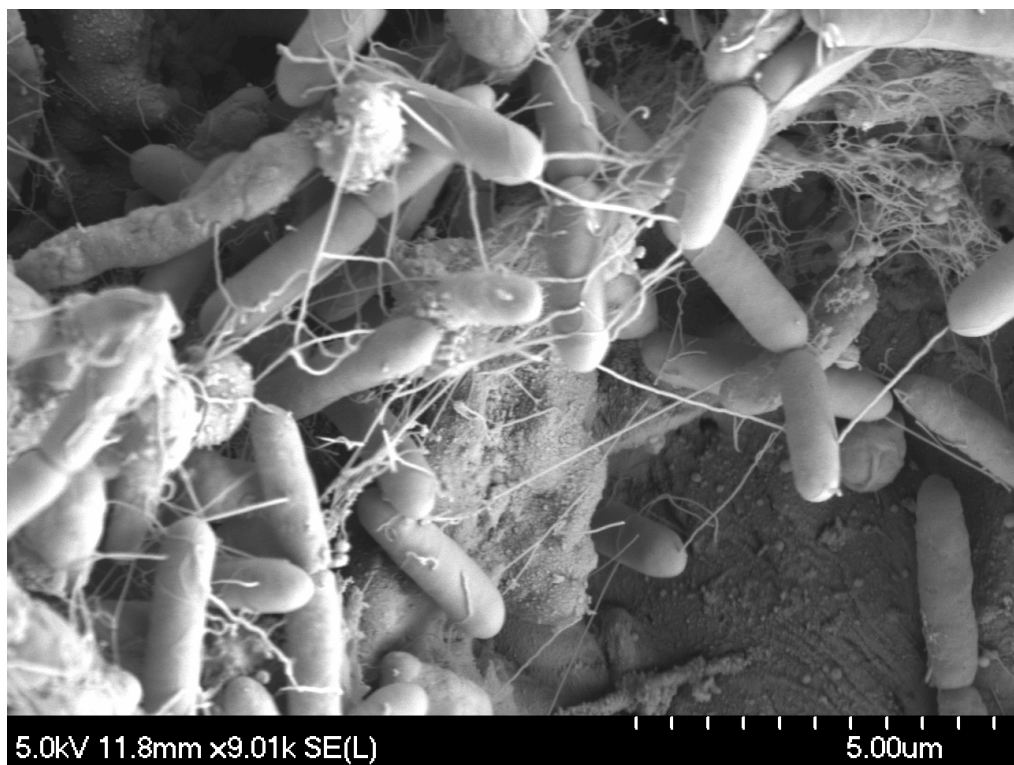Figure 49   SEM image, biofilm of *Bacillus mycoides* in TSB

Figure 50   SEM image, biofilm of *Paenbacillus tundrae* in TSB
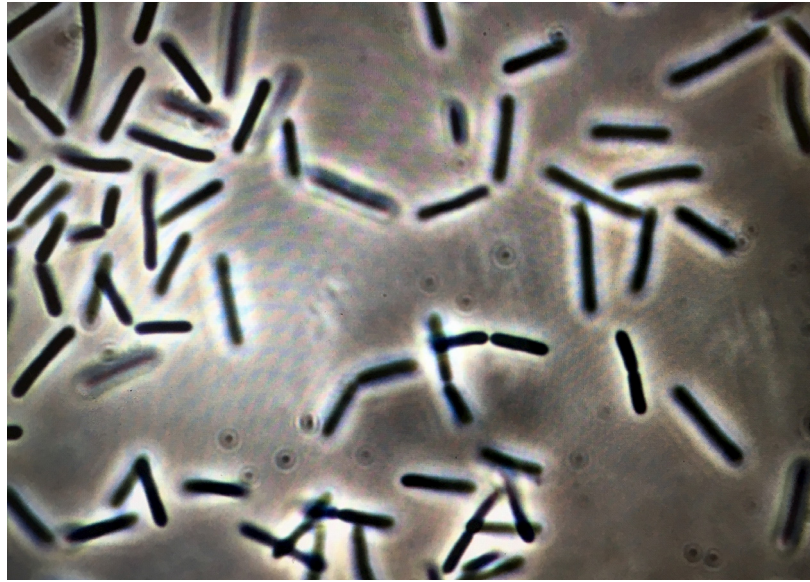
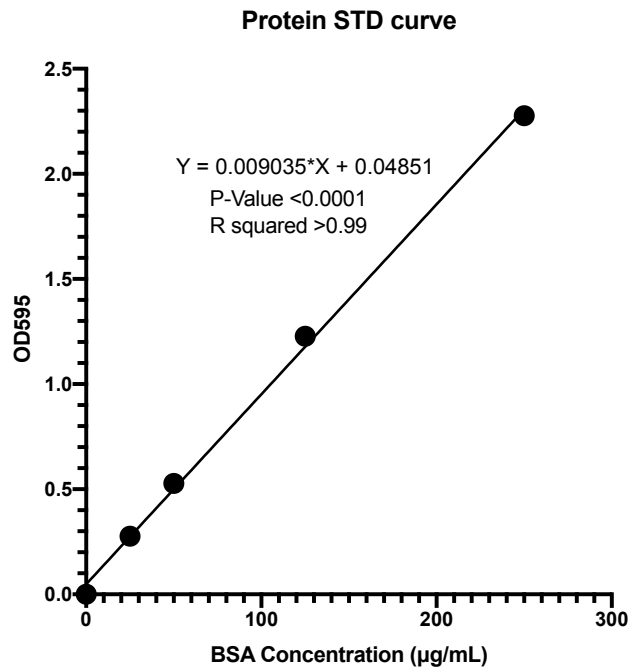Figure 51   Microscopic image of *B. mycoides*

Figure 52   Protein standard curve for calorimetric measurement of EPS-protein
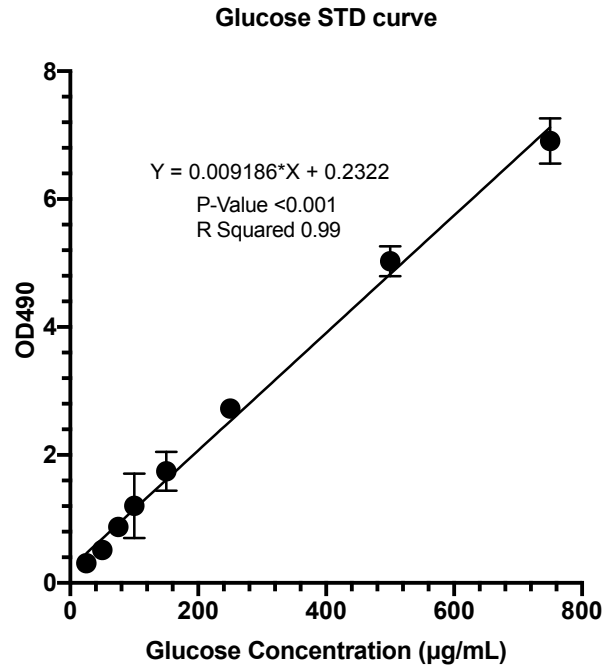
Glucose STD curve

Y = 0.009186*X + 0.2322

P-Value <0.001
R Squared 0.99

OD490

Glucose Concentration (µg/mL)

Figure 53   Glucose standard curve for colorimetric analysis of EPS-carbohydrate

APPENDIX F – COPYRIGHT PERMISSION LETTER FOR CHAPTER III

Dear Leili,

Thank you for your email.

Permission is granted for you to use the material requested for your thesis/dissertation subject to the usual acknowledgements (author, title of material, title of book/journal, ourselves as publisher) and on the understanding that you will reapply for permission if you wish to distribute or publish your thesis/dissertation commercially.

You should also duplicate the copyright notice that appears in the Wiley publication in your use of the Material. Permission is granted solely for use in conjunction with the thesis, and the material may not be posted online separately.

Any third-party material is expressly excluded from this permission. If any material appears within the article with credit to another source, authorisation from that source must be obtained.

Should you require any further information, please do not hesitate to contact me.

Kind regards,

Paisley Chesters
Permissions Co-Ordinator

Wiley
The Atrium
Southern Gate
Chichester
West Sussex
PO19 8SQ
www.wiley.com

WILEY

John Wiley & Sons Limited is a private limited company registered in England with registered number 641132.
Registered office address: The Atrium, Southern Gate, Chichester, West Sussex, United Kingdom.
PO19 8SQ

From: Leili Abkar <abkar@Dal.Ca>
Sent: 28 October 2019 14:56
To: Wiley Global Permissions <permissions@wiley.com>
Subject: Re-print permission for PhD thesis

Dear Madam/Sir,

I hope this email finds you well.

I am contacting you regarding the article titled "SEDIMENTATION: HYDRAULIC IMPROVEMENT OF DRINKING WATER BIOFILTRATION" published in AWWA Water Science, DOI :10.1002/aws2.1160.

This article represent a chapter in my phd thesis in Dalhousie university. I would like to kindly ask for re-print permission to use this article as a chapter in my thesis.

Best regards,

Leili